WILEY-VCH

Edited by
Zbigniew L. Pianowski

# Molecular Photoswitches

## Chemistry, Properties, and Applications

Foreword by B. L. Feringa

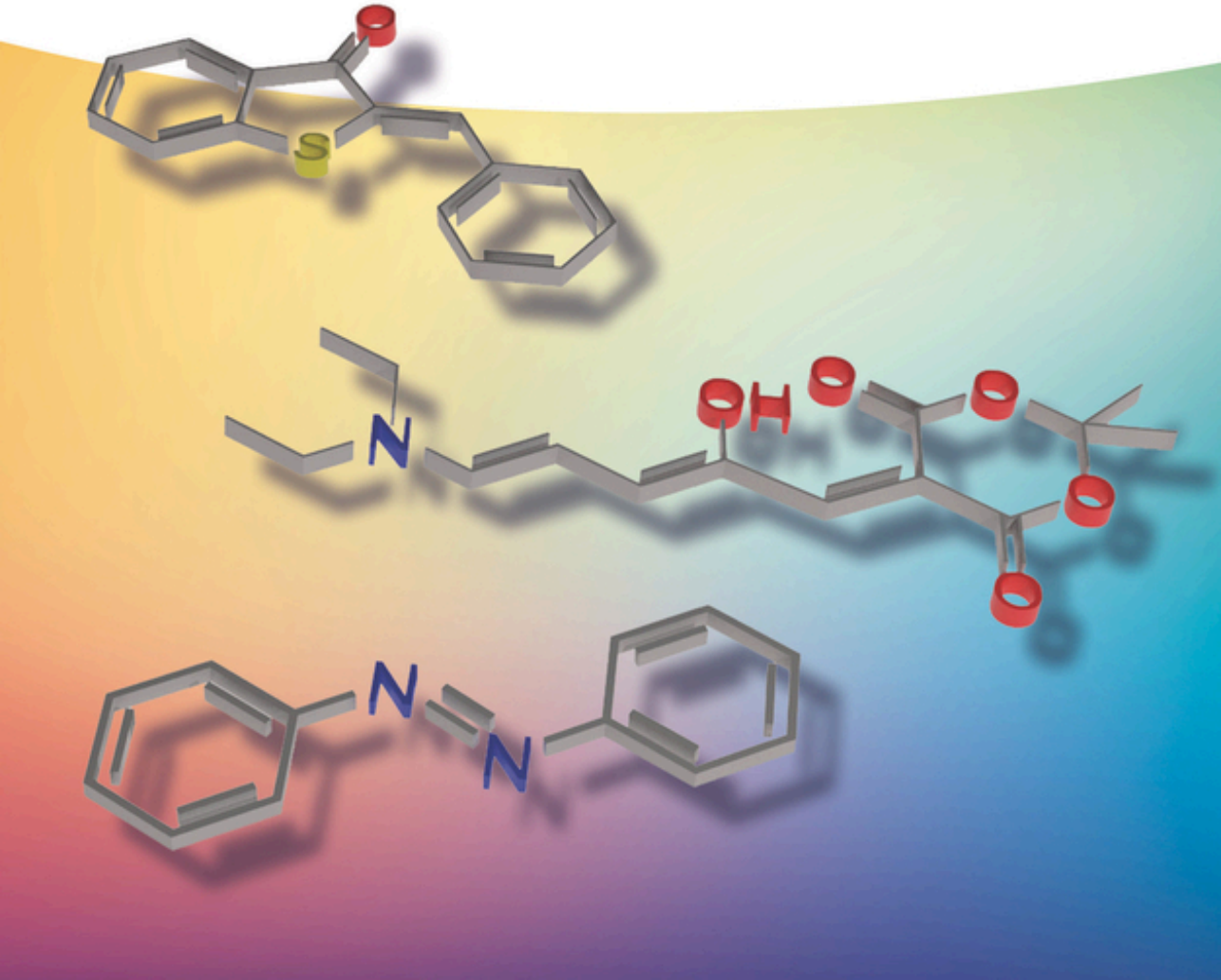

**Molecular Photoswitches**

# Molecular Photoswitches

Chemistry, Properties, and Applications

*Edited by*
*Zbigniew L. Pianowski*

Volume 1

WILEY-VCH

# Molecular Photoswitches

Chemistry, Properties, and Applications

*Edited by*
*Zbigniew L. Pianowski*

Volume 2

WILEY-VCH

***Editor***

***Dr. Zbigniew L. Pianowski***
Karlsruhe Institute of Technology
Institute of Organic Chemistry
Fritz-Haber-Weg 6
76131 Karlsruhe
Germany

Karlsruhe Institute of Technology
Institute of Biological and Chemical
Systems – Functional Molecular Systems
(IBCS-FMS)
Hermann-von-Helmholtz-Platz 1
76344 Eggenstein-Leopoldshafen
Germany



**Library of Congress Card No.:** applied for

**British Library Cataloguing-in-Publication Data**
A catalogue record for this book is available from the British Library.

**Bibliographic information published by the Deutsche Nationalbibliothek**
The Deutsche Nationalbibliothek lists this publication in the Deutsche Nationalbibliografie; detailed bibliographic data are available on the Internet at <http://dnb.d-nb.de>.



**Print ISBN:** 978-3-527-35103-9
**ePDF ISBN:** 978-3-527-82760-2
**ePub ISBN:** 978-3-527-82761-9
**oBook ISBN:** 978-3-527-82762-6

**Cover Design** SCHULZ Grafik-Design, Fußgönheim, Germany
**Typesetting** Straive, Chennai, India

Printed on acid-free paper

10 9 8 7 6 5 4 3 2 1

# Contents

**Volume 2**

# Contents

**Volume 2**

# Foreword

That you can read the title of this book "Molecular Photoswitches" and do not get lost during a fascinating journey through it is due to the billions of tiny molecular switches working frantically in your eyes. Arguably vision is one of the most magnificent results of biological evolution, and it is intriguing that the fundamental process behind it is in fact a *Z*–*E* photoisomerization of an alkene unit in the cis-retinal photoswitch triggered by visible light. But it is more than this as the photoswitch does not operate on its own. To exert its function, the switch is integrated within a dynamic multicomponent system that interfaces it with the complex machinery of life. This duality is reflected in several of current research objectives in the field of artificial molecular photoswitches.

Unsurprisingly, beyond tuning the well-known classes of switches for specific functions, the design of novel molecular photoswitches, and elucidating the fundamental mechanisms of the photochemical event itself, major future challenges are associated with the exploration of these trigger elements in complex dynamic systems ranging from responsive materials all the way to the control of biological function in cells. Drawing inspiration from Nature, numerous chemists have contributed over the last decades to the blooming field of artificial molecular photoswitches, which is testimony to its prominent role in the transition from molecules to dynamic molecular systems in contemporary chemical sciences.

In this timely volume the "Molecular Photoswitch Community" has joined forces to provide an in-depth and balanced account of the progress as well as challenges and perspectives in this flourishing and highly dynamic field under the editorship of Zbigniew Pianowski.

The study of the interplay of light and matter, i.e. photoresponsive molecules, continues to offer remarkable new insights not in the least due to the advances in transient spectroscopies and computational methods. These developments guide the design of novel photoswitches toward specific applications. It is amazing how "revisiting" more classical photochromic compounds, such as azobenzenes, stilbenes, and spiropyrans, is stimulated by the quest for visible light switching, enhanced bistability or compatibility with the molecular systems or materials in which they are to exert their function. It has initiated many unforeseen opportunities. The introduction of new classes of switches such as overcrowded alkenes, arylhydrazones, diazocines, indigoids, and Stenhouse adducts has significantly

enlarged our playground for instance toward multistate or multicomponent orthogonal switching systems.

The discussion of adaptive materials based on molecular photoswitches in Section II again illustrates a vibrant research field. Introducing switching functions in liquid crystal polymers, a variety of soft materials, and supramolecular systems enables the amplification of the molecular triggering event along the length scales to macroscopic function, ranging from responsive surfaces to mechanical muscle-type movement. In addition, the confinement of photoswitches on nanoparticles or in 2D and 3D assemblies, including porous frameworks, addresses issues of functioning at interfaces and cooperative action, and brings entirely new dimensions to the field.

Among the most spectacular developments over the past decade is the use of molecular switches for the photomodulation of biological systems. It is evident that the rapidly emerging area of photopharmacology has its roots in the field of photoswitches, in particular azobenzenes which were reported by Mitscherlich as early as 1834. The control of the activity of a drug by light with high spatiotemporal precision holds promise for precision therapy, smart pharmaceuticals, and imaging techniques. In addition, Section III illustrates how photochromic systems can be applied in a much broader perspective, including control of peptides, oligonucleotides, saccharides, and ion channels. Photoregulation of specific pathways in complex biochemical networks, cellular communication, transcription, or membrane transport are fascinating examples of the opportunities that emerge. It is also evident that the photoswitch community has to tackle many challenges entering the realm of biology – not least in how to make these molecular switches biocompatible, operate in the aqueous environment of the cells, be compatible with multi-chromophore functional systems, and switchable with visible or NIR light. Answering these questions will ultimately allow the application of molecular photoswitches in vivo.

Arguably the question as to how to use molecular switches and achieve controlled movement at the nanoscale has been essential in the discoveries leading toward molecular machines. With the expected key role of chemistry in future complex systems, molecular information science, and soft robotics, taking advantage of the solid basis in molecular photoswitches as presented here will likely become increasingly important. Indeed, this book showcases many novel approaches and opportunities in this vibrant field and without doubt will guide molecular explorers in their odyssey in the world of responsive molecular systems.

*Ben L. Feringa*

# Preface

Light is a traceless reagent, which can be dosed with high spatiotemporal precision. It has been consciously used for almost 200 years to perform chemical reactions, since the report of light-induced rearrangement followed by dimerization of α-santonin by Trommsdorff in 1834. A few decades later, light-induced processes resulting in reversible color changes have been described: photooxidation of tetracene by Fritzche (1867), photoisomerization of benzylidenehydrazines (Wislicenus 1893), osazones (Blitz 1899), or the reversible color change of 2,3,4,4-tetrachloronaphthalen-1(4H)-one in the solid state by Markwald (1899). The latest author introduced the German term "Phototropie," which evolved into what we now call "photochromism" – the reversible transformation of a chemical species between two forms with distinct absorption spectra, by the absorption of electromagnetic radiation. Photochromism often manifests itself as a reversible change of color upon exposure to light.

In 43 chapters of this book, authors describe photochromic organic compounds – molecular photoswitches – which undergo reversible photoisomerization and change their molecular properties, such as geometry, polarity, or rigidity. Properly designed systems containing molecular photoswitches can transform the energy of light into a wide range of functions. Very often, fascinating macroscopic effects can be achieved, which go far beyond the simple color change.

After introductory chapters on the photophysics of the switches and relevant computational methods, the first volume of the book demonstrates the broad variety of classes of photochromic chemical compounds. The photochromic scaffolds established for decades, such as spiropyrans, diarylethenes, or azobenzenes, are followed by compounds whose photochromism was just recently exploited – such as indigoids or donor–acceptor Stenhouse adducts. Some classes have a distinctive functional bias, such as molecular motors for chirooptical switches, conversion of the solar energy by norbornadienes, or molecular electronic systems relying on dihydroazulenes. This section is complemented with a report on photochromic coordination compounds and on systems used for photomodulation of catalytic processes.

The second volume of this book is dedicated to the variety of materials based on molecular photoswitches. Its scope spans from light-induced phase transitions, through photochromic porous materials, liquid crystals, or nanoparticles, to light-responsive molecular machines and logic devices. The last section in

the same volume pertains to the applications of molecular photoswitches in the biological context. There, properties and applications of photoswitchable biopolymers – oligonucleotides, peptides, or saccharides – are described. Other contributions are focused on photochromic bioactive small molecules and their applications – such as light-modulated antibiotics, cytotoxins, or ion channel inhibitors. This section is concluded with light-propelled artificial muscles and implementation of molecular photoswitches into computational design of proteins.

The aim of this book is to provide a balanced overview – to specialists and non-experts – on the rapidly growing field of molecular photoswitches, with a particular focus on the achievements and discoveries from the last decade. We hope that this book may inspire younger colleagues to enter into the fascinating realm of photochromic compounds and materials. We also hope that it will support lecturers worldwide in preparing courses related to this subject. In the name of all the readers, the editor wants to appreciate the effort of contributing authors in providing clear and balanced chapters, rich in carefully selected information and complemented with sources for the further advanced reading. The editor also sincerely apologizes for the omissions and mistakes that might appear in the book despite the careful planning and revision process.

Germany *Dr. Zbigniew L. Pianowski*

# Section I

# Interplay of Light and Matter

# 1 Physicochemical Aspects of Photoswitching

Petr Klán and Jakob Wirz

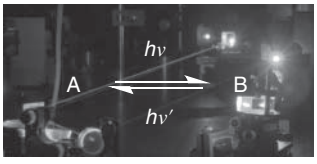


**Characteristic Features**

This chapter offers a short prologue to the basics of photophysics and photochemistry and introduces fundamental concepts such as quantum yield and photostationary state. On two examples of common photoswitches, the reader is acquainted with steady-state and time-resolved spectroscopic methods commonly used to study photochromic systems.

**Key References**

Klan, P. and Wirz, J. (2009). *Photochemistry of Organic Compounds: From Concepts to Practice*, 1st ed. Chichester: Wiley.

Ward, C.L. and Elles, C.G. (2012). Controlling the excited-state reaction dynamics of a photochromic molecular switch with sequential two-photon excitation. *J. Phys. Chem. Lett.*, 3: 2995–3000.

Quick, M., Dobryakov, A.L., Gerecke, M. et al. (2014). Photoisomerization dynamics and pathways of *trans*- and *cis*-azobenzene in solution from broadband femtosecond spectroscopies and calculations. *J. Phys. Chem. B*, 118: 8756–8771.

# 1

# Physicochemical Aspects of Photoswitching

*Petr Klán*[1] *and Jakob Wirz*[2]

[1] *Department of Chemistry and RECETOX, Faculty of Science, Masaryk University, Kamenice 5, 62500, Brno, Czech Republic*
[2] *Department of Chemistry, Institute of Physical Chemistry, University of Basel, Klingelbergstrasse 80, CH-4056, Basel, Switzerland*

## 1.1 Introduction

The expression photochromism is used for reversible structural rearrangements that are triggered by light in one or both directions, which connect two related species (isomers) with different absorption spectra [1]. Such molecules are also called photoswitches. Photoactivation can give access to a thermodynamically less stable isomer. Several types of photoreactions can be involved, such as light-triggered electrocyclization, cycloaddition, *E*,*Z*-isomerization, intramolecular hydrogen, group or electron transfer, or dissociation. Each of them requires specific reaction and illumination conditions and, in particular, detailed knowledge of the mechanism when sufficient control over the scope of photoswitching is needed. Photoswitches have attracted attention in many fields, spanning from applications of optical filters, photography, protection from sunlight, actinometry, imaging, holography, solar energy conversion, energy storage, and molecular electronics to drug delivery and photopharmacology [2–9].

Azobenzene derivatives, spiropyrans, fulgides, and diarylethenes (Scheme 1.1) are probably the most common classes of organic photochromic compounds. The *E*- and *Z*-forms of azobenzene possess similar and strongly overlapping absorption spectra, whereas the two forms of the latter photoswitches are distinctively different thanks to a considerable change of electron distribution during the electrocyclization reaction.

When designing a chromophore as a photoswitch, the number of cycles that a molecule can repeat without degradation is of utmost importance; the loss of any of the photochromic component during irradiation, for example, by oxidative degradation, is termed "fatigue" [1]. Thus, one needs to consider the following properties depending on the application aimed at:

- A reliable, simple synthesis and variability for tailor-made compounds
- Photoswitching efficiency (quantum yield)

*Molecular Photoswitches: Chemistry, Properties, and Applications*,
First Edition. Edited by Zbigniew L. Pianowski.

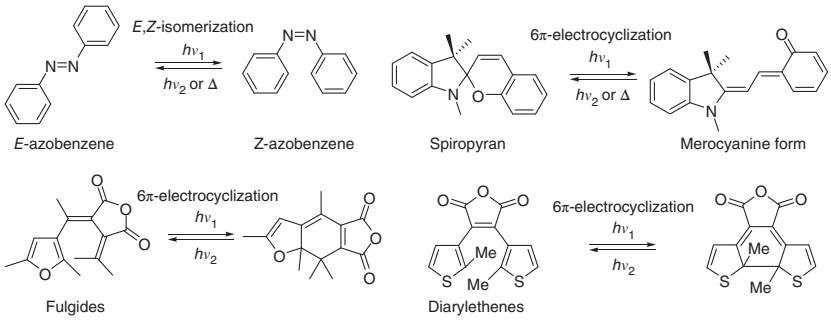


**Scheme 1.1** Major families of photochromic compounds.

- Sufficiently different absorption spectra of both isomers
- Excitation wavelength
- Reversibility and bidirectional switching
- Photodegradation, fatigue
- The desired lifetime of switch setting:
  - T-type: rapid thermal reversion
  - P-type: thermally irreversible or slow
- Fluorescence

## 1.2 Essentials of Photophysics

Some knowledge of photochemistry is required to design and study a photoswitch. Here, we give a short introduction to the basics of photophysics and photochemistry.

We start with a short introduction defining photophysical processes, which are usually depicted in a *Jabłonski diagram* [10] (Figure 1.1). Molecular electronic states are represented by thick horizontal lines (—) that are arranged in a vertical order to indicate relative energies and are labeled consecutively by increasing energy, beginning with the singlet ground state $S_0$, followed by excited singlet

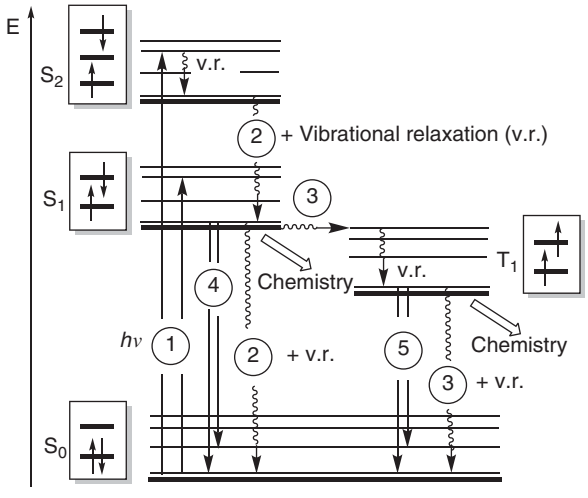


**Figure 1.1** Jabłonski diagram.

states $S_1$, $S_2$, etc. Vibrational states, represented here by thin lines (—), are usually not shown explicitly. States of a given *multiplicity* (singlet, triplet) are collected in separate columns. Horizontal displacement does *not* indicate a change in structure. The energy levels represent minima on the potential energy surfaces of a given electronic state. The corresponding structures will be somewhat different for each state. For molecules with a singlet ground state, the left-hand column collects the electronic singlet states and that to the right the triplet states. The lowest triplet state is labeled $T_1$, followed by $T_2$, etc.

*Photophysical processes* are *radiative* or *radiationless transitions* by which molecules are promoted from one electronic state to another. No chemical change takes place, although the bond lengths and angles generally differ somewhat in different electronic states. Radiative transitions are associated with the absorption or emission of a photon and are represented as straight arrows (↑ or ↓), while radiationless transitions, including vibrational relaxation (v.r.), are not associated with absorption or emission and are shown as wavy arrows (⇝).

The major transitions depicted in Figure 1.1 involve: ① *Absorption* of a photon generating an electronically excited state ($S_0$ to $S_1$ and $S_0$ to $S_2$ shown); ② *internal conversion* (IC) as a radiationless transition between two electronic states of the same multiplicity ($S_2$ to $S_1$ and $S_1$ to $S_0$ shown); ③ *intersystem crossing* (ISC) as a radiationless transition between two electronic states of different multiplicity ($S_1$ to $T_1$ and $T_1$ to $S_0$ shown); ④ *fluorescence* – emission of a photon associated with the generation of a lower-energy state of the same multiplicity ($S_1$ to $S_0$ shown); and ⑤ *phosphorescence* – emission of a photon associated with the generation of a lower-energy state of different multiplicity ($T_1$ to $S_0$ shown). IC ② and ISC ③ are isoenergetic processes of energy redistribution within the excited molecule by which electronic energy is distributed over many vibrational modes of the lower excited state. IC and ISC are essentially irreversible processes because they are associated with an entropy increase (high density of states in the lower-energy electronic state) and because the following vibrational relaxation is very fast (picosecond timescale) in solution. The lowest $S_1$ and $T_1$ states are typically not only associated with emission but also with primary chemical processes (depicted as "chemistry").

### 1.2.1 Quantum Yield

The term *quantum yield* $\Phi_x(\lambda)$ is equal to the amount $n_x$ of photochemical or photophysical events x that have occurred, divided by the amount $n_p$ of photons at the irradiation wavelength $\lambda$ that were absorbed by the reactant, Eq. (1.1) [10].

$$\Phi_x(\lambda) = n_x/n_p \tag{1.1}$$

Both $n_x$ and $n_p$ are measured in moles or einstein (1 einstein = 1 mol of photons) and the dimension of $\Phi_x$ is unity. The photochemical or photophysical process x must be defined explicitly. In general, quantum yields lie in the range $0 \leq \Phi_x \leq 1$ and represent the probability that a molecule undergoes the defined process x after absorption of a photon.

According to *Kasha's rule*, polyatomic molecules generally luminesce only from the lowest excited state of a given multiplicity [10]. By extension of Kasha's rule,

quantum yields are often independent of the excitation wavelength. The same rule can be applied to photochemical processes as depicted in Figure 1.1. There are many exceptions, however.

### 1.2.2 Photostationary State

In a reversible photoreaction between two photoswitch isomers A and B that are stable in the dark, the ratio of their amounts, $n_A$ and $n_B$, formed by exhaustive irradiation at a given wavelength $\lambda_{irr}$, is given by Eq. (1.2) [10],

$$\mathrm{A} \underset{h\nu'}{\overset{h\nu}{\rightleftharpoons}} \mathrm{B}$$

$$\frac{n_B}{n_A}(\lambda_{irr}) = \frac{\Phi_{A\to B}\varepsilon_A(\lambda_{irr})}{\Phi_{B\to A}\varepsilon_B(\lambda_{irr})} \tag{1.2}$$

where $\varepsilon_A(\lambda_{irr})$ and $\varepsilon_B(\lambda_{irr})$ are the molar absorption coefficients of A and B at the wavelength of irradiation, and $\Phi_{A\to B}$ and $\Phi_{B\to A}$ are the quantum yields of photoisomerization of A to B and of B to A, respectively. The ratio $n_B/n_A$ is called the photostationary state (PSS); it defines how well the position of a photoswitch can be controlled by monochromatic irradiation at a given wavelength $\lambda_{irr}$.

### 1.2.3 Photoactivation

Photoswitching processes are typically activated by one-photon excitation, by UV light at least in one direction, and the interconversion itself can originate from either the singlet or triplet excited state. The nature of the excited state, its lifetime, and susceptibility to undergo unwanted competing side reactions, such as oxidation in the presence of oxygen, is one of the main factors in the design and application of photoswitches. When a visible- or near-infrared-light phototrigger is needed, specific modifications of the chromophore, such as the extension of a π-system or designing a push–pull system, can be utilized [11]. In another approach, a high-energy excited state can also be accessed via two-photon excitation [12].

In biological or medical applications, the wavelengths of photoactivation are restricted by the adverse effects of UV light, by tissue absorption due to endogenous chromophores, and by optical scattering, which restrict the depth of tissue penetration. Thus, photolysis by light within the so-called tissue-transparent or phototherapeutic window, limited by the absorption of hemoglobin below 600 nm and by the absorption of water above 900 nm [13], is important for biological and medical applications, and there is a demand for photoswitches that can be activated in this wavelength range.

## 1.3 Spectroscopy of Photoswitching

Steady-state absorption and emission spectroscopies provide invaluable information about the electronic properties and structures of individual photoswitch forms, and

they can also be used for the determination of the composition of reaction mixtures and the identification of reaction (unwanted) side products, especially in combination with other analytical techniques, such as HPLC. The time evolution of the absorbance spectra is particularly important for the evaluation of the photokinetics of slow transformations. Global analysis of spectral data is a very useful tool to validate a proposed model of photoswitch transformation [10].

NMR spectroscopy became one of the essential tools in the structural identification of long-lived intermediates and photoproducts formed during a photochromic process, in conformational analyses, and it can be used for monitoring the extent of photoswitching [14]. NMR can also provide valuable quantitative information about the mixtures without the need to perform other analytical determination methods. Detailed examination of the chemical shifts and spin–spin couplings in the spectra gives additional information about intermolecular interactions, aggregations, etc.

The primary reactions of photoswitches are commonly very fast, taking place on a picosecond timescale and faster. Such reactions can be studied using modern spectroscopy of short-lived reaction intermediates. Following excitation of the photoswitch by an intense, short laser pulse, the resulting transient intermediates are commonly observed by their absorption (transient absorbance difference spectroscopy). More informative spectroscopic techniques for the detection and identification of reactive intermediates have been developed, in particular EPR, IR and Raman spectroscopy, NMR, mass spectrometry, electron microscopy, and X-ray diffraction.

Most optical flash photolysis apparatuses with excitation pulses of nanosecond and longer duration operate in the kinetic mode, that is, the transient absorption is monitored with a photomultiplier at a single wavelength as a function of time, providing accurate reaction rate constants up to about $10^8\ s^{-1}$ [10]. For faster reactions, excitation by laser pulses of shorter duration is required. The pump–probe method provides transient absorption spectra at a given time delay with respect to the excitation pulse. The laser pulse is split into two portions. The major part of the laser pulse (the pump pulse) is used to excite the sample and trigger the process under investigation; the rest (the probe pulse) is focused onto some material to produce a supercontinuum pulse with a strongly broadened spectrum, which is then sent to the sample over an optical delay line. As the speed of light is $c = 3 \times 10^8\ m\ s^{-1} = 0.3\ m\ ns^{-1}$, a delay line of 30 cm length delays the probe pulse by 1 ns with respect to the pump pulse. The probe signal is typically averaged over many pulses. A fast detector is not required. The temporal resolution is fundamentally limited only by the duration of the pump and probe pulses. By varying the time delay between the pump and probe pulses, it is possible to assemble absorption spectra as a function of time after the excitation pulse. Basically, both the kinetic and the pump–probe spectrographic setup measure one-dimensional slices of the same physical information that consists of a two-dimensional array A of absorbances $A\ (\lambda,t)$ as a function of wavelength $\lambda$ and time $t$ after excitation of the sample.

Time-resolved IR and Raman spectroscopies have also been recognized as excellent methods for the characterization of transient chemical species [10]. Both IR and

Raman spectra provide fingerprints that allow for unambiguous identification of simple molecules or their mixtures. The dynamics of fast chemical transformations of photoswitches are successfully evaluated with sensitive Fourier-transform instruments. In picosecond and femtosecond time-resolved Raman spectroscopy, the sample is pumped and probed by well-defined laser pulses, producing a full vibrational spectrum in the 1000–2000 $cm^{-1}$ range with up to <100 fs temporal and < 35 $cm^{-1}$ spectral resolution.

## 1.4 Two Case Examples

This chapter provides two examples of spectroscopic approaches used to study the transformations of photoswitches and highlights some difficulties that can occur in interpreting data. The provided information is not comprehensive; it should only introduce the reader to the spectroscopic methods, which are used to study photochemistry of photoswitches.

### 1.4.1 Diarylethenes

Photochemically induced 6π-electrocyclic cyclization and cycloreversion of diarylethenes (Scheme 1.2) are very fast processes, and their reaction dynamics can be studied by ultrafast time-resolved spectroscopic methods [15–17]. The photocyclization of the simplest example of diarylethenes, (*Z*)-stilbene, occurs from the singlet $^1\pi,\pi^*$ state [10]. The orbital symmetry allowed conrotatory closure results in the formation of *trans*-dihydrophenanthrene, which can be oxidized to phenanthrene in nearly quantitative yield [18, 19] (Scheme 1.2). Many derivatives of 1,2-bis(hetero)arylethenes, in which the phenyl groups of stilbene are replaced with five-membered heterocyclic (e.g. thiophene or furan) rings, have received special attention as photoswitches [16, 17].

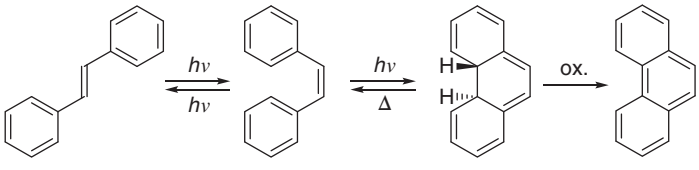


**Scheme 1.2** Stilbene photochemistry.

For example, the photochromic pair of compounds **1a** and **1b** (Scheme 1.3) is a fatigue-resistant [20] photoswitch showing distinct absorption spectra of the open- and closed-ring forms (Figure 1.2) [21, 22]. The π-conjugated system of **1a** is localized on the UV-absorbing thiophene rings, whereas the visible-light-absorbing π-system of **1b** is delocalized throughout the molecule. The lack of absorption of **1a** above 400 nm allows for a complete cycloreversion of **1b** upon irradiation by visible light.

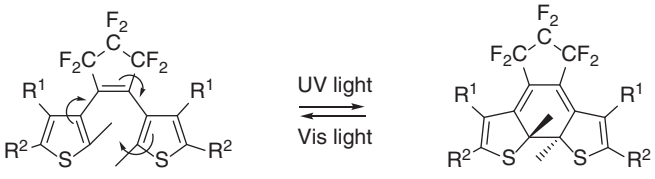


**1a**: $R^1 = CH_3$, $R^2$ = Ph — **1b**
**2a**: $R^1 = CH_3$, $R^2 = p\text{-}(C_6H_4)N(C_2H_5)_2$ — **2b**
**3a**: $R^1$ = H, $R^2$ = Ph — **3b**
**4a**: $R^1$ = H, $R^2 = CH_3$ — **4b**

**Scheme 1.3** Photochemical cyclization and cycloreversion of dithienylethenes.

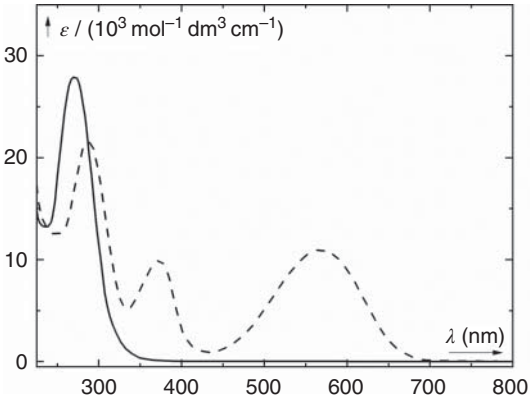


**Figure 1.2** Absorption spectra of **1a** (solid line) and **1b** (dashed line) (R = Ph) in hexane. Source: Adapted from Ward et al. [21].

The **1b→1a** conversion ($x$/%) in dilute solutions is calculated under photostationary-state conditions according to Eq. (1.3) [22]. When the ratio of $\boldsymbol{\Phi_{1b\rightarrow 1a}\varepsilon_{1b}/\Phi_{1a\rightarrow 1b}\varepsilon_{1a}}$ is high, the conversion is large.

$$x = \frac{\boldsymbol{\Phi_{1b\rightarrow 1a}\varepsilon_{1b}}}{\boldsymbol{\Phi_{1b\rightarrow 1a}\varepsilon_{1b} + \Phi_{1a\rightarrow 1b}\varepsilon_{1a}}} \times 100 \tag{1.3}$$

The quantum yields and the efficiencies of any side-reactions may vary with temperature, the nature of substituents, solvent, conformational behavior, etc. [16]. For example, the ring-opening quantum yields decrease by introducing an electron-donating substituent to the *p*-position of the phenyl $R^2$ groups in **2a** (Scheme 1.3) [22]. 1,2-Bis(hetero)arylethenes attain two conformations with the two rings in a parallel or antiparallel arrangement, but the photocyclization can occur only from the latter conformation (Scheme 1.4) [22, 23]. In the case that

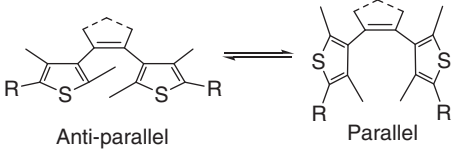


**Scheme 1.4** Antiparallel and parallel arrangements of 1,2-bis(hetero)arylethenes.

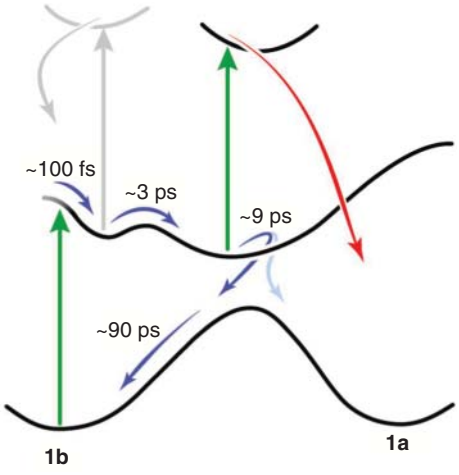


**Figure 1.3** The reaction dynamics for one- and two-photon excitation of **1b**. Source: Reproduced by permission of Ward and Elles [26].

the population ratio of the two conformers is 1 : 1, the cyclization quantum yield cannot exceed 0.5. This ratio, and thus the magnitude of the quantum yield, can be controlled by structural changes and confined environment [16, 17].

Ultrafast kinetics of the cyclization and cycloreversion reactions have been investigated by pico- and femtosecond time-resolved absorption spectroscopy [15, 24]. Polarization-selective nonlinear transient-absorption spectroscopy with a 90–110 fs time resolution was used to study the ring-closing reaction of **3a** (Scheme 1.3) in cyclohexane by Duppen and coworkers [25]. The population and orientational dynamics supported by theoretical calculations revealed that, upon excitation, three events follow: pre-switching due to excited state mixing (50 fs), the ring closure (0.9 ps), and post-switching related to vibrational cooling (100 ps). The fs pump–probe one- [26] and two-color [21] pump–repump–probe spectroscopies were used to study the cycloreversion of **1b** (Scheme 1.3). The excited molecule $^{1}$**1b*** has to cross an activation barrier in ∼3 ps, before reaching the access to a conical intersection with the ground state (Figure 1.3). When a secondary excitation with a delay of ∼5 ps between the primary and secondary excitation events is used, the highest cycloreversion efficiency to give **1a** is observed [26]. It was suggested that the method can be used to selectively control the extent of photoswitching.

A different approach was utilized with picosecond time-resolved Stokes and anti-Stokes Raman spectroscopies to study the cyclization and cycloreversion reactions of **4a**, **4b** (Scheme 1.3) photochemical interconversion [27]. The cyclization, monitored by the time evolution of specific Raman bands attributed to the ring-closed form **4b**, was found to occur in 4 ps followed by vibrational cooling within 10 ps.

Femtosecond transient absorption spectroscopy and ultrafast electron diffraction crystallography [28–30] were also utilized in the study of the cyclization reaction of **1a** in a single crystal. While there is a coexistence of two conformations of **1a** in solution (Figure 1.4), the conformation in the crystal is confined in an antiparallel arrangement, allowing for the cyclization. Femtosecond time-resolved diffraction experiments showed that an initial motion occurring upon excitation brings the central carbon atoms involved in the bond formation into close proximity [30].

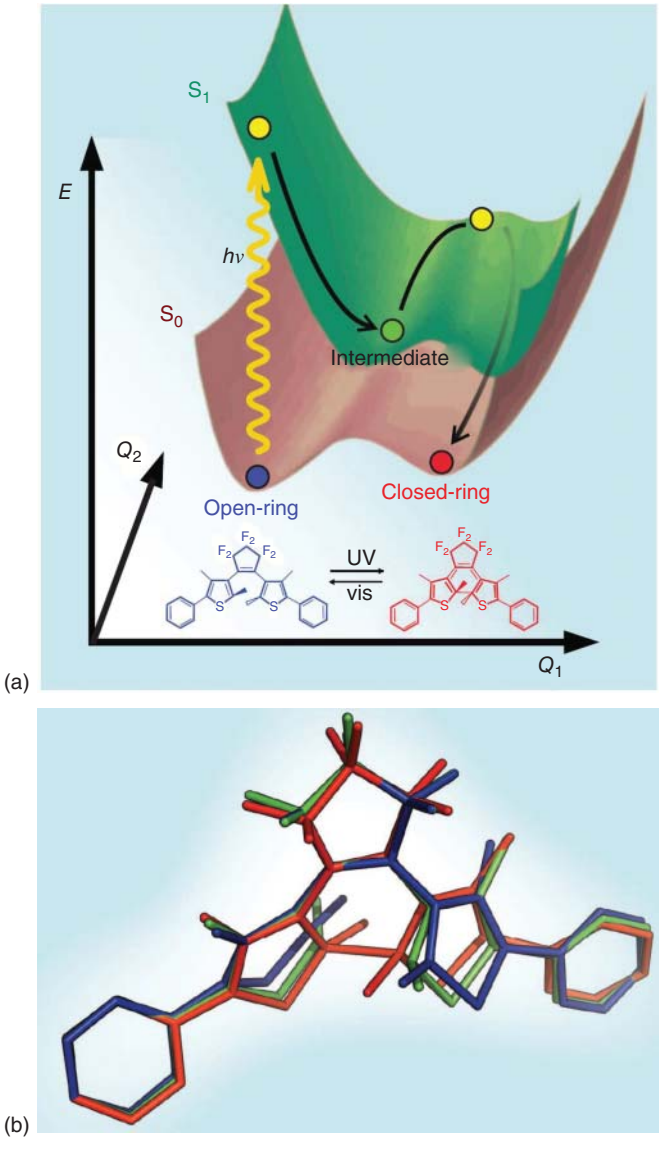


**Figure 1.4** (a) The primary motions involved in the photocyclization of **1a** in a single crystal studied by femtosecond time-resolved diffraction and a simplified reaction coordinate. (b) Motions determined by fs electron diffraction studies. Source: Reproduced by permission of Miller [30].

### 1.4.2 Azobenzene and Its Derivatives

Azobenzene and its derivatives are the most commonly used photoswitches, which undergo a reversible *E*–*Z* photoisomerization (Scheme 1.1) [31–36]. Both isomers possess weak ($n$,$\pi^*$; $S_0 \rightarrow S_1$) and strong ($\pi$,$\pi^*$; $S_0 \rightarrow S_2$) absorption bands. These transitions can be very close in energy in azobenzenes bearing electron-donating

substituents, and the π,π* state becomes the $S_0 \rightarrow S_1$ transition in push–pull systems. Differences in the absorption properties of (*E*)- and (*Z*)-azobenzene allow us to select the irradiation wavelength to obtain the (*Z*)-isomer preferentially, and the photostationary ratio (Eq. (1.2)) of the isomers can be affected by competing thermal $Z \rightarrow E$ processes. The forward and back isomerization quantum yields depend on the irradiation wavelength, the solvent, and the excited-state multiplicity [37].

Precise knowledge of the absorption spectra of both photoisomers is essential to choose the optimum wavelength for switching in either direction and to determine the quantum yields. A recent study [38] revealed that in all previous work, the reported spectrum of *E*-azobenzene had been contaminated by small amounts of the *Z*-isomer. For azobenzene in methanol solution the ratio $\varepsilon_E/\varepsilon_Z$ is the highest at 347 nm reaching 91, and the inverse ratio $\varepsilon_Z/\varepsilon_E$ is the highest at 413 nm reaching 3.3 (Figure 1.5) [39]. These wavelengths of irradiation provide the highest purity of the desired isomer. For complete photoswitching, these numbers should be ∞ and 0, respectively.

The rate constant for the *thermal* $Z \rightarrow E$ isomerization is $1.2 \times 10^{-5}$ $s^{-1}$ at 45 °C, so that essentially pure *E*-azobenzene is obtained by keeping a methanol solution in the dark at 45 °C for five days. At 25 °C, the rate constant amounts to $1.1 \times 10^{-6}$ $s^{-1}$ [39], which is sufficiently slow for many applications. The reaction enthalpy of $Z \rightarrow E$ isomerization in *n*-heptane was reported to be $\Delta H = \sim 48.9$ kJ $mol^{-1}$ [40]. Clearly, the properties of azobenzene fulfill many requirements for a P-type photoswitch. Several structure–property relationship studies helped to design azobenzene photoswitches that possess high *Z*-isomer stability, as complete photoswitching as possible, and bathochromically shifted spectra [31, 32]. For example, *para*-electron-donating substituents of azobenzene can accelerate this thermal back isomerization [41], whereas *ortho*-chloro [42], fluoro [43, 44], or methoxy [45] substituents slow it down.

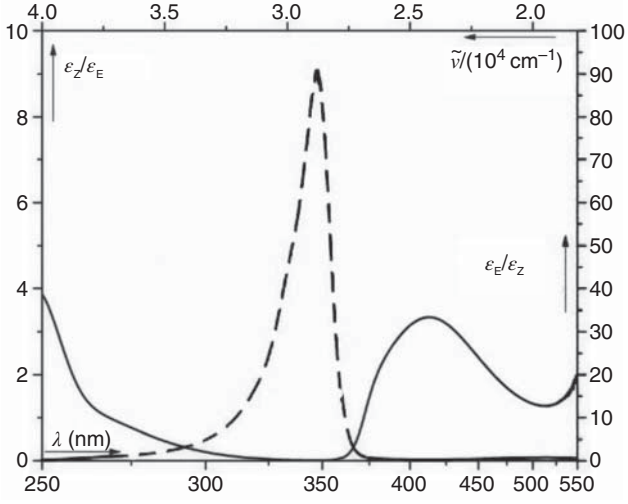


**Figure 1.5** The ratio of molar absorption coefficients $\varepsilon_Z/\varepsilon_E$ (solid line) and $\varepsilon_E/\varepsilon_Z$ (dashed line) of azobenzene in methanol. Source: Adapted from Vetráková et al. [38].

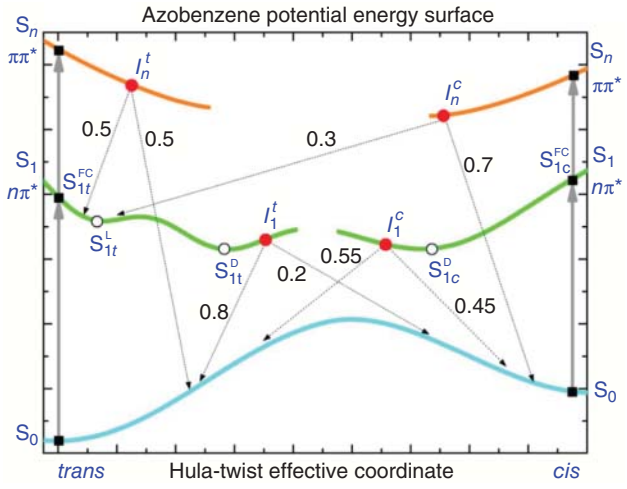


**Figure 1.6** Potential energy surface and relaxation/isomerization pathways of azobenzene [46]. Filled squares mark wavepacket positions upon $n,\pi^*$ ($S_1$) or $\pi,\pi^*$ ($S_n$) excitation, while open and filled circles show stationary points and conical intersections (*I*), respectively. Dotted arrows marked with yields indicate relaxation/isomerization via the intersections. Source: Reproduced by permission of Quick et al. [46].

The quantum yields of isomerization are less than unity and depend on the excitation wavelength, thus violating Kasha rule [37]; in methanol solution, they amount to $\Phi_{E\to Z}(280\,\text{nm}, \pi,\pi^*) = 0.16$, $\Phi_{Z\to E}(280\,\text{nm}, \pi,\pi^*) = 0.36$; $\Phi_{E\to Z}(313\,\text{nm}, \pi,\pi^*) = 0.14$, $\Phi_{Z\to E}(313\,\text{nm}, \pi,\pi^*) = 0.33$; $\Phi_{E\to Z}(405\,\text{nm}, \text{n},\pi^*) = 0.29$, $\Phi_{Z\to E}(405\,\text{nm}, n,\pi^*) = 0.45$ [39].

The excited-state evolution of azobenzene is summarized in the potential energy scheme (Figure 1.6). The photoisomerization was studied by broadband transient absorption spectroscopy [46]. Following $n,\pi^*$-excitation at 444 nm in acetonitrile, the $E\to Z$ reaction takes place with a lifetime of 16 ps, and the reverse reaction rate is bi-exponential with lifetimes of 0.1 and 1 ps. The 16-ps time constant of the former is attributed to the isomerization process that encounters a barrier of 12 kJ mol$^{-1}$, and not to vibrational cooling. Upon $\pi,\pi^*$-excitation, 50% of the population relaxes to an $S_1$ region, which is not accessible under n,$\pi^*$-excitation. The fast decay of the excited states prevents any side reactions, so that the switch can be operated indefinitely without noticeable fatigue.

Time-resolved Raman spectroscopy also provides valuable information about the dynamics of singlet excited states of azobenzene [31, 47]. With the probe wavelength at 410 nm in resonance with a transient absorption appearing after the $S_0\to S_2$ ($\pi,\pi^*$) photoexcitation, transient Raman bands assigned to the $S_1$ state are found. Its lifetime is solvent-dependent; the values of ~2.5 ps in ethylene glycol and ~1 ps in hexane were determined [48].

Nitrogen atoms of the N=N bond of azobenzene possess an in-plane lone electron pair in an n orbital involved in two limiting mechanisms of photoisomerization (rotation akin to that of simple alkenes or in-plane inversion) [10, 31]. A femtosecond

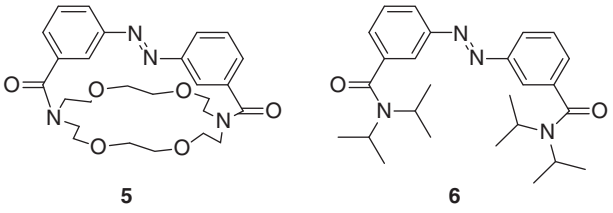

**Figure 1.7** Azobenzene derivatives **5** and **6**.

time-resolved fluorescence up-conversion spectroscopy of rotation-restricted **5** and rotation-free **6** *E*-azobenzene derivatives (Figure 1.7) revealed very similar fluorescence lifetimes [49]. Because **5** cannot isomerize by rotation about the central N=N bond, it was suggested that the interconversion occurs via the inversion mechanism.

## References


1 Dürr, H. and Bouas-Laurent, H. (2003). *Photochromism: Molecules and Systems*. Amsterdam: Elsevier Science.

2 Abdollahi, A., Roghani-Mamaqani, H., and Razavi, B. (2019). Stimuli-chromism of photoswitches in smart polymers: recent advances and applications as chemosensors. *Prog. Polym. Sci.* 98, 101149.

3 Boelke, J. and Hecht, S. (2019). Designing molecular photoswitches for soft materials applications. *Adv. Opt. Mater.* 7, 1900404.

4 Jia, S., Fong, W.K., Graham, B., and Boyd, B.J. (2018). Photoswitchable molecules in long-wavelength light-responsive drug delivery: from molecular design to applications. *Chem. Mater.* 30: 2873–2887.

5 Sun, C.L., Wang, C.X., and Boulatov, R. (2019). Applications of photoswitches in the storage of solar energy. *ChemPhotoChem* 3: 268–283.

6 Tian, Z.Y., Wu, W.W., and Li, A.D.Q. (2009). Photoswitchable fluorescent nanoparticles: preparation, properties and applications. *ChemPhysChem* 10: 2577–2591.

7 Zhou, X.X. and Lin, M.Z. (2013). Photoswitchable fluorescent proteins: ten years of colorful chemistry and exciting applications. *Curr. Opin. Chem. Biol.* 17: 682–690.

8 Broichhagen, J., Frank, J.A., and Trauner, D. (2015). A roadmap to success in photopharmacology. *Acc. Chem. Res.* 48: 1947–1960.

9 Morstein, J. and Trauner, D. (2019). New players in phototherapy: photopharmacology and bio-integrated optoelectronics. *Curr. Opin. Chem. Biol.* 50: 145–151.

10 Klan, P. and Wirz, J. (2009). *Photochemistry of Organic Compounds: From Concepts to Practice*, 1st ed. Chichester: Wiley.

11 Bléger, D. and Hecht, S. (2015). Visible-light-activated molecular switches. *Angew. Chem. Int. Ed.* 54: 11338–11349.

12 Kobayashi, Y., Mutoh, K., and Abe, J. (2018). Stepwise two-photon absorption processes utilizing photochromic reactions. *J. Photochem. Photobiol. C* 34: 2–28.

**13** Konig, K. (2000). Multiphoton microscopy in life sciences. *J. Microsc.* 200: 83–104.

**14** Delbaere, S. and Vermeersch, G. (2008). NMR spectroscopy applied to photochromism investigations. *J. Photochem. Photobiol. C* 9: 61–80.

**15** Kumpulainen, T., Lang, B., Rosspeintner, A., and Vauthey, E. (2017). Ultrafast elementary photochemical processes of organic molecules in liquid solution. *Chem. Rev.* 117: 10826–10939.

**16** Irie, M., Fukaminato, T., Matsuda, K., and Kobatake, S. (2014). Photochromism of diarylethene molecules and crystals: memories, switches, and actuators. *Chem. Rev.* 114: 12174–12277.

**17** Irie, M. (2000). Diarylethenes for memories and switches. *Chem. Rev.* 100: 1685–1716.

**18** Waldeck, D.H. (1991). Photoisomerization dynamics of stilbenes. *Chem. Rev.* 91: 415–436.

**19** Laarhoven, W.H. (1983). Photochemical cyclizations and intramolecular cycloadditions of conjugated arylolefins. Part I: photocyclization with dehydrogenation. *Recl. Trav. Chim. Pays-Bas* 102: 185–204.

**20** Irie, M., Lifka, T., Uchida, K. et al. (1999). Fatigue resistant properties of photochromic dithienylethenes: by-product formation. *Chem. Commun.* 747–750.

**21** Ward, C.L. and Elles, C.G. (2014). Cycloreversion dynamics of a photochromic molecular switch via one-photon and sequential two-photon excitation. *J. Phys. Chem. A* 118: 10011–10019.

**22** Irie, M., Sakemura, K., Okinaka, M., and Uchida, K. (1995). Photochromism of dithienylethenes with electron-donating substituents. *J. Org. Chem.* 60: 8305–8309.

**23** Uchida, K., Nakayama, Y., and Irie, M. (1990). Thermally irreversible photochromic systems. reversible photocyclization of 1,2-bis(benzo[*b*]thiophen-3-yl) ethene derivatives. *Bull. Chem. Soc. Jpn.* 63: 1311–1315.

**24** Tamai, N. and Miyasaka, H. (2000). Ultrafast dynamics of photochromic systems. *Chem. Rev.* 100: 1875–1890.

**25** Hania, P.R., Telesca, R., Lucas, L.N. et al. (2002). An optical and theoretical investigation of the ultrafast dynamics of a bisthienylethene-based photochromic switch. *J. Phys. Chem. A* 106: 8498–8507.

**26** Ward, C.L. and Elles, C.G. (2012). Controlling the excited-state reaction dynamics of a photochromic molecular switch with sequential two-photon excitation. *J. Phys. Chem. Lett.* 3: 2995–3000.

**27** Okabe, C., Nakabayashi, T., Nishi, N. et al. (2003). Picosecond time-resolved stokes and anti-stokes Raman studies on the photochromic reactions of diarylethene derivatives. *J. Phys. Chem. A* 107: 5384–5390.

**28** Jean-Ruel, H., Cooney, R.R., Gao, M. et al. (2011). Femtosecond dynamics of the ring closing process of diarylethene: a case study of electrocyclic reactions in photochromic single crystals. *J. Phys. Chem. A* 115: 13158–13168.

**29** Jean-Ruel, H., Gao, M., Kochman, M.A. et al. (2013). Ring-closing reaction in diarylethene captured by femtosecond electron crystallography. *J. Phys. Chem. B* 117: 15894–15902.

**30** Miller, R.J.D. (2014). Femtosecond crystallography with ultrabright electrons and X-rays: capturing chemistry in action. *Science* 343: 1108.

**31** Bandara, H.M.D. and Burdette, S.C. (2012). Photoisomerization in different classes of azobenzene. *Chem. Soc. Rev.* 41: 1809–1825.

**32** Dong, M., Babalhavaeji, A., Samanta, S. et al. (2015). Red-shifting azobenzene photoswitches for in vivo use. *Acc. Chem. Res.* 48: 2662–2670.

**33** Beharry, A.A. and Woolley, G.A. (2011). Azobenzene photoswitches for biomolecules. *Chem. Soc. Rev.* 40: 4422–4437.

**34** Natansohn, A. and Rochon, P. (2002). Photoinduced motions in azo-containing polymers. *Chem. Rev.* 102: 4139–4176.

**35** Merino, E. and Ribagorda, M. (2012). Control over molecular motion using the *cis-trans* photoisomerization of the azo group. *Beilstein J. Org. Chem.* 8: 1071–1090.

**36** Calbo, J., Thawani, A.R., Gibson, R.S.L. et al. (2019). A combinatorial approach to improving the performance of azoarene photoswitches. *Beilstein J. Org. Chem.* 15: 2753–2764.

**37** Bortolus, P. and Monti, S. (1979). *Cis-trans* photoisomerization of azobenzene. Solvent and triplet donors effects. *J. Phys. Chem.* 83: 648–652.

**38** Vetráková, Ľ., Ladányi, V., Al Anshori, J. et al. (2017). The absorption spectrum of *cis*-azobenzene. *Photochem. Photobiol. Sci.* 16: 1749–1756.

**39** Ladányi, V., Dvořák, P., Al Anshori, J. et al. (2017). Azobenzene photoisomerization quantum yields in methanol redetermined. *Photochem. Photobiol. Sci.* 16: 1757–1761.

**40** Adamson, A.W., Vogler, A., Kunkely, H., and Wachter, R. (1978). Photocalorimetry. Enthalpies of photolysis of *trans*-azobenzene, ferrioxalate and cobaltioxalate ions, chromium hexacarbonyl, and dirhenium decarbonyl. *J. Am. Chem. Soc.* 100: 1298–1300.

**41** Bahamonde, M.I., Taura, J., Paoletta, S. et al. (2014). Photomodulation of G protein-coupled adenosine receptors by a novel light-switchable ligand. *Bioconjugate Chem.* 25: 1847–1854.

**42** Konrad, D.B., Frank, J.A., and Trauner, D. (2016). Synthesis of redshifted azobenzene photoswitches by late-stage functionalization. *Chem. Eur. J.* 22: 4364–4368.

**43** Hansen, M.J., Lerch, M.M., Szymanski, W., and Feringa, B.L. (2016). Direct and versatile synthesis of red-shifted azobenzenes. *Angew. Chem. Int. Ed.* 55: 13514–13518.

**44** Bléger, D., Schwarz, J., Brouwer, A.M., and Hecht, S. (2012). *o*-Fluoroazobenzenes as readily synthesized photoswitches offering nearly quantitative two-way isomerization with visible light. *J. Am. Chem. Soc.* 134: 20597–20600.

**45** Beharry, A.A., Sadovski, O., and Woolley, G.A. (2011). Azobenzene photoswitching without ultraviolet light. *J. Am. Chem. Soc.* 133: 19684–19687.

**46** Quick, M., Dobryakov, A.L., Gerecke, M. et al. (2014). Photoisomerization dynamics and pathways of *trans*- and *cis*-azobenzene in solution from broadband femtosecond spectroscopies and calculations. *J. Phys. Chem. B* 118: 8756–8771.

**47** Fujino, T. and Tahara, T. (2000). Picosecond time-resolved Raman study of trans-azobenzene. *J. Phys. Chem. A* 104: 4203–4210.

**48** Lednev, I.K., Ye, T.Q., Matousek, P. et al. (1998). Femtosecond time-resolved UV-visible absorption spectroscopy of *trans*-azobenzene: dependence on excitation wavelength. *Chem. Phys. Lett.* 290: 68–74.

**49** Pancur, T., Renth, F., Temps, F. et al. (2005). Femtosecond fluorescence upconversion spectroscopy of a rotation-restricted azobenzene after excitation to the $S_1$ state. *Phys. Chem. Chem. Phys.* 7: 1985–1989.

# 2 Computational Methods and Photochromism

Martial Boggio-Pasqua

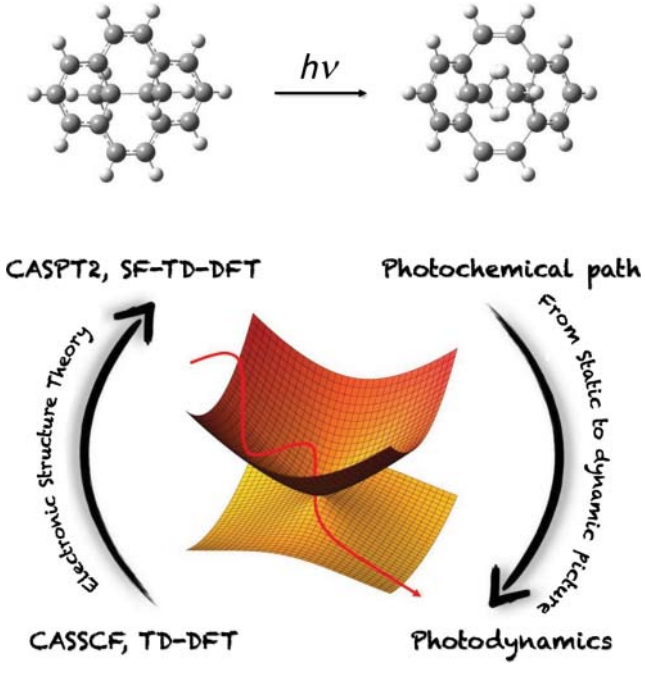


**Characteristic Features**

Computational photochemistry at work in the theoretical study of the photoswitching mechanisms of photochromic compounds. Illustration of dihydroazulene and dihydropyrene photochromism.

**Key References**

Boggio-Pasqua, M., Bearpark, M.J., Hunt, P.A. et al. (2002). Dihydroazulene/vinylheptafulvene photochromism: a model for one-way photochemistry via a conical intersection. *J. Am. Chem. Soc.* 124: 1456–1470.

Boggio-Pasqua, M., Bearpark, M.J., and Robb, M.A. (2007). Towards a mechanistic understanding of the photochromism of dimethyldihydropyrenes. *J. Org. Chem.* 72: 4497–4503.

# 2

# Computational Methods and Photochromism

*Martial Boggio-Pasqua*

*CNRS et Université Toulouse III – Paul Sabatier, LCPQ UMR 5626, 118 route de Narbonne, 31062, Toulouse, France*

## 2.1 Introduction

In the field of photochemistry, photochromism represents an increasing area of research because of its actual and potential applications [1–3]. It can be defined as a reversible phototransformation of a molecule between two forms having different spectral properties. Photochromic compounds thus convert photonic energy into chemical energy on an ultrafast timescale. The change in electronic and molecular structures following light irradiation results in a modification of physical properties, which forms the basis of many applications in biology [4], nano, and material sciences [5–13].

The vast majority of reported photochromic compounds relies on organic molecules undergoing photoinduced electrocyclic reactions, cycloadditions, *cis-trans* (*E*/*Z*) isomerizations, intramolecular hydrogen or group transfers, dissociation processes, or electron transfers (redox) [1]. Moreover, transition metal complexes have also been designed to display photochromic properties. These systems are often based on linkage isomerizations between the metal center and ambidentate ligands (e.g. nitrosyls [14, 15] and sulfoxides [16, 17]).

Given the importance and many possible applications of photoswitches to which photochromic compounds belong, a large number of computational studies have been carried out to (i) rationalize experimental observations, (ii) unravel the key steps of the underlying reaction mechanism at the origin of the photochromism, (iii) predict the properties and help in the design of new photochromic systems to be synthesized.

Computational photochemistry [18–20] is an essential tool for rationalizing the photochemical behavior of such compounds. While early interpretations of photochemical processes were based on vertical excitations at the Franck–Condon (FC) geometry, advances in electronic structures methods and in computational tools have allowed the exploration of other regions of the complex multidimensional potential energy surfaces (PESs) and the characterization of electronically

*Molecular Photoswitches: Chemistry, Properties, and Applications*,
First Edition. Edited by Zbigniew L. Pianowski.

excited-state reaction paths. The general strategy often relies on a combination of quantum chemistry calculations and nonadiabatic dynamics simulations in order to characterize the main photochemical pathways connecting the initial excited-state reactants to the final ground-state photoproducts and to simulate the photodynamics of the system. This synergy between accurate and global static calculations and either quantum or semiclassical nonadiabatic dynamics simulations has allowed major breakthroughs in the understanding of photochemical and photophysical processes, in particular in the field of photochromism. The purpose of this chapter is to provide a general introduction to the computational methods and strategies used in the theoretical studies of such compounds and to give some illustrations with notable examples in which computations were used to explain nonintuitive experimental observations.

## 2.2 Basics of Computational Photochemistry

### 2.2.1 Electronic Structure Methods

To describe the ground and excited electronic states involved in the photodynamics of a system, a quantum mechanical method that provides a balanced description of all these states is required. The method needs to describe the electronic states consistently along the entire photochemical pathway (e.g. along the photoisomerization pathway in the context of electrocyclic reactions as illustrated below), meaning that the important electronic rearrangements taking place in all the states considered must be accounted for along the reaction path. In addition, a method with analytical energy gradients available is also required to explore any photochemical process, whether statically through geometry optimizations and minimum energy path (MEP) calculations or dynamically through ab initio nonadiabatic molecular dynamics (NAMD) simulations. Because of the important nonadiabatic effects often involved in the excited-state dynamics, particularly around conical intersections (CoIns) [21], it is also desirable to use a method that allows a proper description of the electronic state couplings in the corresponding regions of the PESs.

For all these reasons, multiconfigurational wavefunction-based methods, such as the popular complete active space self-consistent field (CASSCF) method, have often been used to compute excited-state PESs or to investigate ab initio NAMD on-the-fly of photochromic compounds. Within the CASSCF framework, one chooses a set of active orbitals over which the active electrons can be distributed to generate all the electronic configurations, as in a configuration interaction (CI) calculation. Both CI coefficients and orbitals are optimized for a given (set of) state(s). The most critical feature of this kind of calculations is the choice of the active electrons and orbitals, known as the active space. A judicious choice of active space has to be selected [22] in order to describe all the electronic rearrangements that will occur during the photoisomerization of the photochromic compound under investigation. It allows a reliable description of the static (or non-dynamical) electron correlation. However, to obtain accurate PESs, post-CASSCF treatments

are usually necessary to recover the dynamic electron correlation missing at the CASSCF level. This is the case in the complete active space second-order perturbation theory (CASPT2), which has become the post-CASSCF method of reference widely employed in photochemistry today [23, 24], including for the studies of photochromic compounds. To obtain useful mechanistic information in photochemical studies, the CASSCF approximation is often sufficient. However, if quantitative agreement with experiment is sought or if CASSCF does not provide a balanced description of the excited states involved because of the lack of dynamic electron correlation, then CASPT2 becomes necessary.

However, both CASSCF and CASPT2 approaches rapidly become prohibitively expensive with the system and active space sizes. Although promising approaches to reduce the scaling of such methods have been developed recently based most notably on the density matrix renormalization group (DMRG) [25], these methods are not widely applicable yet to investigate photochemical mechanisms because of the lack of analytical energy gradients. Thus, alternative approaches capable of computing excited-state energies and their associated gradients need to be used when the system size forbids the use of CASSCF and CASPT2. This is the case of several efficient single-reference methods [26] such as time-dependent density functional theory (TD-DFT), approximate second-order coupled-cluster (CC2), and algebraic diagrammatic construction (ADC) scheme. Among these, TD-DFT is one of the most popular approaches to study excited states of medium to large-size systems, including in the context of the photoisomerization of photochromic compounds. Unlike the CASSCF and CASPT2 approaches, it is simple and straightforward to use once an appropriate functional has been chosen for the considered system. It can be efficiently used to study NAMD on the fly [27]. However, it suffers from deficiencies of the underlying mono-configurational description of the ground state in regions of bond breaking and bond formation, and it is known to encounter severe problems in describing valence states of molecules exhibiting extended $\pi$ systems, doubly excited states, charge-transfer excited states [26], and CoIns between ground and excited states [28, 29]. Triplet state instabilities [30] are also a serious issue when such states are involved in the photochemical process. For all these reasons, TD-DFT may only give qualitative information on the photoisomerization mechanisms of photochromic compounds. Note that developments in TD-DFT are ongoing to solve these issues and to make TD-DFT truly reliable in the context of computational photochemistry [31, 32].

In addition, approaches based on semiempirical configuration interaction methods (e.g. FOMO/CI [33], GUGA [34], OM2/MRCI [35], MMVB [36–38]) have also been developed specifically for excited-state calculations and for simulating photochemical processes taking place through CoIns. Such methods neglect many of the two-electron integrals computed in ab initio calculations and use parameters for most of the one- and two-electron integrals that cannot be neglected. These low-cost methods can be considered as an alternative to the ab initio methods described above for studies of photochemical processes in large-size molecules or when a large number of trajectories are necessary to simulate the dynamics of the system. However, these methods require transferable, large-scale parameterization

over many elements to obtain a single-molecule-independent set of parameters. Moreover, it is often necessary to re-optimize these parameters to generate a molecule-specific set of parameters allowing description of the excited-state critical structures (stationary points and CoIns) on the PESs to make them truly reliable for modeling photochemical processes. In such cases, the method becomes cumbersome in practice and unsatisfactory from a conceptual point of view.

For more details about the various electronic structure methods available in computational photochemistry and their capabilities, the interested reader can consult a number of excellent review articles and books dedicated to this topic [20, 28, 39–41].

### 2.2.2 Photochemical Pathway and Conical Intersections

To understand the fate of photoexcited molecules such as in the case of photochromic compounds, it is not only necessary to understand their excited-state properties but also to determine how the system will evolve chemically in terms of bond making and bond breaking in these excited states. Thus, it is crucial to understand the reaction pathway describing the passage from the excited-state reactants to the final photoproducts evolving along the PESs of the photochemically relevant electronic states (see Figure 2.1 for an illustration involving one excited state). This reaction path is called *photochemical reaction path* or *photochemical pathway*. It is determined by following the detailed relaxation and reaction paths of the molecule along the relevant PESs from the Franck-Condon (FC) point (i.e. vertically excited geometry) to the ground state. Static calculations are performed to investigate the topology of the PESs. It requires finding all the relevant critical structures (minima, saddle points, barriers, surface crossings) involved along the reaction path and

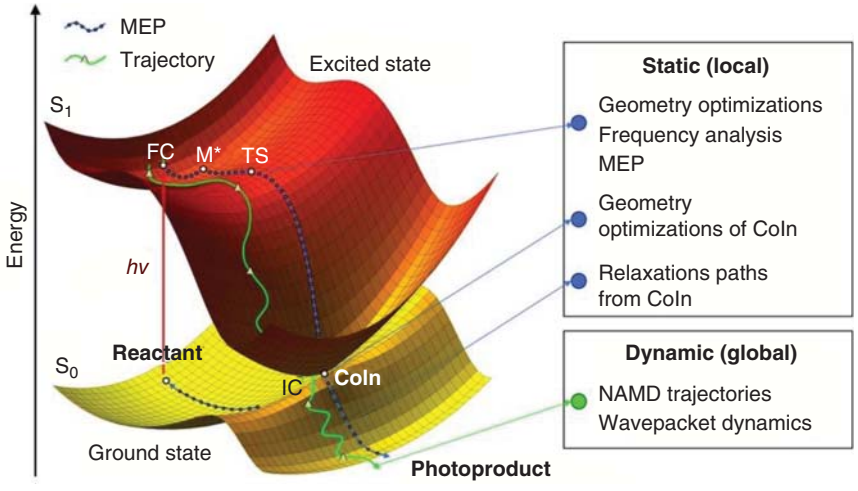


**Figure 2.1** Illustration of the photoreaction path modeling with static and dynamic approaches for a two-state photochemical reaction. FC, Franck–Condon point; M*, excited-state minimum; TS, transition state; CoIn, conical intersection; IC, internal conversion; MEP, minimum energy path.

understanding how all these critical points are interconnected on the PESs. This interconnection is often determined by MEP calculations or sometimes by exploring potential energy profiles using linearly interpolated geometries between optimized structures. Once the potential energy landscape for all the relevant electronic states is understood, very detailed mechanistic information can be derived on the photochemistry of the system such as the identification of the transient species involved, the radiative and nonradiative deactivation pathways, the barrierless or activated nature of the photochemical reaction, and its feasibility in terms of forming new photoproducts (photochemical paths) against the regeneration of the initial ground-state species (photophysical paths).

It is important to state at this stage that the photochemical reaction path requires computing relaxation pathways in the excited states up to the eventual PES crossings before exploring what are the different relaxation paths arising from such crossings down to the ground state. One of the common pitfalls is to try to deduce photoinduced reaction mechanisms based solely on the excited-state potential energy profiles computed along the ground-state (thermal) reaction paths. While these profiles can be interesting as an initial exploration of the excited-state PESs and may sometimes provide indications of possible PES crossings, they do not describe the correct reaction path in the excited states, as the nuclei feel an excited-state potential after the system is photoexcited. It is therefore crucial to follow the excited-state path along which the system is evolving, otherwise important mechanistic features of the photochemical reaction may be completely overlooked.

The information obtained from this static approach is mainly structural, i.e. the computed photochemical path describes the motion of a vibrationally cold molecule moving with infinitesimal momenta. While this path does not represent any *real* trajectory, it allows for a qualitative understanding of different experimental data such as excited-state lifetimes, nature of the photoproducts formed, and quantum yields. Beyond the static approach, detailed information about the time-evolution of a molecule after photoexcitation can be obtained from nonadiabatic dynamics simulations. Dynamics studies become all the more important when the system does not follow MEPs. In such cases, regions of the PESs far from the computed static photochemical pathway may become important, and mechanistic pictures deduced solely from the topological investigation of the PESs may be erroneous. Moreover, dynamics simulations can bring semiquantitative information on important experimental data such as excited-state lifetimes and quantum yields provided that a sufficient sampling of the system can be achieved. Thus, calculations of PESs and characterization of the static photochemical pathway are often complemented by dynamics simulations to gain a more complete understanding of the molecular photochemistry.

These simulations can be performed using two distinct strategies. The first and most conventional method is to simulate the direct dynamics of the system using semiclassical approaches such as ab initio NAMD by computing the potential energies and couplings on the fly along trajectories. This method is largely used in photochromic compounds due to the large number of internal degrees of freedom that needs to be handled. The second approach resorts to more accurate and

computationally demanding grid-based quantum wavepacket dynamics [42] such as in the multi-configuration time-dependent Hartree method [43] (MCTDH), which requires that the PESs and couplings are modeled along the most relevant (photochemically active) internal degrees of freedom using a vibronic-coupling Hamiltonian. This approach is much more challenging to use in the context of photochromic compounds, but the MCTDH dynamics study of benzopyran taken as a model compound for photochromic spiropyrans is a beautiful example [44].

Over the last three decades, it has become more and more evident that photochemical pathways were evolving through CoIns, which correspond to PES crossings responsible for efficient nonradiative decay of excited-state species. While first thought as an exception, it is now very well established that CoIns are central mechanistic features in organic photochemistry [45–47]. This is particularly the case in the photoswitching mechanisms of photochromic systems, as CoIns have been identified along the photoisomerization paths of azobenzenes [48], spiropyrans [49], aromatic Schiff bases [50], dihydroazulenes [51], dithienylethenes [52], chromenes [53], oxazines [54], dihydropyrenes [55], dihydronaphthalene [56], and fulgides [57], to cite a few examples.

Thus, CoIns need to be located as they act as funnels for electronic radiationless transitions between electronic states. In an analogy to transition states, which are bottleneck structures separating the reactant from the product in a ground-state reaction, CoIns form a bottleneck for electronic relaxation in a photochemical reaction. The main difference is that CoIns act as bifurcations leading possibly to different products, and they are not isolated crossing points on the PESs but are part of extended crossing seams [58–60]. CoIns are characterized by the two vectors (nuclear vibrations) that lift the degeneracy at first order: the gradient difference ($\mathbf{x}_1$) and the interstate coupling ($\mathbf{x}_2$) vectors, which form the so-called *branching space*. As a consequence, the two crossing PESs intersect as a double cone if they are plotted in the two dimensions of the branching space vectors. For a molecule with $N^{\text{int}}$ internal degrees of freedom, it is possible to find $N^{\text{int}} - 2$ coordinates orthogonal to the branching space, which preserve the degeneracy at first order. This $(N^{\text{int}} - 2)$-dimensional space is a hyperline of degeneracy and is also called *intersection space* or *intersection seam*. This seam will then appear as a crossing line if the two intersecting PESs are plotted along one branching space coordinate and one intersection space coordinate.

A first consequence of this intrinsic multidimensional nature of a CoIn is that it makes the state crossings all the more accessible during the course of the photochemical reaction. Moreover, this high dimensionality can be crucially important, as different regions of the associated extended crossing seam can be sampled by the system during excited-state vibrational relaxations, and these regions can potentially lead to different products. Thus, the search for the most relevant photochemical funnels aims at finding minimum energy crossing points (also called minimum energy CoIns) within the crossing seams. But one has to keep in mind that energetically accessible crossing segments away from such minima can also play a major role in the outcome of a photochemical reaction.

## 2.3 Applications: Photoswitching Mechanisms of Photochromic Compounds

In this section, we will illustrate the insightful potential of computational photochemistry with two notable examples of photochromic systems for which computations were used to explain nonintuitive experimental observations. For each system, the main experimental observations will be summarized, the computational method succinctly presented, and the main results deduced from the calculations allowing for a detailed interpretation of their photoswitching mechanism will be described.

### 2.3.1 Dihydroazulene Photochromism

The dihydroazulene (DHA)/vinylheptafulvene (VHF) photochromic couple (Scheme 2.1) has attracted a lot of interest because of its applications as photoswitch and thermoswitch. The photoinduced ring-opening reaction has a very high quantum yield (close to unity) in solution at room temperature, and the VHF photoproduct is formed on an ultrafast picosecond timescale, suggesting the presence of a CoIn [61]. Surprisingly, whereas DHA and VHF absorb in different spectral regions with no spectral overlap, irradiation of VHF in its first excited state does not produce DHA. The cyclization reaction can be achieved thermally or by two-photon excitation [62]. Moreover, no fluorescence is observed from VHF even at low temperature in contrast to DHA [63]. We will show in the following that most of these experimental observations can be explained by a CoIn between the $S_1$ and $S_0$ electronic states [49].

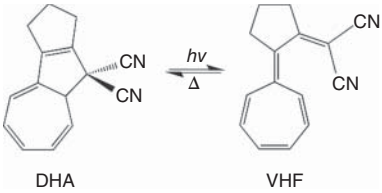


**Scheme 2.1** The dihydroazulene (DHA)/vinylheptafulvene (VHF) photochromic system.

The reference theoretical study of the photoswitching mechanism of this system was performed two decades ago [51]. It relied on the static and dynamical investigations of various model systems at the CASSCF level of theory. To account for the electronic reorganization taking place along the photoisomerization, it is necessary to include all the valence π orbitals of DHA plus the pair of σ, σ* orbitals describing the σ-bond that breaks during the ring-opening reaction. This active space naturally correlates with the full valence π system of VHF. It is important to note that CASPT2 calculations on such systems were not feasible at that time but would be required for accurate energetics of the PESs. However, the CASSCF method is sufficient to

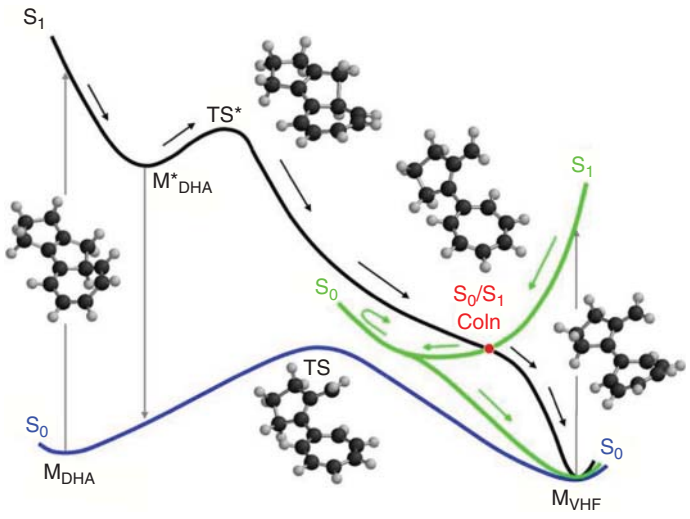


**Figure 2.2** Schematic $S_0$ and $S_1$ potential energy profiles for a model DHA/VHF system. Gray vertical arrows indicate absorption and emission processes. The black and green curves show the nonadiabatic DHA→VHF and VHF→VHF reaction pathways, respectively. Source: Adapted from Boggio-Pasqua et al. [51].

provide the correct topology of the PESs and thus the central mechanistic features for this system.

Based on this computational methodology, the $S_0$ and $S_1$ potential energy profiles obtained along the photochemical reaction path are shown in Figure 2.2 along with the main relaxation pathways. Upon photoexcitation to the $S_1$ state of DHA, the system relaxes to a local $S_1$ DHA biradicaloid minimum ($M^*_{DHA}$) following a complete inversion of single and double bonds within the π-system. Then, upon stretching the σ-bond that breaks to produce VHF, the system reaches a transition state TS* (about 10 kcal mol$^{-1}$ above $M^*_{DHA}$ but more than 20 kcal mol$^{-1}$ below the $S_1$ Franck–Condon energy) characterized by a transition vector dominated by an adiabatic σ-bond breaking. Beyond the transition structure, the system proceeds downhill to a conical intersection, $S_0/S_1$ CoIn. The associated minimum energy CoIn corresponds to the lowest energy point on the $S_1$ PES (over 50 kcal mol$^{-1}$ below $M^*_{DHA}$). This crossing presents a VHF-like structure, i.e. the 5-membered ring is opened, and at this funnel, efficient radiationless decay to $S_0$ will take place producing the VHF isomer ($M_{VHF}$). This picture is consistent with the observation of fluorescence following photoexcitation of DHA, as there is a local DHA $S_1$ minimum ($M^*_{DHA}$). The DHA→VHF isomerization quantum yield increases, at the expense of the emission efficiency, when the temperature is increased. This is consistent with the activated process to reach the funnel for photoisomerization.

In fact, the MEP calculated from TS* in the VHF direction does not actually reach the minimum energy $S_0/S_1$ CoIn itself, the lowest-energy point optimized on the intersection. Instead, the MEP terminates at a higher energy point on the intersection seam, denoted as $S_0/S_1$ CoIn*, which is over 30 kcal mol$^{-1}$ above the minimum

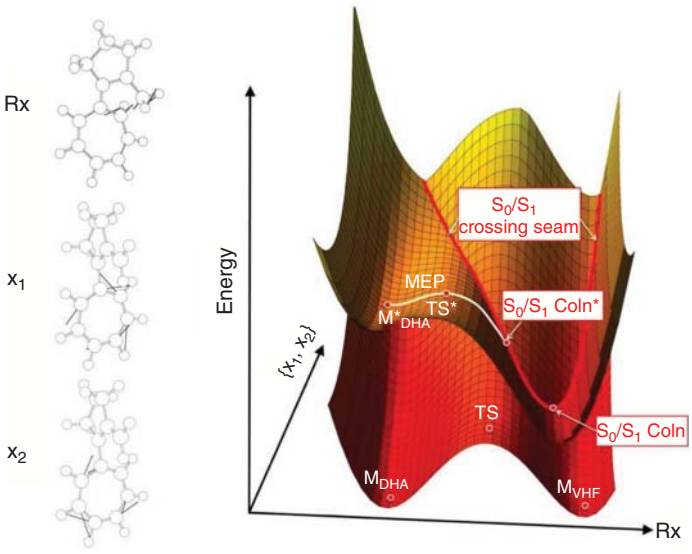


**Figure 2.3** $S_0$ and $S_1$ potential energy landscapes along the reaction path (Rx) corresponding to the DHA→VHF photoisomerization. The MEP computed at TS* is indicated by the white line and shows how it is intercepted by the intersection seam at the structure $S_0/S_1$ CoIn*, lying much higher in energy than the minimum energy conical intersection, $S_0/S_1$ CoIn. The relevant coordinates for mechanistic photochemistry are shown on the left for a DHA/VHF model system: the reaction coordinate Rx is orthogonal to the branching space.

energy CoIn (Figure 2.3). This is made possible because the ring-opening reaction coordinate involves mainly a C—C σ-bond breaking, while the branching space coordinates $\{\mathbf{x}_1, \mathbf{x}_2\}$ at the minimum energy $S_0/S_1$ CoIn are dominated by rearrangements of the seven-membered ring. Thus, the crossing seam appears as a line of degeneracy along the DHA→VHF reaction path, as illustrated in Figure 2.3. In addition to its higher energy, $S_0/S_1$ CoIn* is characterized by a shorter C—C bond distance for the broken σ-bond of 2.45 Å compared with the 3.45 Å C—C bond distance at the minimum energy $S_0/S_1$ CoIn. This confirms that the MEP is intercepted by the crossing seam well before reaching the minimum energy CoIn. Analysis of the decay routes at $S_0/S_1$ CoIn* shows that the system may return to $M_{DHA}$ or form $M_{VHF}$ but, for inertial reasons, product formation will be highly favored over reactant regeneration.

Upon photoexcitation to the $S_1$ state of VHF, the system relaxes directly toward the minimum energy $S_0/S_1$ CoIn (green arrows in Figure 2.2). The relaxation coordinate corresponds to the gradient difference $\mathbf{x}_1$ vector characterizing this crossing. Consequently, the MEP on $S_1$ is naturally driven to the minimum energy $S_0/S_1$ CoIn. The topological feature on $S_0$ around this CoIn only allows the system to reform VHF. After nonradiative decay to $S_0$ at the minimum energy CoIn, the system encounters a steep rise in the ground-state energy (Figure 2.2), and molecules approaching the minimum energy $S_0/S_1$ CoIn from the VHF side will therefore be reflected on this barrier back toward $M_{VHF}$. These particular topological features around the CoIn account for the high photostability of VHF. Moreover, the presence of the minimum

energy $S_0/S_1$ CoIn as the lowest critical point on the $S_1$ PES in the VHF region also explains the lack of fluorescence upon excitation of VHF.

Both the highly efficient DHA→VHF photoisomerization and high VHF photostability were confirmed by on-the-fly CASSCF [51] and MMVB [37] molecular dynamics. All the trajectories performed from TS* ended up producing VHF, while none of the trajectories started from VHF produced DHA. In addition, these dynamics simulations also illustrated the access of the higher energy part of the crossing seam in the region of $S_0/S_1$ CoIn* during the DHA→VHF photoisomerization.

### 2.3.2 Dihydropyrene Photochromism

Dihydropyrenes (DHPs) belong to a well-known class of photochromic compounds: the diarylethene family, whose most famous representative is the dithienylethene (DTE) photochrome [8]. However, in contrast to DTEs, DHPs have the particularity to be negative photochromes, which makes them highly interesting because the thermally stable isomer is the more colored one, while positive photochromes such as DTEs have the more stable form colorless. The colored form, associated with the highly conjugated closed-ring DHP isomer, bleaches upon exposure to visible light corresponding to the formation of the less aromatic open-ring cyclophanediene (CPD) isomer and returns to the DHP isomer upon exposure to UV light or thermally (Scheme 2.2) [64, 65]. However, the low DHP to CPD isomerization quantum yields combined with a fast rate of thermal back reaction in these compounds were representing an obstacle for their use as efficient photochromic systems.

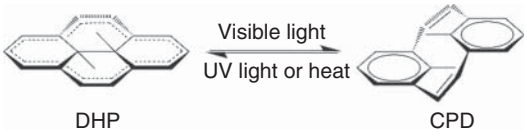


**Scheme 2.2** The dimethyldihydropyrene (DHP)/cyclophanediene (CPD) photochromic system.

The reasons behind this lack of efficiency were first rationalized based on a CASSCF/CASPT2 ab initio study of the reference compound shown in Scheme 2.2 back in 2007 [55]. Unlike the DHA/VHF system presented above, which can be approximated as a two-electronic-state problem, the DHP/CPD is much more challenging because several coupled excited states of different nature (covalent/ionic, singly-/doubly-excited) are involved in the photoswitching mechanism. In addition, the natural active space to describe this electrocyclic reaction requires to include the valence $\pi$ orbitals of the annulene ring at the periphery of DHP plus the pair of $\sigma$, $\sigma^*$ orbitals describing the $\sigma$-transannular bond that breaks during the ring-opening reaction. This amounts to distributing 16 electrons in 16 orbitals for this unsubstituted DHP, representing a formidable task for computing CASSCF and CASPT2 PESs. An additional challenge arises from the difficulty to describe simultaneously covalent and zwitterionic excited states for which the dynamic electron correlation

is very different. In such a particular case, the CASSCF method fails to provide accurate relative energies between these states, and the CASPT2 level is necessary to obtain the right order of the states [66]. Thus, this system falls in the case where both static and dynamic electron correlations need to be described accurately between the various electronic states. The CASSCF is then only useful to optimize structures and to provide approximate adiabatic relaxation pathways assuming that these are correctly described without accurate description of the dynamic electron correlation. These relaxation pathways cannot be computed with standard MEP calculations because of their prohibitive computational cost at the CASSCF(16,16) level. More approximate paths based on linearly interpolated geometries in internal coordinates between optimized structures had to be used instead.

Following such a computational strategy, the photoisomerization path was derived from the static exploration of the PESs as represented in Figure 2.4. On this figure, only the most relevant excited states are shown. These states are (i) the $S_1(L_b)$ covalent state described as a combination of the HOMO–1→LUMO and HOMO→LUMO+1 excitations, (ii) the $S_2(L_a)$ zwitterionic state dominated by the HOMO→LUMO transition, and (iii) the $S_6(\cdot\cdot)$ biradicaloid state described by a mixture of singly and doubly excited configurations and dominated upon vibrational relaxation by the ground-state configuration and the $HOMO^2 \rightarrow LUMO^2$ excitation. Irradiation of the unsubstituted DHP (Scheme 2.2) in its first singlet excited state $S_1(L_b)$ does not lead to CPD formation, whereas photoisomerization is observed from the $S_2(L_a)$ state upon irradiation at 480 nm in aerated cyclohexane with a ring-opening quantum yield of only 0.006 [65]. This very low ring-opening quantum yield was rationalized theoretically by the efficient depopulation of the initially excited $S_2(L_a)$ photoactive state (i.e. state that leads to photoisomerization) to the lower $S_1(L_b)$ unreactive state (i.e. state that does not lead to photoisomerization). This is illustrated by the yellow path in Figure 2.4 showing the nonradiative decay from $S_2(L_a)$ to $S_1(L_b)$ via a $S_1/S_2$ CoIn. While vibrational relaxation on the $S_2$ state leads to a CPD precursor (CPD*; Figure 2.4) characterized by an elongated transannular C—C bond and a loss of planarity of the DHP core relative to the ground-state structure, the $S_1$ state relaxes to an excited-state minimum (DHP*; Figure 2.4) with a similar structure as ground-state DHP. From DHP*, the system deactivates back to the initial ground-state DHP either radiatively or nonradiatively. To undergo the DHP to CPD ring-opening reaction, the system needs to reach a biradical intermediate via the population of CPD* on $S_2$ followed by internal conversion at a CoIn between the zwitterionic and biradicaloid states. Upon population of the biradical intermediate, the system can then decay to the ground state at a nearby $S_0/S_1$ CoIn leading to product formation. This is illustrated by the purple path in Figure 2.4. Note that this path is an activated process as it needs to reach two CoIns higher in energy than CPD*. The $S_0/S_1$ CoIn is the expected photochemical funnel for CPD formation. This CoIn belongs to a well-known class of conical intersections involving three weakly coupled π-electrons. This type of CoIn has also been encountered in the photoswitching mechanism of DTEs [52].

Since this seminal theoretical study, more efficient DHP derivatives such as benzo [*e*]-fused-DHPs and pyridinium-appended-DHPs were studied computationally

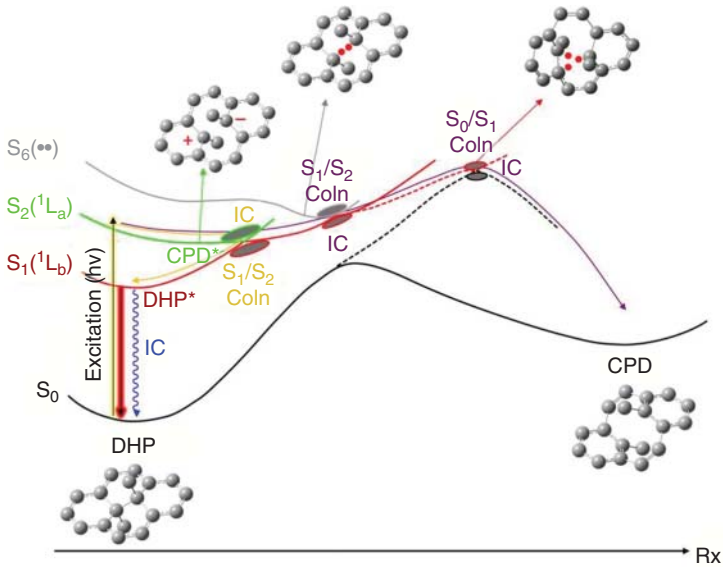


**Figure 2.4** Schematic potential energy profiles of the relevant electronic states involved in the DHP/CPD photochromism based on CASPT2 energies along CASSCF adiabatic relaxation pathways. IC: internal conversion, CoIn: conical intersection. Relevant structures for which hydrogen atoms have been omitted for clarity are shown. Yellow curved arrow: photophysical pathway; purple curved arrow: photoisomerization (photochemical) pathway.

[67, 68]. Because of the size of these derivatives, the CASSCF/CASPT2 approach employed to study the reference compound (Scheme 2.1) becomes impractical. Instead, TD-DFT can be used efficiently. While the biradicaloid excited state cannot be described with TD-DFT because of the doubly excited nature of this electronic state, TD-DFT is expected to describe the $S_2 \rightarrow S_1$ deactivation pathway, as both states result from single excitations as described above. This was first verified for the reference compound [67]. After validation of the description of the $S_2 \rightarrow S_1$ photophysical path at the TD-DFT level, the pathway leading to CPD* and to the $S_1/S_2$ CoIn was investigated for these improved DHP derivatives. Figure 2.5 illustrates this relaxation pathway for a simple benzo[*e*]-fused-DHP. For this system, the more efficient ring-opening reaction is made possible by the inversion of states occurring between $S_1$ and $S_2$, $S_1$ becoming the $L_a$ state and $S_2$ the $L_b$ state. Thus, CPD* formation takes place directly on the lowest $S_1$ PES, and no internal conversion with another excited state is involved. This study showed that in these systems, the CPD* minimum is the lowest excited-state minimum in contrast to the reference system for which it is DHP*. As CPD* is the transient species required to photoisomerize, more efficient formation of this intermediate is associated here to an improved ring-opening efficiency. More recently, it was explained theoretically why the ring-opening efficiency is dependent on the number of electron-withdrawing pyridinium groups appended to the DHP core [69].

Note that the photochemical funnels ($S_0/S_1$ CoIn) have yet to be identified in these substituted DHP derivatives. As TD-DFT is not suitable to describe such crossings

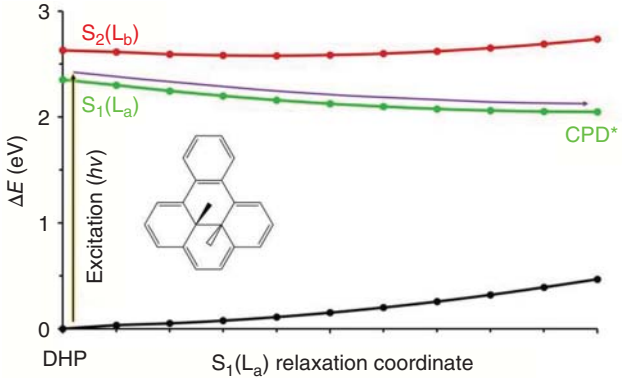


**Figure 2.5** TD-DFT potential energy profiles for the first three electronic states of a simple benzo[*e*]-fused DHP along the $S_1$ relaxation coordinate leading to CPD*. Purple curved arrow: $S_1$ relaxation pathway.

(biradical character of $S_0$ at the $S_0/S_1$ CoIn and wrong $S_0$-$S_1$ coupling at this level of theory), other variants of TD-DFT (e.g. spin-flip TD-DFT and multiconfigurational DFT) [31, 32, 70], which allow both the multiconfigurational description of the ground state and its correct electronic coupling with excited states, will be required to investigate the complete photoisomerization pathway of these systems.

## 2.4 Conclusions and Perspectives

In this chapter, we have given an outlook of the potential of computational photochemistry applied in the context of photochromic systems. Computational photochemistry is the branch of computational chemistry devoted to the study of chemical reactions induced by light. We have reviewed succinctly the various important aspects of such studies. It includes a short description of the most popular electronic structure methods allowing the reliable simultaneous description of ground and excited electronic states. We have presented the general strategy to determine a photochemical reaction mechanism with both static and dynamic exploration of the PESs allowing description of the sequence of molecular structures (traveling points on the PESs) through which the photoreaction proceeds on its way from reactant to photoproducts. We have recalled the central role of CoIns in ultrafast photochemistry in general but also in the context of the photoswitching of photochromic systems. CoIns provide the critical funnels through which the system is nonradiatively decaying between electronic states. Eventually, CoIns provide the reactive channels (photochemical funnels) for the photoproducts formation in the ground state.

Two illustrative examples of computational studies of photochromic systems have been given. The first one is the unidirectional photoswitching of DHA to VHF, which can be explained by the particular topological features of the $S_0/S_1$ CoIn seam. The second example is the low-efficient photoinduced ring opening of DHP into CPD, which can be accounted for by the presence of an unreactive

deactivation pathway via an easily accessible $S_1/S_2$ CoIn. The improved efficiency of some DHP derivatives can be rationalized theoretically by the effective removal of this unreactive deactivation pathway.

The developments of efficient and accurate quantum chemistry methods capable of describing excited-state reaction paths, CoIns, and photodynamics are needed to deal with complex and large photoactive systems. Recent advances in the field [32, 71] hold great promises in the future exploration of photochromic compounds, not only at the molecular level but also at the nanoscale [72], which is of high relevance to understand the efficiencies of photochromic materials for various optoelectronic applications. We can thus anticipate that computational photochemistry will carry on playing a major role in the understanding of photochromic compounds, and its predictive power will prove valuable in the design of novel photochromic materials in the future.

## References


1 Dürr, H. and Bouas-Laurent, H. (ed.) (1990). *Photochromism: Molecules and Systems*. Amsterdam: Elsevier.

2 Crano, J.C. and Guglielmetti, R. (1999). *Organic Photochromic and Thermochromic Compound*. New York: Plenum Press.

3 Feringa, B.L. and Browne, W.R. (ed.) (2011). *Molecular Switches*. Wiley-VCH Verlag GmbH & Co. KGaA.

4 Szymanski, W., Beierle, J.M., Kistemaker, H.A.V. et al. (2013). Reversible photocontrol of biological systems by the incorporation of molecular photoswitches. *Chem. Rev.* 113: 6114–6178.

5 Feringa, B.L. (2007). The art of building small: from molecular switches to molecular motors. *J. Org. Chem.* 72: 6635–6652.

6 Kim, T., Zhu, L., Al-Kaysi, R.O., and Bardeen, C.J. (2014). Organic photomechanical materials. *ChemPhysChem* 15: 400–414.

7 Asadirad, A.M., Boutault, S., Erno, Z., and Branda, N.R. (2014). Controlling a polymer adhesive using light and a molecular switch. *J. Am. Chem. Soc.* 136: 3024–3027.

8 Irie, M. (2000). Diarylethenes for memories and switches. *Chem. Rev.* 100: 1685–1716.

9 Berkovic, G., Krongauz, V., and Weiss, V. (2000). Spiropyrans and spirooxazines for memories and switches. *Chem. Rev.* 100: 1741–1753.

10 Yokoyama, Y. (2000). Fulgides for memories and switches. *Chem. Rev.* 100: 1717–1739.

11 Szacilowski, K. (2008). Digital information processing in molecular systems. *Chem. Rev.* 108: 3481–3548.

12 Andréasson, J. and Pischel, U. (2010). Smart molecules at work – mimicking advanced logic operations. *Chem. Soc. Rev.* 39: 174–188.

13 Pianowski, Z.L. (2019). Recent implementations of molecular photoswitches into smart materials and biological systems. *Chem. Eur. J.* 25: 5128–5144.

**14** Coppens, P., Novozhilova, I., and Kovalevsky, A. (2002). Photoinduced linkage isomers of transition-metal nitrosyl compounds and related complexes. *Chem. Rev.* 102: 861–883.

**15** Bitterwolf, T.E. (2006). Photochemical nitrosyl linkage isomerism/metastable states. *Coord. Chem. Rev.* 250: 1196–1207.

**16** Rack, J.J. (2009). Electron transfer triggered sulfoxide isomerization in ruthenium and osmium complexes. *Coord. Chem. Rev.* 253: 78–85.

**17** McClure, B.A. and Rack, J.J. (2010). Isomerization in photochromic ruthenium sulfoxide complexes. *Eur. J. Inorg. Chem.* 3895–3904.

**18** Kutateladze, A.G. (2005). *Computational Methods In Photochemistry*. CRC Press.

**19** Olivucci, M. (2005). *Computational Photochemistry*. Elsevier.

**20** Robb, M.A. (2018). *Theoretical Chemistry for Electronic Excited States*, Theoretical and Computational Chemistry Series. London: The Royal Society of Chemistry.

**21** Worth, G.A. and Cederbaum, L.S. (2004). Beyond Born-Oppenheimer: molecular dynamics through a conical intersection. *Annu. Rev. Phys. Chem.* 55: 127–158.

**22** Veryazov, V., Malmqvist, P.Å., and Roos, B.O. (2011). How to select active space for multiconfigurational quantum chemistry? *Int. J. Quantum Chem.* 111: 3329–3338.

**23** Garavelli, M. (2006). Computational organic photochemistry: strategy, achievements and perspectives. *Theor. Chem. Acc.* 116: 87–105.

**24** Roca-Sanjuán, D., Aquilante, F., and Lindh, R. (2012). Multiconfiguration second-order perturbation theory approach to strong electron correlation in chemistry and photochemistry. *WIREs Comput. Mol. Sci.* 2: 585–603.

**25** Yanai, T., Saitow, M., Xiong, X.-G. et al. (2017). Multistate complete-active-space second-order perturbation theory based on density matrix renormalization group reference states. *J. Chem. Theory Comput.* 13: 4829–4840.

**26** Dreuw, A. and Head-Gordon, M. (2005). Single-reference ab initio methods for the calculation of excited states of large molecules. *Chem. Rev.* 105: 4009–4037.

**27** Curchod, B.F.E., Rothlisberger, U., and Tavernelli, I. (2013). Trajectory-based nonadiabatic dynamics with time- dependent density functional theory. *ChemPhysChem* 14: 1314–1340.

**28** Levine, B.G., Ko, C., Quenneville, J., and Martínez, T.J. (2006). Conical intersections and double excitations in time-dependent density functional theory. *Mol. Phys.* 104: 1039–1051.

**29** Cordova, F., Doriol, L.J., Ipatov, A. et al. (2007). Troubleshooting time-dependent density-functional theory for photochemical applications: oxirane. *J. Chem. Phys.* 127: 164111.

**30** Peach, M.J.G., Williamson, M.J., and Tozer, D.J. (2011). Influence of triplet instabilities in TDDFT. *J. Chem. Theory Comput.* 7: 3578–3585.

**31** Casida, M. and Huix-Rotllant, M. (2012). Progress in time-dependent density-functional theory. *Annu. Rev. Phys. Chem.* 63: 287–323.

**32** Herbert, J.M., Zhang, X., Morrison, A.F., and Liu, J. (2016). Beyond time-dependent density functional theory using only single excitations: methods for computational studies of excited states in complex systems. *Acc. Chem. Res.* 49: 931–941.

**33** Granucci, G., Persico, M., and Toniolo, A. (2001). Direct semiclassical simulation of photochemical processes with semiempirical wave functions. *J. Chem. Phys.* 114: 10608.

**34** Koslowski, A., Beck, M.E., and Thiel, W. (2003). Implementation of a general multireference configuration interaction procedure with analytic gradients in a semiempirical context using the graphical unitary group approach. *J. Comput. Chem.* 24: 714.

**35** Silva-Junior, M.R. and Thiel, W. (2010). Benchmark of electronically excited states for semiempirical methods: MNDO, AM1, PM3, OM1, OM2, OM3, INDO/S, and INDO/S2. *J. Chem. Theory Comput.* 6: 1546–1564.

**36** Bernardi, F., Olivucci, M., and Robb, M.A. (1992). Simulation of MC-SCF results on covalent organic multi-bond reactions: molecular mechanics with valence bond (MM-VB). *J. Am. Chem. Soc.* 114: 1606–1616.

**37** Bearpark, M.J., Boggio-Pasqua, M., Robb, M.A., and Ogliaro, F. (2006). Excited states of conjugated hydrocarbons using the molecular mechanics - valence bond (MMVB) method: conical intersections and dynamics. *Theor. Chem. Acc.* 116: 670–682.

**38** Bearpark, M.J., Ogliaro, F., Vreven, T. et al. (2007). CASSCF calculations for photoinduced processes in large molecules: choosing when to use the RASSCF, ONIOM and MMVB approximations. *J. Photochem. Photobiol., A* 190: 207–227.

**39** González, L., Escudero, D., and Serrano-Andrés, L. (2012). Progress and challenges in the calculation of electronic excited states. *ChemPhysChem* 13: 28–51.

**40** Lischka, H., Nachtigallová, D., Aquino, A.J.A. et al. (2018). Multireference approaches for excited states of molecules. *Chem. Rev.* 118: 7293–7361.

**41** Mai, S. and González, L. (2020). Molecular photochemistry: recent developments in theory. *Angew. Chem. Int. Ed.* 59: 16832–16846.

**42** Kosloff, R. (1988). Time-dependent quantum-mechanical methods for molecular dynamics. *J. Phys. Chem.* 92: 2087–2100.

**43** Meyer, H.-D., Gatti, F., and Worth, G.A. (ed.) (2009). *Multidimensional Quantum Dynamics: MCTDH Theory and Applications*. Weinheim: Wiley VCH.

**44** Gonon, B., Lasorne, B., Karras, G. et al. (2019). A generalized Vibronic-coupling hamiltonian for molecules without symmetry: application to the photoisomerization of benzopyran. *J. Chem. Phys.* 150: 124109.

**45** Robb, M.A., Bernardi, F., and Olivucci, M. (1995). Conical intersections as a mechanistic feature of organic photochemistry. *Pure Appl. Chem.* 67: 783–789.

**46** Bernardi, F., Olivucci, M., and Robb, M.A. (1996). Potential energy surface crossings in organic photochemistry. *Chem. Soc. Rev.* 25: 321–328.

**47** Robb, M.A., Garavelli, M., Olivucci, M., and Bernardi, F. (2000). A computational strategy for organic photochemistry. *Rev. Comput. Chem.* 15: 87–146.

**48** Cattaneo, P. and Persico, M. (1999). An ab initio study of the photochemistry of azobenzene. *Phys. Chem. Chem. Phys.* 1: 4739–4743.

**49** Celani, P., Bernardi, F., Olivucci, M., and Robb, M.A. (1997). Conical intersection mechanism for photochemical ring opening in benzospiropyran compounds. *J. Am. Chem. Soc.* 119: 10815–10820.

**50** Zgierski, M.Z. and Grabowska, A. (2000). Photochromism of salicylideneaniline (SA). How the photochromic transient is created: a theoretical approach. *J. Chem. Phys.* 112: 6329–6337.

**51** Boggio-Pasqua, M., Bearpark, M.J., Hunt, P.A., and Robb, M.A. (2002). Dihydroazulene/vinylheptafulvene photochromism: a model for one-way photochemistry via a conical intersection. *J. Am. Chem. Soc.* 124: 1456–1470.

**52** Boggio-Pasqua, M., Ravaglia, M., Bearpark, M.J. et al. (2003). Can diarylethene photochromism be explained by a reaction path alone? A CASSCF study with model MMVB dynamics. *J. Phys. Chem. A* 107: 11139–11152.

**53** Migani, A., Gentili, P.L., Negri, F. et al. (2005). The ring-opening reaction of Chromenes: a photochemical mode-dependent transformation. *J. Phys. Chem. A* 109: 8684–8692.

**54** Maurel, F., Aubard, J., Millie, P. et al. (2006). Quantum chemical study of the photocoloration reaction in the naphthoxazine series. *J. Phys. Chem. A* 110: 4759–4771.

**55** Boggio-Pasqua, M., Bearpark, M.J., and Robb, M.A. (2007). Towards a mechanistic understanding of the photochromism of dimethyldihydropyrenes. *J. Org. Chem.* 72: 4497–4503.

**56** Tomasello, G., Ogliaro, F., Bearpark, M.J. et al. (2008). Modeling the photophysics and photochromic potential of 1,2-dihydronaphthalene (DHN): a combined CASPT2//CASSCF-topological and MMVB-dynamical investigation. *J. Phys. Chem. A* 112: 10096–10107.

**57** Tomasello, G., Bearpark, M.J., Robb, M.A. et al. (2010). Significance of a zwitterionic state for fulgide photochromism: implications for the design of mimics. *Angew. Chem. Int. Ed.* 49: 2913–2916.

**58** Yarkony, D.R. (1996). Diabolical conical intersections. *Rev. Mod. Phys.* 68: 985–1013.

**59** Robb, M.A. (2011). *Conical Intersections in Organic Photochemistry, in Conical Intersections: Theory, Computation and Experiment*, vol. 17 (ed. W. Domcke, D.R. Yarkony and H. Köppel), Chap. 1, pp. 3–50. Singapore: World Scientific.

**60** Blancafort, L. (2014). Photochemistry and photophysics at extended seams of conical intersection. *ChemPhysChem* 15: 3166–3181.

**61** Ern, J., Petermann, M., Mrozek, T. et al. (2000). Dihydroazulene/vinylheptafulvene photochromism: dynamics of the photochemical ring-opening reaction. *Chem. Phys.* 259: 331–337.

**62** De Waele, V., Schmidhammer, U., Mrozek, T. et al. (2002). Ultrafast bidirectional dihydroazulene/vinylheptafulvene (DHA/VHF) molecular switches: photochemical ring closure of vinylheptafulvene proven by a two-pulse experiment. *J. Am. Chem. Soc.* 124: 2438–2439.

**63** Görner, H., Fischer, C., Gierisch, S., and Daub, J. (1993). Dihydroazulene/vinylheptafulvene photochromism: effects of substituents, solvent, and temperature in the photorearrangement of dihydroazulene to vinylheptafulvenes. *J. Phys. Chem.* 97: 4110–4117.

**64** Mitchell, R.H. (1999). The metacyclophanediene-dihydropyrene photochromic π switch. *Eur. J. Org. Chem.* 2695–2703.

**65** Sheepwash, M.A.L., Mitchell, R.H., and Bohne, C. (2002). Mechanistic insights into the photochromism of *trans*-10b,10c-dimethyl-10b-10c-dihydropyrene derivatives. *J. Am. Chem. Soc.* 124: 4693–4700.

**66** Sarkar, R., Heitz, M.-C., Royal, G., and Boggio-Pasqua, M. (2020). Electronic excited states and UV-Vis absorption spectra of the dihydropyrene/cyclophanediene photochromic couple: a theoretical investigation. *J. Phys. Chem. A* 124: 1567–1579.

**67** Boggio-Pasqua, M. and Garavelli, M. (2015). Rationalization and design of enhanced photoinduced cycloreversion in photochromic dimethyldihydropyrenes by theoretical calculations. *J. Phys. Chem. A.* 119: 6024–6032.

**68** Roldan, D., Cobo, S., Lafolet, F. et al. (2015). A multi-addressable switch based on the dimethyldihydropyrene photochrome with remarkable proton-triggered photo-opening efficiency. *Chem. Eur. J.* 21: 455–467.

**69** Lognon, E., Heitz, M.-C., Bakkar, A. et al. (2020). Dependency of the dimethyldihydropyrene photochromic properties on the number of Pyridinium electron-withdrawing groups. *ChemPhysChem* 21: 1571–1577.

**70** Ghosh, S., Verma, P., Cramer, C.J. et al. (2018). Combining wave function methods with density functional theory for excited states. *Chem. Rev.* 118: 7249–7292.

**71** Park, J.W. and Shiozaki, T. (2017). On-the-Fly CASPT2 surface-hopping dynamics. *J. Chem. Theory Comput.* 13: 3676–3683.

**72** Levine, B.G., Esch, M.P., Fales, B.S. et al. (2019). Conical intersections at the nanoscale: molecular ideas for materials. *Annu. Rev. Phys. Chem.* 70: 21–43.

# Section II

# Chemical Classes of Molecular Photoswitches

# 3 Azobenzenes: The Quest for Visible Light Triggering

Vanessa Koch and Stefan Bräse

**Photochromism**

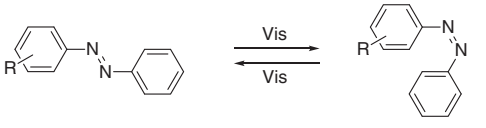


**Characteristic Features**

This chapter aims to summarize the synthetic approaches (including Mills reactions), the design concepts of different kinds of azobenzene photoswitches reversibly switchable with visible light, regarding their applications (especially in biological systems) as well as their physical properties.

**Synthetic Methods**

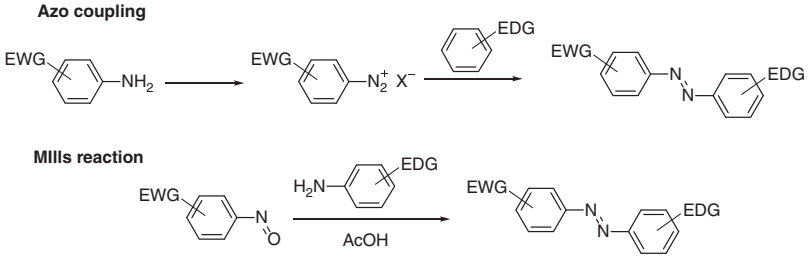


**First Reference**

Robertson, P.W. (1913). *J. Chem. Soc. Trans.* 103: 1472–1479.

**Key References**

Bléger, D., Schwarz, J., Brouwer, A.M. et al. (2012). *J. Am. Chem. Soc.* 134: 20597–20600.

Banghart, M., Borges, K., Isacoff, E. et al. (2004). *Nat. Neurosci.* 7: 1381–1386.

Dong, M., Babalhavaeji, A., Samanta, S. et al. (2015). *Acc. Chem. Res.* 48: 2662–2670.

Hansen, M.J., Lerch, M.M., Szymanski, W. et al. (2016). *Angew. Chem. Int. Ed.* 55: 13514–13518.

# 3

# Azobenzenes: The Quest for Visible Light Triggering

*Vanessa Koch*[1,2] *and Stefan Bräse*[1,2]

[1] *Karlsruhe Institute of Technology (KIT), Institute of Organic Chemistry, Organic Chemistry I, Fritz-Haber-Weg 6, Karlsruhe, 76131, Germany*
[2] *Karlsruhe Institute of Technology (KIT), Biological and Chemical Systems – Functional Molecular Systems (IBCS-FMS), Hermann-von-Helmholtz-Platz 1, Eggenstein-Leopoldshafen, D-76344, Germany*

## 3.1 Introduction

The discovery of azo compounds goes back to the mid-1800s when Eilhard Mitscherlich found that the distillation of nitrobenzene over burnt lime gave a so far unknown red solid compound that he called azobenzene (AB) due to its elemental analysis, which is ambiguous for a molecule with one or two nitrogen atoms. Its structure was determined over 30 years later by August Kekulé, but the configuration of the N=N double bond remained unsolved till G.S. Hartley discovered the photoisomerization of ABs in 1937 [1]. During his studies of the solubility properties of ABs, he observed a lack of reproducibility in the measurement of absorbance spectra and the color change of the solution when being exposed to sunlight. By a tremendous purification process, he was able to isolate the product that was responsible for the color change and determined its physical and chemical properties. As it thermally reverts to the *trans*-AB, G. S. Hartley concluded that he discovered the *cis*-form of AB and therefore also the photoisomerization of *trans*-ABs to *cis*-ABs by sunlight. In the following years, many AB derivatives were synthesized and their photophysical properties were studied.

The present book chapter aims to summarize the synthetic approaches, the design concepts of different kinds of AB photoswitches regarding their applications (especially in biological systems) as well as their physical properties. In the end, selected applications were given to show the overall potential of ABs. Thereby, the cited literature and reviews serve as sources to be consulted for deeper understanding [2–5]. Aliphatic derivatives are not covered, while heteroaromatic azoarenes (six- [6–10] or five-membered ones [11–14]) are compared with classical ones – a more detailed discussion is found in this book (Chapter 5 by Matthew Fuchter) [15]. Multiple [16] and cyclic [17] azobenzenes are only discussed very briefly.

*Molecular Photoswitches: Chemistry, Properties, and Applications*,
First Edition. Edited by Zbigniew L. Pianowski.

### 3.1.1 Azobenzene and Its Physical Characteristics

ABs have two geometric isomers (*Z*/*E* or *cis*/*trans*) from which the *E*-isomer is circa 12 kcal mol$^{-1}$ more stable than the *Z*-isomer. As the energy barrier of the photoexcited state is about 23 kcal mol$^{-1}$, the *trans*-isomer is predominant in the dark at room temperature with 99.99%. When irradiated with a wavelength between 320 and 350 nm, the *trans*-AB isomerizes to the *cis*-form on a picosecond timescale, thus being substantially faster than most biological processes, qualifying ABs for biological investigations. The reaction is reversible either by irradiation with light of a wavelength between 400 and 450 nm, heating, or thermal relaxation (milliseconds to days) the *trans*-isomer back. The reversibility of the process and the changes in physical properties, such as molecular geometry, their absorption spectra, or dipole moment, identify ABs as valuable photoswitches. The change of the geometry leads to a decrease in the end-to-end distance of *trans*-located carbons from 9.0 to 5.5 Å. This goes along with a change of the dipole moment μ as the *cis*-isomer is bent and one of the aryl rings twists 50° out of the plane to avoid electronical repulsion resulting in μ = 3.0 D while the *trans*-AB is almost flat. This effect can be also observed in the $^1$H NMR (nuclear magnetic resonance) spectrum. Due to the anisotropic effect of the π cloud of the aromatic, the aromatic signals of the *cis*-AB are shifted toward a higher field compared with those of the *trans*-AB (Figure 3.1).

The UV–vis absorption spectra of both isomers of the AB show two characteristic absorption bands, which are distinct but overlap each other. *trans*-AB shows a very intense π→π* transition band near 320 nm and a weak n→π* transition band near 440 nm – as this transition is not allowed by symmetry rules. In comparison, the *cis*-AB has a stronger n→π* transition band at a similar wavelength (as it is allowed) and two absorption bands at shorter wavelengths of 280 and 240 nm. It is worth noting that photoisomerization takes place with high quantum yields, and only negligible photobleaching is observed.

The photophysics of heterocyclic azobenzenes has been discussed in detail elsewhere [15]. Recently, azobenzenes have been used for the self-assembly of nanoparticles [18] and the design of visible-light switchable or orthogonally switchable systems [19–21].

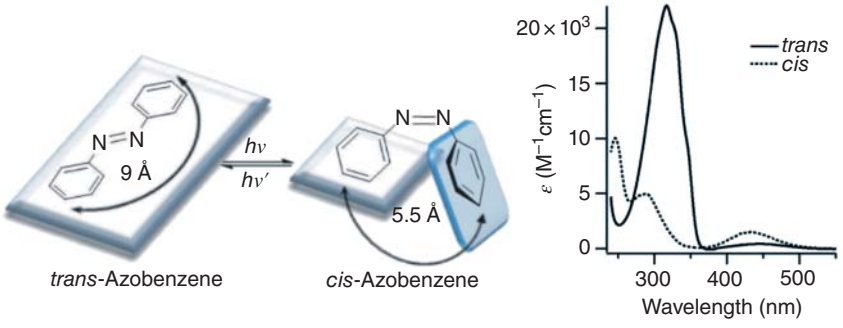


**Figure 3.1** Photoisomerization of azobenzene (Source: Reprinted from Ref. [5]) and the absorption spectrum of the two isomers. Source: Reprinted with permission from Beharry and Woolley [2].

## 3.2 Synthesis of Azobenzenes

Since ABs are broadly used both in the industry and in academia, a variety of synthetic methods have been developed since their discovery in the mid-1800s. Some of these will be presented in the following chapter, for more detailed information, several reviews can be found in the literature [22, 23]. Even though many new methods have been developed, most syntheses of ABs are still based on classical methods such as the azo coupling or the Mills reaction.

### 3.2.1 Synthesis of Symmetrical Azobenzenes by Oxidation of Anilines

The synthesis of symmetrical AB derivatives has been accomplished via the oxidation of anilines – either by electrolytic oxidation or oxidizing reagents comprising metallic and nonmetallic ones. Among the huge variety of oxidants presented in the literature reaching over $MnO_2$, $KMnO_4$, $Ag_2CO_3$ $Pb(OAc)_4$, and hypervalent iodides such as $PhI(OAc)_2$ to aerial oxidants such as $O_2$/*t*BuOK, $O_2/CuCl_2$/pyridine or peroxidase/$H_2O_2$, $MnO_2$, and NaOCl are most commonly used in practice. The oxidation of anilines bearing electron-withdrawing groups (EWGs) in *meta*- and/or *para*-position was realized in refluxing toluene with $MnO_2$ affording the ABs in mostly excellent yields (Scheme 3.1, top). Apart from classical methods, greener alternatives by solvent-free permanganate oxidation were provided to access ABs carrying, for example, *para*-chloro substituents, but also di-*ortho*-*para*-methyl residues (Scheme 3.1, bottom).

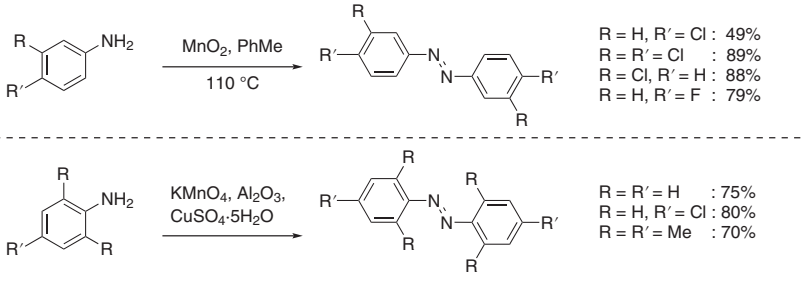


**Scheme 3.1** Oxidation of anilines with $MnO_2$ and $KMnO_4$.

The oxidation of anilines sometimes suffers from poor yields in dependency on the substitution pattern. For example, the oxidation of 2,4,6-trichloroaniline using NaOCl as oxidant afforded the tetra-*ortho*-chloro AB (**Cl4**) only in 19% yield (Scheme 3.2, left). Hence, the development of new and alternative methods is still under investigation and provides new solutions for specific synthetic problems. An approach to access different tetra-*ortho*-chloro ABs of the type **Cl4** was recently introduced by the Trauner group using a palladium-catalyzed late-stage C–H chlorination (Scheme 3.2, right) [24].

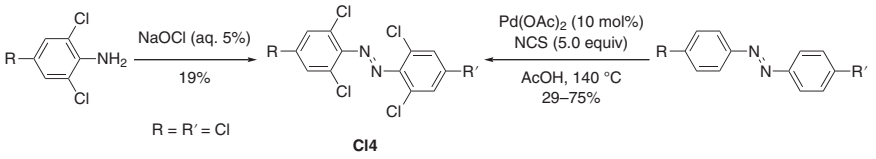


**Scheme 3.2** Oxidation of anilines and late-stage C–H chlorination for the synthesis of tetra-*ortho*-chloro azobenzene.

### 3.2.2 Azo Coupling

The most widespread and classical (1860, Grieß) method to access unsymmetrical ABs is still the azo coupling, based on the initial diazotization of an aniline derivative, which is then supposed to react with an electron-rich aromatic nucleophile carrying typical electron-donating groups (EDGs) such as ethers or amines (Scheme 3.3). The reaction proceeds usually in a short time and good yields; nevertheless, the temperature of the reaction has to be controlled and the stability of the diazonium salt has to be carefully considered as some of these are explosive. For example, diazonium chlorides are unstable – decomposing explosively when they are stored at a temperature above 5 °C, whereby tetrafluoroborates or hexafluorophosphates show higher stability in the solid state and can even be stored for longer periods.

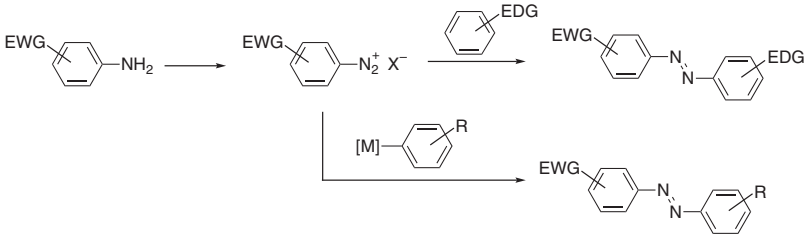


**Scheme 3.3** Azo coupling of diazonium salts and electron-rich aromatics.

Due to the electron-donating character of the nucleophile, the azo coupling occurs in *para*-position to the donor group. When this position is already occupied by another functional group, *ortho*-substitution is favored instead. An alternative is the reaction of diazonium salts with organometallics such as Grignard, lithium, or zinc reagents (see also Scheme 3.7).

### 3.2.3 Mills Reaction

Another classical method for the synthesis of unsymmetrical AB derivatives was developed by Mills and includes the reaction between an aromatic nitroso derivative and anilines under acetic conditions (Scheme 3.4). The nitroso compound was first synthesized by the oxidation of an aromatic methylhydroxyl amine,

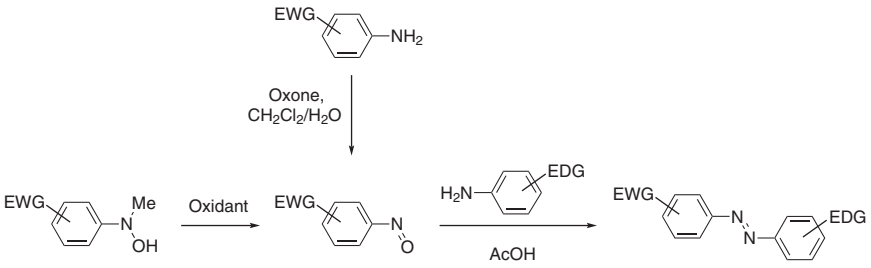


**Scheme 3.4** Mills reaction starting of the aromatic nitroso compound with anilines. The nitroso compound can be prepared by oxidation of aromatic methylhydroxyl amines or anilines.

whereby many oxidants are described in the literature, e.g. *tert*-butyl hypochlorite, $FeCl_3$, *m*-CPBA, or $H_2O_2$ in the presence of rhenium, tungsten, or molybdenum catalysts (Scheme 3.4, left). Nevertheless, the nitrosoarene is often only obtained in low yields, because competing side reactions such as the decomposition of the hydroxylamine, the overoxidation of the nitroso to nitro compound, or the condensation of the hydroxylamine and the nitro compound are difficult to control. To overcome these drawbacks, heterogeneous two-phase systems such as Oxone® in a mixture of $CH_2Cl_2$ and $H_2O$ were developed. These separate the less water-soluble nitrosoarene from the *N*-hydroxylamine intermediates and the aniline derivate and prevent therefore the condensation reaction (Scheme 3.4, top).

Variants of the Mills reaction include the deoxygenation of aromatic nitro compounds under basic reaction conditions to form the nitroso derivative, which reacts then with *N*-acylamines, or the reaction of nitroso derivatives with triphenylarsine phenylamine as a nucleophile. The latter reacts upon heating with the nitroso compound in a Wittig-type mechanism giving the corresponding azo compound (Scheme 3.5).

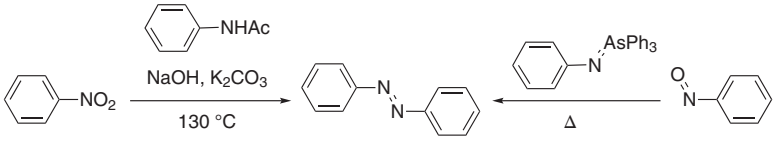


**Scheme 3.5** Modified reaction conditions of the Mills Reaction.

### 3.2.4 Modern Methods

A plethora of new methods arises in the current literature accessing azobenzenes including the usage of metal–organic reagents, late-stage C–H activation reactions, metal catalysts as well as electrocatalytic approaches from which only selected examples will be presented in the following. A particular focus relies on the synthesis of tetra-*ortho*-substituted ABs, as the yields are often unsatisfying when classical methods are applied (Scheme 3.6).

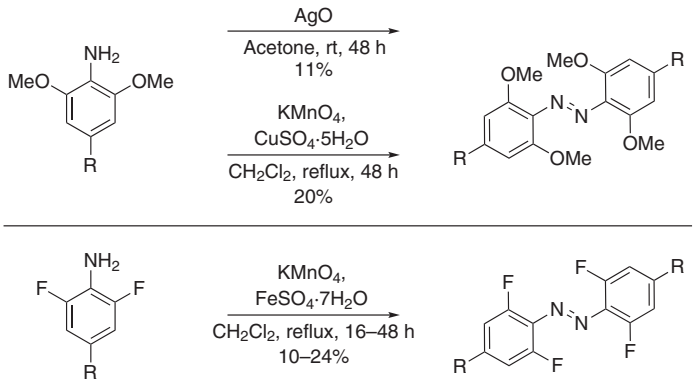


**Scheme 3.6** Classical synthetic methods toward tetra-*ortho*-substituted azobenzenes.

In addition to the *ortho*-chlorination of ABs to access tetra-*ortho*-chloroazobenzenes (Scheme 3.2) [24], Feringa and coworkers proposed to use a directed *ortho*-lithiation of the aromatic precursor and its subsequent reaction with aryldiazonium salts (Scheme 3.7). This approach accesses symmetric and unsymmetrical ABs in improved yields ranging from 77% to 92% but lacks a broad functional group tolerance as they have to be compatible with lithium organyls [25].

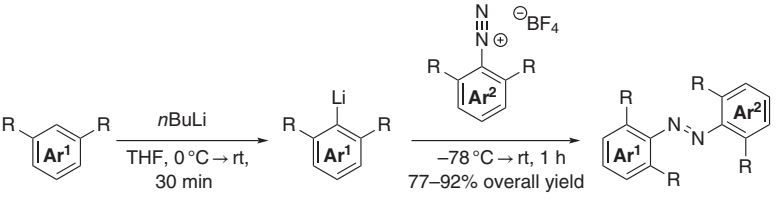


**Scheme 3.7** Novel synthetic methods toward tetra-*ortho*-substituted azobenzenes based on the addition of lithium organyls to diazonium compounds.

Lin et al. showed that symmetrical ABs can be easily synthesized by an oxidative homocoupling in a one-step procedure starting from aniline derivatives using the stable and inexpensive reagents *N*-chlorosuccinimide (NCS) and 1,8-diazabicyclo [5.4.0]undec-7-ene (DBU) (Scheme 3.8). The protocol includes the synthesis of several tetra-*ortho*-fluoroazobenzenes in good yields of c. 60% [26].

Mellah and coworker reported on an electrocatalytic approach based on the reduction of nitroarenes toward ABs using electrogenerated samarium diiodide

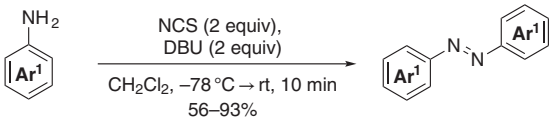


**Scheme 3.8** Oxidative coupling of aniline derivatives for the synthesis of symmetric azobenzenes.

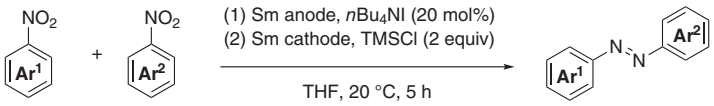


**Scheme 3.9** Novel synthetic methods for azobenzenes.

as a reducing reagent (Scheme 3.9). This method allows accessing a variety of symmetrical ABs bearing different kinds of functional groups in all positions, but also unsymmetrical ABs by using different molar ratios (1,3 of $Ar^1$-$NO_2$/$Ar^2$-$NO_2$). This includes di-*ortho*-substituted ABs in general as well as the tetra-*ortho*-methylazobenzenes [27].

## 3.3 Visible Light-Activated Azobenzenes as Photoswitches

Since UV light is highly energetic and hence, detrimental to the surroundings and sometimes even to the photoswitch itself, several strategies have been developed to avoid the irradiation with UV light and replace it with visible light or even near-infrared (NIR) light.

In principle, three different strategies divided by their mechanism were developed so far. The first strategy is based on the combination of a photoswitch with a photosensitizer such as a two-photon fluorophore, a triplet sensitizer, or an upconverting nanoparticle that can absorb the irradiated light and transfer the energy to the molecular switch. The latter can happen through different modes of action, e.g. Förster resonance energy transfer, triplet–triplet transfer, or simple emission and reabsorption.

The second strategy involves redox reactions where a sensitizer is excited either by irradiation or electrochemically and initiates the catalytic chain through photoinduced electron transfer.

The third and most direct approach tries to engineer the direct photoexcitation by influencing the energy gap between the highest occupied molecular orbital (HOMO) and the lowest occupied molecular orbital (LUMO) by the molecular design. This can be achieved by the extension of the π system resulting in a redshift of the π→π* band. Since the n→π* band is only slightly affected, the absorption bands of the two isomers overlap, and thus, the isomers cannot be addressed selectively [4]. Hence, the incorporation of EWGs or EDGs to influence the energy of the orbitals represents the preferred approach (Figure 3.2). Besides, so-called push–pull systems in which one ring of the ABs bears an EWG, while the other an EDG, were investigated. In this case, the π→π* and n→π* bands are overlapping as well, making a light-driven control of the isomerization processes impossible. Besides, it is worth mentioning that half-lives of the respective *Z*-isomers are rather short and typically range from nanoseconds to seconds. For an early example, see reference [28].

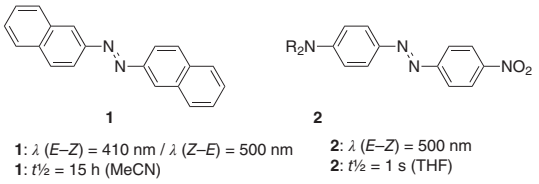


**Figure 3.2** Examples for red-shifted azobenzenes by the extension of the π system (left) or a push–pull substitution (right).

### 3.3.1 The Effect of Electron-Donating Groups on Direct Photoexcitation

Several EDGs such as alkyl, amino, methoxy, or thioalkyl residues were incorporated at all positions of the AB structure. Systematic studies on the design of ABs with EDG showed however that the *ortho*-substitution was superior over the *meta*-substitution as the thermal half-life time of the *cis*-isomer in the latter case was too short for most of applications (μs for *meta* in contrast to s for the *ortho*). When adding electron-donating alkyl groups to all four *ortho*-positions, a small separation of the n→π* transition between the *cis*- and *trans*-isomer was observed. The *ortho*-alkylation also led to longer thermal half-lives, which was attributed to the steric clashes between the substituents and the n-orbital of azo nitrogen. By the substitution with stronger EDGs such as amino groups, the absorption wavelength could be shifted toward longer wavelengths and thermal relaxation times in the range of seconds to minutes in water. The degree of the donating effect of the amine was determined by the character of the amino group. A six-membered piperidine residue, for example, caused a loss of $sp^2$ character on the azo nitrogen due to the steric interactions, which was not the case for the five-membered pyrrolidine residue or an acyclic amine. As an undesired side effect of the electron-rich nature of the AB, photobleaching occurred [29] (Figure 3.3).

To avoid photobleaching, less electron-donating methoxy groups were installed at all four *ortho*-positions of an amidoazobenzene **OMe4** (Figure 3.4). This also shifted the n→π* absorption band for the *trans*-isomer to higher wavelengths and led therefore to a separation of the transition bands between the *cis*- and *trans*-isomers ($\Delta\lambda_{n\rightarrow\pi^*} = 35$ nm). This can be explained by the comparison of the relative energies of the orbitals of each isomer. As the HOMO, located at the azo nitrogen, is close to the electron-rich oxygen atom of the methoxy group in the *trans*-isomer, its

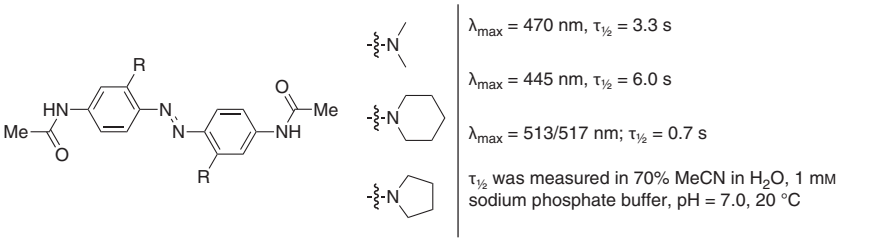


**Figure 3.3** *Ortho*-substituted aminoazobenzenes and their selected physical properties.

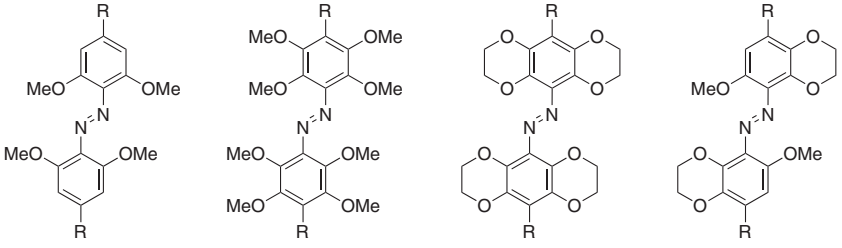


**Figure 3.4** Overview of azobenzenes bearing methoxy groups and/or dioxane rings.

relative energy is higher than in the unsubstituted AB. As a result, the required energy for the *trans*→*cis* isomerization based on the n→π* transition is decreased. For the *cis*-isomer, the methoxy group does not influence the lone pair, which is why **OMe4** shows a similar transition band to its parent compound. This *cis*-isomer was thermally stable with a half-life of 53 hours allowing that both isomers can be readily photogenerated and maintained in the dark granting, for example, the spatial localization of the *cis*-isomer in vivo. Additionally, no photobleaching or photo-oxidation occurred as the photoswitch survived multiple cycles of isomerization and constant high-intensity irradiation with a green light. To tune the (photo)physical properties, a variety of derivatives based on the same concept were explored [30–33]. According to computational studies, the functionalization of all *ortho*- and *meta*-positions of the AB with methoxy groups (**OMe8**) is supposed to lead to a loss of conjugation due to the steric clash of the methoxy groups. Therefore, the conformation was locked by the introduction of 1,4-dioxane moieties. Because of the poor solubility of azobenzene **DOM4**, only one dioxane ring per aryl residue could be attached (**DOM2**). The absorbance maximum of the *trans*-isomer was even further red-shifted to near 600 nm with a clear separation of the n→π* transition of the two isomers. By the nature of the chosen amine R in *the para*-position, the wavelength maximum was affected, but also – and even more importantly – the azonium p$K_a$. This might diminish the absorbance as the azonium and the ammonium species can coexist at physical pH having both different photophysical properties. Regarding their application in biological systems, their sensitivity toward reduction limits their usage to extracellular processes [34].

### 3.3.2 The Effect of Electron-Withdrawing Groups on Direct Photoexcitation

As was the case for EDGs, numerous studies have been carried out to investigate the effect of EWGs on ABs. *Ortho*-EWGs can stabilize both the n orbital of the *cis*-isomer and the π* orbitals of both isomers. This leads to an increased energy of the n→π* transition band for the *cis*-isomer of *ortho*-EWG substituted ABs and hence, in a blue shift of the n→π* band, while the transition energy of the corresponding *trans*-isomer is lowered, and as consequence, a redshift for n→π* transition band is observed compared with the unsubstituted ABs (Figure 3.5).

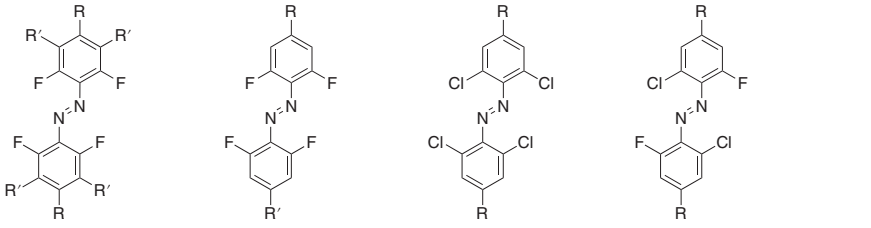


**Figure 3.5** Overview of selected examples of fluoro- and chloroazobenzenes.

As a consequence, the two n→π* transition bands of *ortho*-tetrafluoroazobenzene **F4** are well separated (42 nm) allowing the use of visible light $\lambda = 410$ nm for the $E \rightarrow Z$ isomerization and $\lambda > 500$ nm for the reverse $Z \rightarrow E$ isomerization accompanied with high quantum yields. An interesting feature of these *ortho*-fluoro substituted ABs is their planarity as well as the enhanced thermal stability of the *cis*-form due to the lowered energy of the n orbital. As expected, ABs bearing only two *ortho*-fluorine substituents cause a smaller splitting than **F4**, whereby the opposite effect of an enhanced splitting did not occur when additional fluorine atoms were added (**F6**, **F8**, or **F10**). EDGs lead to a less effective splitting of the n→π* bands and were hence not further investigated. Regarding the photoconversions, best performances were attained for *ortho*-tetrafluoroazobenzenes bearing either amide (**F4-diamide**) or ester groups (**F4-diester**), which additionally facilitate the attachment of biological systems. All fluoro-substituted ABs show longer thermal half-lives of the *cis*-isomer than the unsubstituted AB whereby symmetrical ABs with four or six fluorine atoms (**F4** and **F6**) showed half-lives of more than 90 hours in MeCN at 60 °C. Nevertheless, the studies revealed that *meta*-substitution should be avoided if one is seeking photoswitches with long thermal half-lives. Among the *ortho*-fluoroazobenzenes, **F4-ester** represents the best compromise between high photoconversions in both directions and high thermal stability including also the possibility of an attachment to other systems [35]. For completeness, it is worth mentioning that Woolley et al. investigated at the same time *ortho*-tetrachloroazobenzene **Cl4** with an even higher red-shifted absorption for the n→π* transition, but higher thermal relaxation rates [31, 36].

In most recent reports, the relation between substituents of the *ortho*-tetrachloroazobenzene **Cl4** and the photophysical properties has been in-depth investigated, both spectroscopically and theoretically [20]. Another group demonstrated deeply red-shifted azobenzenes with mixed chloro- and fluoro-substituents in the *ortho*-positions (e.g. **Cl2F2**), less synthetically challenging and more thermally stable than the original **Cl4** structure [21]. Finally, it was shown that appending the **F4** structure with conjugated unsaturated substituents (–CHO or –C=C– groups) in *para*-positions (R, R′) (but not in *meta*-) also results in bathochromic shift of the photoisomerization wavelength. In that case, red light (>630 nm) irradiation can

**Table 3.1** Spectroscopic data including the separation of the n→π* transition bands ($\Delta\lambda_{n\rightarrow\pi^*}$), the composition of the photostationary state (PSS) when irradiated at $\lambda > 500$ nm ($PSS_{(Z)}$) and $\lambda = 410$ nm ($PSS_{(E)}$), and the experimental half-lives $\tau_{1/2}$ in MeCN at 60 °C by Bléger et al. [35].

| Compound | $\Delta\lambda_{n\rightarrow\pi^*}$ (nm) | $PSS_{(Z)}$ (%) | $PSS_{(E)}$ (%) | $\tau_{1/2}$ (h) |
|---|---|---|---|---|
| AB | 14 | — | — | 4 |
| F4 | 42 | 86 | 91 | 92 |
| F6 | 36 | 94 | 91 | 95 |
| F8 | 43 | 92 | 92 | 27 |
| F10 | 40 | 91 | 90 | — |
| F4-diester | 50 | 90 | 97 | 15 |
| F4-ester | 44 | 95 | 95 | 30 |
| F4-diamide | 50 | 92 | 96 | 22 |

Source: Data from Bléger et al. [35].

produce up to 82% of the respective *cis*-isomer (for the bis-aldehyde) with thermal stability similar to the unsubstituted azobenzene (*cis*-isomer with $t_{1/2} = 3.2$ hour at 60 °C in MeCN, see Table 3.1) [37].

### 3.3.3 Further Modification Leading to Visible Light Photoswitches

There are also further approaches to tune the photoswitching properties of ABs. One of these is based on a C2-bridged azobenzene (diazocines), which also has distinct and well-separated n→π* transition bands (Scheme 3.10). In this case, the *cis*-form is thermodynamically more stable than the *trans*-form as the short bridge strains and distorts the latter. The *cis*→*trans* isomerization occurs rapidly with blue light from the near-UV range (λ = 380–400 nm) while the backward reaction is induced by green light, both in very high quantum yields [38]. A more detailed reference can be found in the chapter of Rainer Herges and coworkers [38–59].

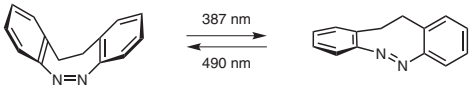


**Scheme 3.10** C2-bridged azobenzene.

Another class of visible-light addressable AB photoswitches are boron-coordinated azo compounds (Scheme 3.11). The introduction of different functional groups in the *para*-position of **azo1** gave a series of AB derivatives emitting green, yellow, orange, and red fluorescence [60, 61]. As the isomerization reaction was locked due to the coordination of the boron atom to the lone pair of the azo nitrogen, structural changes were required. Hence, azo compounds with the general structure **azo2** were synthesized showing well-separated $\pi_{nb}\rightarrow\pi^*$ transitions for the *trans*-

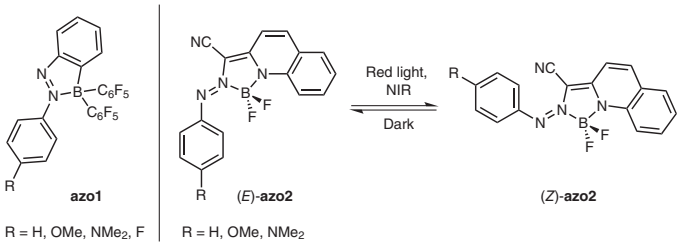


**Scheme 3.11** Boron-coordinated azobenzenes.

and the *cis*-isomer in the visible part of the light spectrum, which is caused by the complexation of the azo group with $BF_2$ in combination with an extended conjugation of the diazo π-electrons. By increasing the electron density through EDGs in the *para*-position of **azo2**, the absorption bands were shifted to the red and even NIR region. Besides the high photoconversion and high photoisomerization quantum yields, the **azo2**-compounds were relatively stable regarding their half-lives ($\tau_{1/2} \approx 10$ hours/20 minutes in deoxygenated/regular $CH_2Cl_2$) and toward reduction by glutathione [62, 63].

### 3.3.4 Complex Molecular and Supramolecular Systems Containing Azobenzenes

Azobenzenes have been incorporated into molecular systems with various degree of complexity. Many specific examples have been discussed in the following chapters of this book. However, we will list here a few representative examples: diazocine homologues with increasing sizes of the central ring [52], further macrocyclic azobenzenes [44, 64, 65], azobenzene-containing crown-ethers [66], or cyclic binaphthyls [67]. One selected example of a complex azobenzene-containing macrocyclic system is shown below (Scheme 3.12) [68].

Over the last year, a vast number of phototriggered materials based on azobenzene photoisomerization have been demonstrated, just to mention photochromic hydrogels [69–73], actuators for upconverting luminescence [74], molecular machines [75], polymers [76], and complex systems [77, 78], as well as photoswitchable MOF [6–10, 79–85] – many discussed in-depth in the following chapters in the Section II of this book.

## 3.4 Applications of Azobenzenes in Biological Systems

Visible light is an interesting tool to study biochemical processes in vivo without external interference. The usage of light offers additionally the possibility to investigate biochemical pathways and interactions with high spatial and temporal precision. Alternative methods do not show spatiotemporal control since genetic approaches often lack temporal resolution, while small molecules can be better temporally controlled but suffer from the target selectivity. To use visible light as an efficient tool, the biomolecule must carry a light-sensitive group such as an AB fulfilling

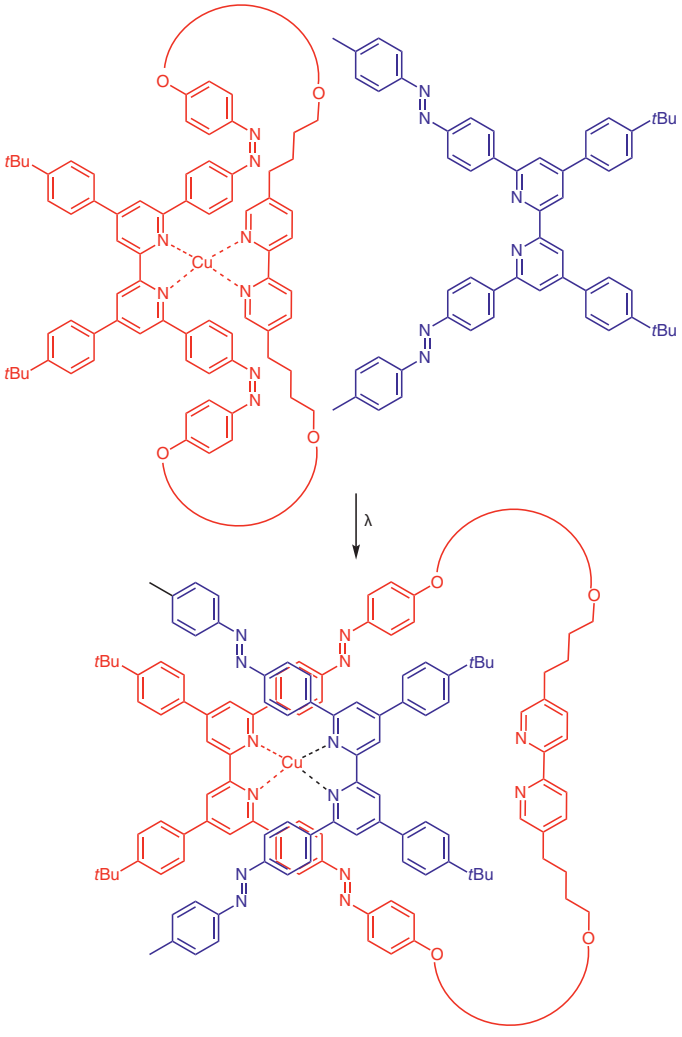


**Scheme 3.12** Switching of an azo crown ether copper complex. Source: Modified from Umeki et al. [68].

certain requirements to be applicable in biological systems. The light-sensitive group has to alter the target upon irradiation in a substantial manner to detect the changes in its biological activity caused, for example, by conformational changes. Second, the absorption of light in an efficient manner is required, meaning that the group either shows a high molar extinction coefficient or undergoes a two-photon cross section. This aspect also includes that the photochemistry of the envisioned modification is efficient to avoid the application of high dosages of light. The selected photoswitch should isomerize with visible or NIR light (between 400 and 900 nm), preferentially in the so-called therapeutic window (600–900 nm), which is only negligibly absorbed by soft body parts or hemoglobin. Hence, that light can penetrate cells

and tissues easily to induce the photoswitch, while UV light in contrast is strongly absorbed by biomolecules such as NADH and scattered by the skin. Another, but not less important, requirement for the photosensitive group is its stability under biological conditions during as well as after the irradiation, meaning that photosensitive groups should be nontoxic and stable toward hydrolysis and reduction. To fulfill these requirements, the core structure of ABs has been modified (see above).

Noteworthy, the reversibility of the photoisomerization of ABs makes them superior toward competing approaches such as the "caging" approach. So far, most applications of ABs to photomodulate biological systems were reported in vitro. For in vivo applications, the target has to be addressed selectively by the AB, or it has to be modified with the AB and then introduced into the living system, which both pose significant technical challenges. In the following section, a selection of examples will be presented to give a rough overview of the milestones that were achieved so far, but also the limitations of ABs as photoswitches.

One application of AB photoswitches to photomodulate properties of biopolymers is based on the idea to control structures of peptides to alter their function by changing their secondary/tertiary structure. As cysteine residues are rarely found in proteins and are easy to introduce by standard molecular biology techniques, cysteine residues are commonly utilized to attach ABs to peptides and proteins. The AB derivative incorporates two chloroacetamide groups to provide chemoselective covalent binding with the cysteine sulfhydryl groups in presence of other aminoacid side chains. Additionally, sulfonate groups were included into the structure of the azobenzene for higher solubility. The peptides were rationally designed after the calculations of the end-to-end distances of both isomers. The UV irradiation of a helical peptide that contains the cross-linked cysteines at the positions $i$ and $i + 11$ matching to the end-to-end distance range of the *trans*-AB leads to a decrease in helicity as the *cis*-isomer has a smaller end-to-end distance and is therefore not compatible with the helical structure (Figure 3.6). This strategy was later transferred to naturally occurring peptides such as the DNA-recognition helix to enable the photo-control of DNA binding by conformational changes [86].

The isomerization of AB has also been used in vivo to open and close pores in cellular membranes to control the transport of ions. One example was presented by Kramer and Trauner [87] using the photoisomerization of ABs to control $K^+$ channels in neurons of rats to switch action potential firing on and off (Figure 3.7). As these voltage-gated $K^+$ channels are blocked by the binding of quaternary ammonium ions, the ABs were equipped with triethylammonium residues on one side. On the other side, a maleimide linker was attached to ensure selective binding to cysteine that was introduced to the channel by exogenous expression replacing Glu422. By irradiation with $\lambda = 380$ nm, photoisomerization is induced shortening the end-to-end distance of the AB about 7 Å, which opens the channel and hence, allows the ions to pass. When the light of $\lambda = 500$ nm is applied, the photoisomerization process is reversed and the channel is blocked again.

Another example of the control of ion channels by photoisomerization is based on the allosteric control of an active site by a remote regulatory binding site and was illustrated for the ionotropic glutamate receptor (iGluR). Therefore, an AB was

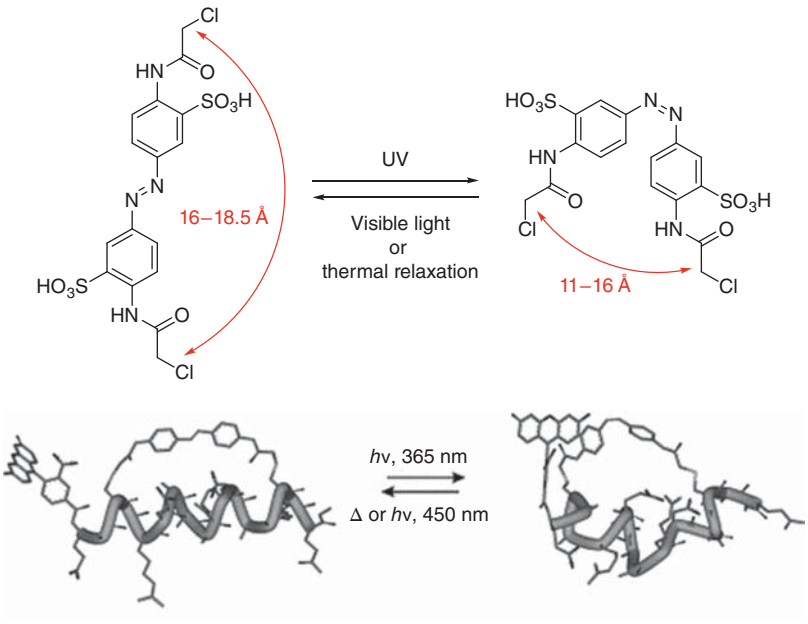


**Figure 3.6** Photocontrol of the α-helical content in secondary structures of peptides connected via two cysteines in position *i* and *i* + *11* to an azobenzene derivative. Source: Adapted with permission from Beharry et al. [86].

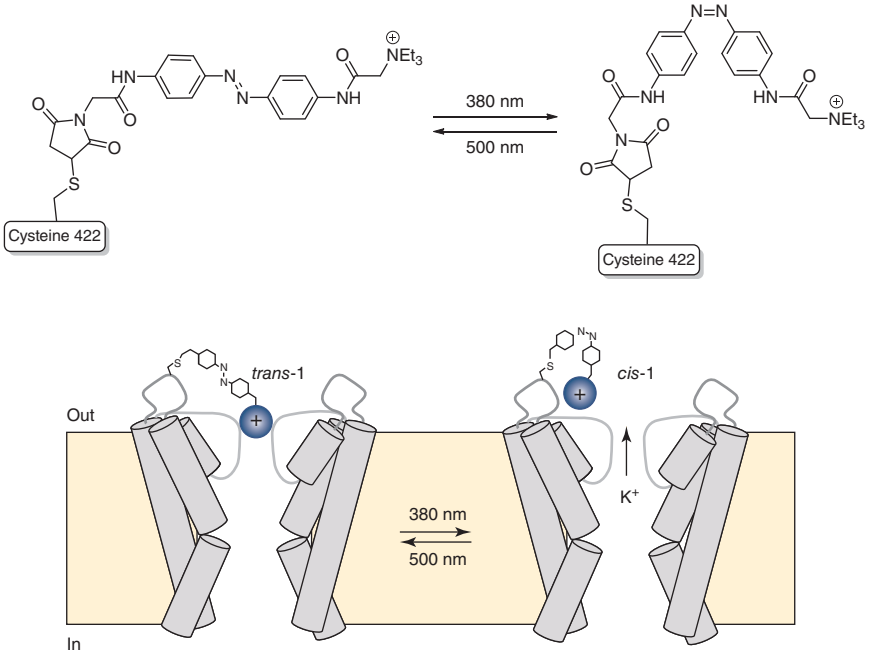


**Figure 3.7** Photocontrol of a $K^+$ channel in the cellular membrane of neurons based on the photoisomerization of an azobenzene derivative, which is connected via a maleimide to the Cys422 of the ion channel. Source: Adapted with permission from Banghart et al. [87].

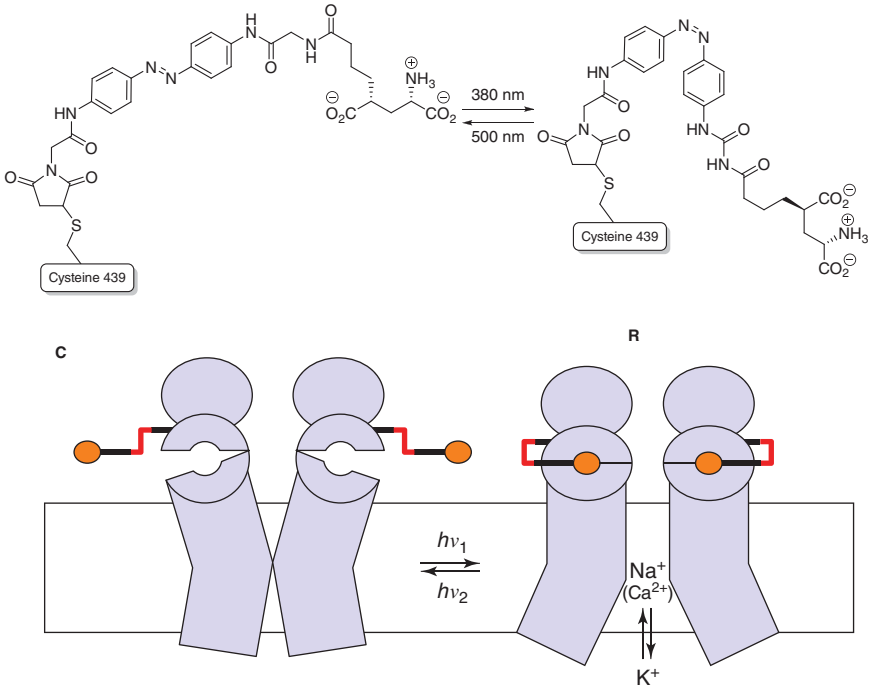


**Figure 3.8** Photocontrol of the ionotropic ion glutamate receptor by the conformational changes of an azobenzene derivative connected to the ion channel via a Cys439. Source: Source: Reprinted with permission from Volgraf et al. [88].

equipped with a maleimide residue enabling the covalent binding to the protein via a cysteine residue (again inserted by mutation, L439C) and a glutamate unit on the other side serving as an agonist for the receptor. Upon irradiation with $\lambda = 380$ nm, photoisomerization occurs allowing the interaction of the glutamate residue with the active site of the protein receptor, which leads to conformational changes of the protein and hence, to channel gating (Figure 3.8). Other applications are directed to other channels [88].

To circumvent systemic and environmental side effects of drugs, photoswitchable drugs with spatial and temporal control over its activity with light are part of numerous investigations in the emerging field of photopharmacology. In this context, Feringa et al. developed a photo-responsive, antibacterial diaminopyrimidine whose activity can be controlled by light with specific wavelengths. The antibacterial diaminopyrimidine unit was attached to a tetra-*ortho*-chloroazobenzene. Whereas (*E*)-**Cl4pyr** is nearly inactive with an $MIC_{50} > 80\,\mu M$, the irradiation with red light ($\lambda = 652$ nm) forms (*Z*)-**Cl4pyr** and leads to bacteriostasis (inhibition of bacteria growth without their destruction) down to 20 μM with an $MIC_{50} = 80\,\mu M$, which corresponds to an eightfold difference before and after irradiation [89]. (Figure 3.9).

Other examples included visible-light-responsive peptide backbone photoswitches [73, 90], intercalators for photocontrol of DNA [91], reversible and

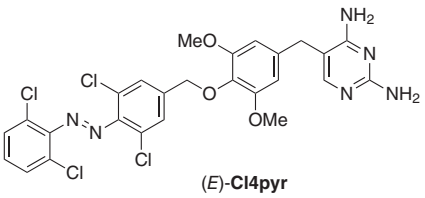


(*E*)-**Cl4pyr**

**Figure 3.9** First example of a photo-responsive antibacterial agent switchable with visible light.

tunable photoswitching of protein function [92], red-shifted azobenzene [93], or azo-bridges [94].

## 3.5 Conclusion

In this chapter, we have summarized the basic photophysical properties, photochromism, and most common synthetic methods of azobenzenes, which are among the most common molecular photoswitches. They are embedded in a variety of functional molecular scaffold and used to construct phototriggered materials and compounds with photomodulated biological activity. Selected classes and examples of such materials will be discussed in the Sections II and III of this book, respectively. Here, we attempted to provide the reader with a brief overview and more detailed references to a few selected topics. While the standard azobenzene chromophore poses numerous limitations on its application scope, the last decade witnessed numerous reports on AB structures optimized for particular applications, especially in hydrophilic biological systems. This was enabled by efficient few-step synthetic strategies available for this particular scaffold, as well as its photostability and chemical robustness.

## References

1 Hartley, G.S. (1937). Cis form of azobenzene. *Nature* 140: 281.
2 Beharry, A.A. and Woolley, G.A. (2011). Azobenzene photoswitches for biomolecules. *Chem. Soc. Rev.* 40 (8): 4422–4437.
3 Dong, M., Babalhavaeji, A., Samanta, S. et al. (2015). Red-shifting azobenzene photoswitches for in vivo use. *Acc. Chem. Res.* 48 (10): 2662–2670.
4 Bléger, D. and Hecht, S. (2015). Visible-light-activated molecular switches. *Angew. Chem. Int. Ed.* 54 (39): 11338–11349.
5 Merino, E. and Ribagorda, M. (2012). Control over molecular motion using the cis–trans photoisomerization of the azo group. *Beilstein J. Org. Chem.* 8: 1071–1090.
6 Wang, Z., Grosjean, S., Bräse, S., and Heinke, L. (2015). Photoswitchable adsorption in metal-organic frameworks based on polar guest-host interactions. *ChemPhysChem* 16 (18): 3779–3783.
7 Dommaschk, M., Peters, M., Gutzeit, F. et al. (2015). Photoswitchable magnetic resonance imaging contrast by improved light-driven coordination-induced spin state switch. *J. Am. Chem. Soc.* 137 (24): 7552–7555.

**8** Fang, L., Chen, S., Zhang, Y., and Zhang, H. (2011). Azobenzene-containing molecularly imprinted polymer microspheres with photoresponsive template binding properties. *J. Mater. Chem.* 21 (7): 2320–2329.

**9** Modrow, A., Zargarani, D., Herges, R., and Stock, N. (2011). The first porous MOF with photoswitchable linker molecules. *Dalton Trans.* 40 (16): 4217–4222.

**10** Wang, Z., Heinke, L., Jelic, J. et al. (2015). Photoswitching in nanoporous, crystalline solids: an experimental and theoretical study for azobenzene linkers incorporated in MOFs. *Phys. Chem. Chem. Phys.* 17 (22): 14582–14587.

**11** Adam, V., Prusty, D.K., Centola, M. et al. (2018). Expanding the toolbox of photoswitches for DNA nanotechnology using arylazopyrazoles. *Chem. Eur. J.* 24 (5): 1062–1066.

**12** Calbo, J., Weston, C.E., White, A.J.P. et al. (2017). Tuning azoheteroarene photoswitch performance through heteroaryl design. *J. Am. Chem. Soc.* 139 (3): 1261–1274.

**13** Simeth, N.A., Crespi, S., Fagnoni, M., and Koenig, B. (2018). Tuning the thermal isomerization of phenylazoindole photoswitches from days to nanoseconds. *J. Am. Chem. Soc.* 140 (8): 2940–2946.

**14** Weston, C.E., Richardson, R.D., Haycock, P.J. et al. (2014). Arylazopyrazoles: azoheteroarene photoswitches offering quantitative isomerization and long thermal half-lives. *J. Am. Chem. Soc.* 136 (34): 11878–11881.

**15** Fuchter, M. (2021). Arylazoheterocycles. In: *Molecular Photoswitches – Synthesis, Properties and Applications* (ed. Z. Pianowski). Wiley-VCH.

**16** Heindl, A.H., Becker, J., and Wegner, H.A. (2019). Selective switching of multiple azobenzenes. *Chem. Sci.* 10 (31): 7418–7425.

**17** Vela, S., Scheidegger, A., Fabregat, R., and Corminboeuf, C. (2020). Tuning the thermal stability and photoisomerization of azoheteroarenes through macrocycle strain. *ChemRxiv* 1–10.

**18** Manna, D., Udayabhaskararao, T., Zhao, H., and Klajn, R. (2015). Orthogonal light-induced self-assembly of nanoparticles using differently substituted azobenzenes. *Angew. Chem. Int. Ed.* 54 (42): 12394–12397.

**19** Zhao, F., Grubert, L., Hecht, S., and Bleger, D. (2017). Orthogonal switching in four-state azobenzene mixed-dimers. *Chem. Commun.* 53 (23): 3323–3326.

**20** Lameijer, L.N., Budzak, S., Simeth, N.A. et al. (2020). General principles for the Design of visible-light-responsive photoswitches: tetra-ortho-chloro-azobenzenes. *Angew. Chem. Int. Ed.* 59: 21663–21670.

**21** Konrad, D.B., Savasci, G., Allmendinger, L. et al. (2020). Computational design and synthesis of a deeply red-shifted and bistable azobenzene. *J. Am. Chem. Soc.* 142 (14): 6538–6547.

**22** Merino, E. (2011). Synthesis of azobenzenes: the coloured pieces of molecular materials. *Chem. Soc. Rev.* 40 (7): 3835–3853.

**23** Hamon, F., Djedaini-Pilard, F., Barbot, F., and Len, C. (2009). Azobenzenes—synthesis and carbohydrate applications. *Tetrahedron* 65 (49): 10105–10123.

**24** Konrad, D.B., Frank, J.A., and Trauner, D. (2016). Synthesis of redshifted azobenzene photoswitches by late-stage functionalization. *Chem. Eur. J.* 22 (13): 4364–4368.

**25** Hansen, M.J., Lerch, M.M., Szymanski, W., and Feringa, B.L. (2016). Direct and versatile synthesis of red-shifted azobenzenes. *Angew. Chem. Int. Ed.* 55 (43): 13514–13518.

**26** Antoine John, A. and Lin, Q. (2017). Synthesis of azobenzenes using *N*-chlorosuccinimide and 1,8-diazabicyclo[5.4.0]undec-7-ene (DBU). *J. Org. Chem.* 82 (18): 9873–9876.

**27** Zhang, Y.-F. and Mellah, M. (2017). Convenient electrocatalytic synthesis of azobenzenes from nitroaromatic derivatives using SmI2. *ACS Catal.* 7 (12): 8480–8486.

**28** Robertson, P.W. (1913). Isomerism of p-Azophenol. *J. chem. Soc. Trans.* 103: 1472–1479.

**29** Sadovski, O., Beharry, A.A., Zhang, F., and Woolley, G.A. (2009). Spectral tuning of azobenzene photoswitches for biological applications. *Angew. Chem. Int. Ed.* 48 (8): 1484–1486.

**30** Samanta, S., Babalhavaeji, A., Dong, M.-x., and Woolley, G.A. (2013). Photoswitching of ortho-substituted azonium ions by red light in whole blood. *Angew. Chem. Int. Ed.* 52 (52): 14127–14130.

**31** Samanta, S., Beharry, A.A., Sadovski, O. et al. (2013). Photoswitching azo compounds in vivo with red light. *J. Am. Chem. Soc.* 135 (26): 9777–9784.

**32** Dong, M., Babalhavaeji, A., Hansen, M.J. et al. (2015). Red, far-red, and near infrared photoswitches based on azonium ions. *Chem. Commun.* 51 (65): 12981–12984.

**33** Beharry, A.A., Sadovski, O., and Woolley, G.A. (2011). Azobenzene photoswitching without ultraviolet light. *J. Am. Chem. Soc.* 133 (49): 19684–19687.

**34** Dong, M., Babalhavaeji, A., Collins, C.V. et al. (2017). Near-infrared photoswitching of azobenzenes under physiological conditions. *J. Am. Chem. Soc.* 139 (38): 13483–13486.

**35** Bléger, D., Schwarz, J., Brouwer, A.M., and Hecht, S. (2012). *o*-Fluoroazobenzenes as readily synthesized photoswitches offering nearly quantitative two-way isomerization with visible light. *J. Am. Chem. Soc.* 134 (51): 20597–20600.

**36** Rullo, A., Reiner, A., Reiter, A. et al. (2014). Long wavelength optical control of glutamate receptor ion channels using a tetra-ortho-substituted azobenzene derivative. *Chem. Commun.* 50 (93): 14613–14615.

**37** Leistner, A.-L., Kirchner, S., Karcher, J. et al. (2021). Fluorinated azobenzenes switchable with red light. *Chem. Eur. J.* 27 (31): 8094–8099.

**38** Böckmann, M., Doltsinis, N.L., and Marx, D. (2010). Unraveling a chemically enhanced photoswitch: bridged azobenzene. *Angew. Chem. Int. Ed.* 49 (19): 3382–3384.

**39** Herges, R. (2021). Diazocines – Bridged Azobenzenes with Unusual Properties. In: *Molecular Photoswitches – Synthesis, Properties and Applications*. Wiley-VCH.

**40** Siewertsen, R., Neumann, H., Buchheim-Stehn, B. et al. (2009). Highly efficient reversible Z-E photoisomerization of a bridged azobenzene with visible light through resolved S1($n\pi^*$) absorption bands. *J. Am. Chem. Soc.* 131 (43): 15594–15595.

**41** Siewertsen, R., Schoenborn, J.B., Hartke, B. et al. (2011). Superior Z E and E Z photoswitching dynamics of dihydrodibenzodiazocine, a bridged azobenzene, by S1(nπ*) excitation at $\lambda$ = 387 and 490 nm. *Phys. Chem. Chem. Phys.* 13 (3): 1054–1063.

**42** Boeckmann, M., Doltsinis, N.L., and Marx, D. (2012). Enhanced photoswitching of bridged azobenzene studied by nonadiabatic ab initio simulation. *J. Chem. Phys.* 137 (22): 22A505/1–22A505/10.

**43** Samanta, S., Qin, C., Lough, A.J., and Woolley, G.A. (2012). Bidirectional photocontrol of peptide conformation with a bridged azobenzene derivative. *Angew. Chem. Int. Ed.* 51 (26): 6452–6455, S6452/1–S6452/10.

**44** Deo, C., Bogliotti, N., Metivier, R. et al. (2016). A visible-light-triggered conformational diastereomer photoswitch in a bridged azobenzene. *Chem. Eur. J.* 22 (27): 9092–9096.

**45** Hammerich, M., Schuett, C., Staehler, C. et al. (2016). Heterodiazocines: synthesis and photochromic properties, trans to cis switching within the bio-optical window. *J. Am. Chem. Soc.* 138 (40): 13111–13114.

**46** Liu, L., Wang, Y., and Fang, Q. (2017). New insights into mechanistic photoisomerization of ethylene-bridged azobenzene from ab initio multiple spawning simulation. *J. Chem. Phys.* 146 (6): 064308/1–064308/8.

**47** Glock, P., Broichhagen, J., Kretschmer, S. et al. (2018). Optical control of a biological reaction-diffusion system. *Angew. Chem. Int. Ed.* 57 (9): 2362–2366.

**48** Jun, M., Joshi, D.K., Yalagala, R.S. et al. (2018). Confirmation of the structure of trans-cyclic azobenzene by X-ray crystallography and spectroscopic characterization of cyclic azobenzene analogs. *ChemistrySelect* 3 (9): 2697–2701.

**49** Schehr, M., Hugenbusch, D., Moje, T. et al. (2018). Synthesis of mono-functionalized S-diazocines via intramolecular Baeyer-Mills reactions. *Beilstein J. Org. Chem.* 14: 2799–2804.

**50** Cabre, G., Garrido-Charles, A., Gonzalez-Lafont, A. et al. (2019). Synthetic photoswitchable neurotransmitters based on bridged azobenzenes. *Org. Lett.* 21 (10): 3780–3784.

**51** Lentes, P., Stadler, E., Roehricht, F. et al. (2019). Nitrogen bridged diazocines: photochromes switching within the near-infrared region with high quantum yields in organic solvents and in water. *J. Am. Chem. Soc.* 141 (34): 13592–13600.

**52** Maier, M.S., Huell, K., Reynders, M. et al. (2019). Oxidative approach enables efficient access to cyclic azobenzenes. *J. Am. Chem. Soc.* 141 (43): 17295–17304.

**53** Reynders, M., Matsuura, B., Berouti, M. et al. (2019). PHOTACs enable optical control of protein degradation. *ChemRxiv* 1–34.

**54** Stadler, E., Tassoti, S., Lentes, P. et al. (2019). In situ observation of photoswitching by NMR spectroscopy: a photochemical analogue to the exchange spectroscopy experiment. *Anal. Chem.* 91 (17): 11367–11373.

**55** Thapaliya, E.R., Zhao, J., and Ellis-Davies, G.C.R. (2019). Locked-azobenzene: testing the scope of a unique photoswitchable scaffold for cell physiology. *ACS Chem. Neurosci.* 10 (5): 2481–2488.

**56** Trads, J.B., Huell, K., Matsuura, B.S. et al. (2019). Sign inversion in photopharmacology: incorporation of cyclic Azobenzenes in photoswitchable potassium channel blockers and openers. *Angew. Chem. Int. Ed.* 58 (43): 15421–15428.

**57** Zhu, Q., Wang, S., and Chen, P. (2019). Diazocine derivatives: a family of azobenzenes for photochromism with highly enhanced turn-on fluorescence. *Org. Lett.* 21 (11): 4025–4029.

**58** Burk, M.H., Schroeder, S., Moormann, W. et al. (2020). Fabrication of diazocine-based photochromic organic thin films via initiated chemical vapor deposition. *Macromolecules* 53 (4): 1164–1170.

**59** Trauner, D., Reynders, M., Matsuura, B. et al. (2020). Preparation of photoswitchable PROTACs for treating diseases and inducing selective degradation of a target protein. WO2020172655A1.

**60** Yoshino, J., Furuta, A., Kambe, T. et al. (2010). Intensely fluorescent azobenzenes: synthesis, crystal structures, effects of substituents, and application to fluorescent vital stain. *Chem. Eur. J.* 16 (17): 5026–5035.

**61** Yoshino, J., Kano, N., and Kawashima, T. (2007). Synthesis of the most intensely fluorescent azobenzene by utilizing the B–N interaction. *Chem. Commun.* 6: 559–561.

**62** Yang, Y., Hughes, R.P., and Aprahamian, I. (2012). Visible light switching of a BF2-coordinated Azo compound. *J. Am. Chem. Soc.* 134 (37): 15221–15224.

**63** Yang, Y., Hughes, R.P., and Aprahamian, I. (2014). Near-infrared light activated azo-BF2 switches. *J. Am. Chem. Soc.* 136 (38): 13190–13193.

**64** Takaishi, K., Kawamoto, M., Muranaka, A., and Uchiyama, M. (2012). Fusion of photochromic reaction and synthetic reaction: photoassisted cyclization to highly strained chiral azobenzenophanes. *Org. Lett.* 14 (13): 3252–3255.

**65** Lin, C., Maisonneuve, S., Metivier, R., and Xie, J. (2017). Photoswitchable carbohydrate-based macrocyclic azobenzene: synthesis, chiroptical switching, and multi-stimuli-responsive self-assembly. *Chem. Eur. J.* 23 (60): 14996–15001.

**66** Shiga, M., Takagi, M., and Ueno, K. (1980). Azo-crown ethers. The dyes with azo group directly involved in the crown ether skeleton. *Chem. Lett.* 8: 1021–1022.

**67** Takaishi, K., Muranaka, A., Kawamoto, M., and Uchiyama, M. (2012). Photoinversion of cisoid/transoid binaphthyls. *Org. Lett.* 14 (1): 276–279.

**68** Umeki, S., Kume, S., and Nishihara, H. (2011). Switching of molecular insertion in a cyclic molecule via photo- and thermal isomerization. *Inorg. Chem.* 50 (11): 4925–4933.

**69** Tamesue, S., Takashima, Y., Yamaguchi, H. et al. (2010). Photoswitchable supramolecular hydrogels formed by cyclodextrins and azobenzene polymers. *Angew. Chem. Int. Ed.* 49 (41): 7461–7464. S7461/1-S7461/17.

**70** Dai, L., Lu, J., Kong, F. et al. (2019). Reversible photo-controlled release of bovine serum albumin by azobenzene-containing cellulose nanofibrils-based hydrogel. *Adv. Compos. Hybrid Mater.* 2 (3): 462–470.

**71** Velema, W.A., Stuart, M.C.A., Szymanski, W., and Feringa, B.L. (2013). Light-triggered self-assembly of a dichromonyl compound in water. *Chem. Commun.* 49 (44): 5001–5003.

**72** Accardo, J.V. and Kalow, J.A. (2018). Reversibly tuning hydrogel stiffness through photocontrolled dynamic covalent crosslinks. *Chem. Sci.* 9 (27): 5987–5993.

**73** Karcher, J. and Pianowski, Z.L. (2018). Photocontrol of drug release from supramolecular hydrogels with green light. *Chem. Eur. J.* 24 (45): 11605–11610.

**74** Jiang, Z., Xu, M., Li, F., and Yu, Y. (2013). Red-light-controllable liquid-crystal soft actuators via low-power excited upconversion based on triplet-triplet annihilation. *J. Am. Chem. Soc.* 135 (44): 16446–16453.

**75** Browne, W.R., Pijper, D., Pollard, M.M., and Feringa, B.L. (2009). Chiroptical molecular switches and motors. In: *Switching at the nanoscale* (ed. D.B. Amabilino), 349–390. Wiley-VCH Verlag GmbH & Co. KGaA.

**76** Yue, Y., Norikane, Y., Azumi, R., and Koyama, E. (2018). Light-induced mechanical response in crosslinked liquid-crystalline polymers with photoswitchable glass transition temperatures. *Nat. Commun.* 9 (1): 1–8.

**77** Weis, P., Wang, D., and Wu, S. (2016). Visible-Light-Responsive Azopolymers with Inhibited π-π Stacking Enable Fully Reversible Photopatterning. *Macromolecules* 49 (17): 6368–6373.

**78** Yan, H., Qiu, Y., Wang, J. et al. (2020). Wholly visible-light-responsive host-guest supramolecular gels based on methoxy azobenzene and β-cyclodextrin dimers. *Langmuir* 36 (26): 7408–7417.

**79** Fan, C.B., Liu, Z.Q., Gong, L.L. et al. (2017). Photoswitching adsorption selectivity in a diarylethene-azobenzene MOF. *Chem. Commun.* 53 (4): 763–766.

**80** Heinke, L., Cakici, M., Dommaschk, M. et al. (2014). Photoswitching in two-component surface-mounted metal-organic frameworks: optically triggered release from a molecular container. *ACS Nano* 8 (2): 1463–1467.

**81** Heinke, L., Tu, M., Wannapaiboon, S. et al. (2015). Surface-mounted metal-organic frameworks for applications in sensing and separation. *Microporous Mesoporous Mater.* 216: 200–215.

**82** Meng, H., Zhao, C., Nie, M. et al. (2018). Optically controlled molecular metallofullerene magnetism via an azobenzene-functionalized metal-organic framework. *ACS Appl. Mater. Interfaces* 10 (38): 32607–32612.

**83** Prasetya, N., Donose, B.C., and Ladewig, B.P. (2018). A new and highly robust light-responsive Azo-UiO-66 for highly selective and low energy post-combustion $CO_2$ capture and its application in a mixed matrix membrane for $CO_2/N_2$ separation. *J. Mater. Chem. A* 6 (34): 16390–16402.

**84** Wang, Z., Mueller, K., Valasek, M. et al. (2018). Series of photoswitchable azobenzene-containing metal-organic frameworks with variable adsorption switching effect. *J. Phys. Chem. C* 122 (33): 19044–19050.

**85** Heinke, L. (2021). Light-triggered metal-organic frameworks. In: *Molecular Photoswitches – Synthesis, Properties and Applications* (ed. Z. Pianowski). Wiley-VCH.

**86** Beharry, A.A., Wong, L., Tropepe, V., and Woolley, G.A. (2011). Fluorescence imaging of azobenzene photoswitching in vivo. *Angew. Chem. Int. Ed.* 50 (6): 1325–1327.

**87** Banghart, M., Borges, K., Isacoff, E. et al. (2004). Light-activated ion channels for remote control of neuronal firing. *Nat. Neurosci.* 7 (12): 1381–1386.

**88** Volgraf, M., Gorostiza, P., Numano, R. et al. (2006). Allosteric control of an ionotropic glutamate receptor with an optical switch. *Nat. Chem. Biol.* 2: 47–52.

**89** Wegener, M., Hansen, M.J., Driessen, A.J.M. et al. (2017). Photocontrol of antibacterial activity: shifting from UV to red light activation. *J. Am. Chem. Soc.* 139 (49): 17979–17986.

**90** Albert, L., Penalver, A., Djokovic, N. et al. (2019). Modulating protein-protein interactions with visible-light-responsive peptide backbone photoswitches. *ChemBioChem* 20 (11): 1417–1429.

**91** Heinrich, B., Bouazoune, K., Wojcik, M. et al. (2019). ortho-Fluoroazobenzene derivatives as DNA intercalators for photocontrol of DNA and nucleosome binding by visible light. *Org. Biomol. Chem.* 17 (7): 1827–1833.

**92** Luo, J., Samanta, S., Convertino, M. et al. (2018). Reversible and tunable photoswitching of protein function through genetic encoding of azobenzene amino acids in mammalian cells. *ChemBioChem* 19 (20): 2178–2185.

**93** John, A.A., Ramil, C.P., Tian, Y. et al. (2015). Synthesis and site-specific incorporation of red-shifted azobenzene amino acids into proteins. *Org. Lett.* 17 (24): 6258–6261.

**94** Hoppmann, C., Maslennikov, I., Choe, S., and Wang, L. (2015). In situ formation of an azo bridge on proteins controllable by visible light. *J. Am. Chem. Soc.* 137 (35): 11218–11221.

## 4 Diazocines: Photoswitches with Excellent Photophysical Properties and Inverted Stabilities

Rainer Herges and Pascal Lentes

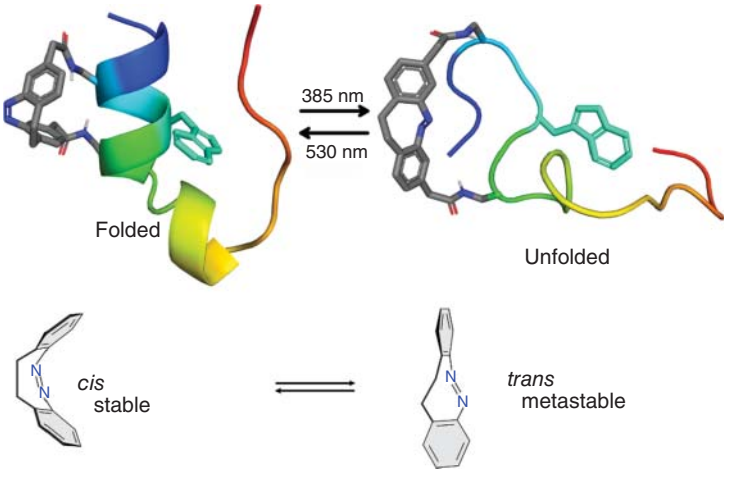


**Characteristic Features**

Diazocines are bridged azobenzenes with superior properties for application in a number of fields, such as light-controlled protein folding, photopharmacology, and materials sciences.

### First reported

R. Siewertsen, R. Herges, F. Temps et al. (2009). Highly efficient reversible Z–E photoisomerization of a bridged azobenzene with visible light through resolved S1($n\pi^*$) absorption bands. *J. Am. Chem. Soc*. 131, 15594–15595.

### Key references

M. Hammerich, C. Schütt, C. Stähler, and P. Lentes (2016). Heterodiazocines: synthesis and photochromic properties, *trans* to *cis* switching within the bio-optical window. *J. Am. Chem. Soc*. 138, 13111–13114.

P. Lentes, E. Stadler, F. Röhricht, and A. Brahms (2019). Nitrogen bridged diazocines: photochromes switching within the near-infrared region with high quantum yields in organic solvents and in water. *J. Am. Chem. Soc*.: 13592–13600.

G. Cabré, A. Garrido-Charles, À. González-Lafont, and W. Moormann (2019). Synthetic photoswitchable neurotransmitters based on bridged azobenzenes. *Org. Lett*. 21, 3780–3784.

# 4

# Diazocines: Photoswitches with Excellent Photophysical Properties and Inverted Stabilities

*Rainer Herges and Pascal Lentes*

*Christian-Albrechts-Universität zu Kiel, Otto-Diels-Institut für Organische Chemie, Otto-Hahn-Platz 4, 24098 Kiel, Germany*

## 4.1 Photophysical Properties and Conformations of Parent Diazocine

Diazocines (11,12-dihydrodibenzo[*c*,*g*][1,2]diazocines) are azobenzenes that are bridged by an ethylene linker connecting the *ortho* positions of both phenyl rings. Parent diazocine (**1**, $-CH_2-CH_2$-bridged) was first discovered in 1910 during an investigation on benzidination reactions [1]. About 100 years after the first report, it was rediscovered as a photoswitch with largely superior properties compared to the parent azobenzene system [2]. The 8-membered central "ocine" core exhibits two configurations, a stable *Z* structure in boat conformation and a metastable *E* isomer (Figure 4.1). As expected for an unsaturated 8-membered ring, the *Z*-boat structure is about 8–10 kcal mol$^{-1}$ more stable than the *E* configuration, which has a strain energy of ∼17 kcal mol$^{-1}$ [3, 4]. Diazocines, therefore, have an inverse thermal stability compared to azobenzene, which has a stable *E* configuration [5].

UV-spectra and photoisomerization mechanisms of diazocine also differ from azobenzene. Parent *E* and *Z* azobenzene exhibit ππ* transitions at 314 nm (*E*) and 275 nm (*Z*). Upon irradiation into the ππ* band of the *E* isomer of azobenzene with UV light of 290–350 nm, the *Z* isomer is formed (92%). Back-isomerization is achieved by irradiation into the nπ* band of the *Z* isomer with violet light (∼420 nm). However, the photoconversion is incomplete (79% *E*) because the nπ* bands of both isomers strongly overlap (*E*: $\lambda_{max}$ 445 nm, *Z*: $\lambda_{max}$ 435 nm). Nevertheless, a reasonable photoconversion yield is observed since the molar extinction coefficients of the nπ* bands of both isomers differ (*E*: 390, *Z*: 1100 L mol$^{-1}$ cm$^{-1}$). The difference in molar absorption arises from the fact that *E* azobenzene is planar and the nπ* transition is symmetry forbidden, whereas the *Z* isomer is slightly distorted [6, 7].

Diazocines exhibit a rather different photoswitching mechanism. In contrast to azobenzene, the nπ* bands of *Z* and *E* diazocine are clearly separated ($\lambda_{max}$: 404 and 490 nm) and have higher molar extinction coefficients (*Z*: 479; *E*: 770 L$^{-1}$ mol cm$^{-1}$)

*Molecular Photoswitches: Chemistry, Properties, and Applications*,
First Edition. Edited by Zbigniew L. Pianowski.

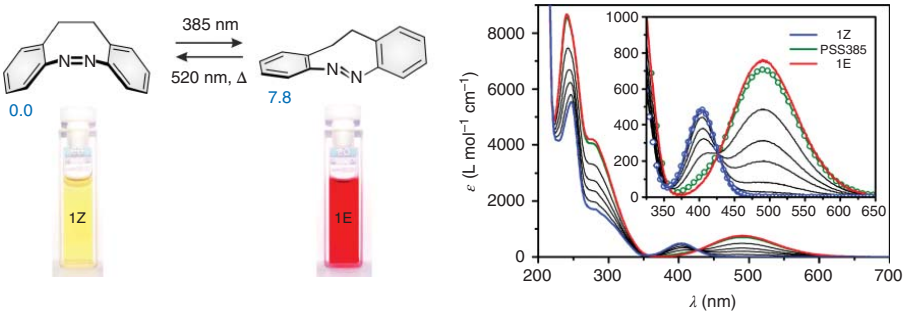


**Figure 4.1** Left: Structures of parent diazocine **1** in the *Z*-boat conformation and the *E*-twist conformation. Relative energies $E_{rel}$ in kcal mol$^{-1}$ are given in blue color. Right: UV spectra of *Z*-diazocine (blue), photostationary equilibrium upon irradiation with 385 nm (PSS 385, green, and pure *E*-diazocine [red]) [2]. Source: Adapted with permission of the American Chemical Society from Siewertsen et al. [2].

because both isomers are non-planar. Hence, the two nπ* bands can be selectively addressed with violet light (385–400 nm, $Z \rightarrow E$ isomerization) and green or yellow light (520–600 nm, $E \rightarrow Z$) (see Figure 4.1 and Table 4.1) [2]. Photoconversion yields are excellent ($E \rightarrow Z > 99\%$ and $Z \rightarrow E \sim 92\%$). The metastable $E$ configuration thermochemically isomerizes back to the stable $Z$ isomer with a half-life of 4.5 hours at 28.5 °C in hexane.

With quantum yields of 0.7 ($Z \rightarrow E$) at 385 nm and 0.9 ($E \rightarrow Z$) at 520 nm [4], parent diazocine **1** well competes with the most efficient natural systems such as rhodopsin (see Figure 4.2). Azobenzene exhibits significantly smaller quantum yields of 0.47 ($Z \rightarrow E$, 436 nm) and 0.16 ($E \rightarrow Z$, 317 nm) [9].

Efficient photochemical conversions, high quantum yields, and switching wavelengths in the visible region lead to very high efficiencies in the conversion of light to chemical energy (7.6% at 400 nm). Substituted diazocines attain efficiencies of up to 18.1% [8], which are the highest among photochromic compounds. Unexpectedly, the isomerization dynamics of parent diazocine **1** ($S_1$ life-time ~30–40 fs) are one order of magnitude faster than the isomerization of azobenzene ($S_1$ life-time ~365–400 fs). The ultrafast excited state decay is counter-intuitive since the bridge reduces the flexibility of the molecule [5, 10, 11].

As compared to azobenzene, the conformational degrees of freedom in diazocine are reduced. The ethylene bridge locks the rotation of the phenyl rings. Nevertheless, several temperature-dependent conformational movements complicate the interpretation of nuclear magnetic resonance (NMR) spectra (Figure 4.3). The stable $Z$ isomer undergoes a boat inversion, which is slow on the NMR timescale at room temperature. The calculated activation barrier is 33.3 kcal mol$^{-1}$ at the M062X(D3)/def2TZVP level of density-functional theory (DFT). The metastable $E$-diazocine exists in a twist or a chair conformation, whereby the $E$-twist conformation is about 2–3 kcal mol$^{-1}$ more stable than the $E$-chair conformation. Hence, the predominant $E$ species is the twisted form. DFT calculations revealed that both $E$-conformations (twist and chair) are rotamers and are in equilibrium with each other by a crank-type movement. Due to its $C_2$ symmetry, both $E$-twist structures are enantiomers. The chair and the twist, however, do not directly interconvert with their enantiomeric structure, the intermediate structure of the chair–chair conversion is the twist form and vice versa [12].

The nπ*-transition of the $E$-chair is almost isoenergetic with the nπ*-transition of the $Z$-boat ($\lambda_{max} \sim 400$ nm), while the nπ*-transition of the $E$-twist conformation is strongly bathochromic shifted ($\lambda_{max} = 490$ nm). This is an important finding. Upon designing new diazocine derivatives, care should be taken that the $E$-twist conformation is more stable than the $E$-chair conformation. If the $E$-chair would be the predominant species in the conformational equilibrium, this would decrease the photoconversion yield drastically due to an overlap of the $Z$-boat nπ*-transition and the $E$-chair nπ*-transition [3, 4].

The switching properties of substituted azobenzenes may differ from the unsubstituted parent system, albeit diazocines are less susceptible to substitution effects. An overview of recent literature [13–17] indicates that the energies of

**Table 4.1** Comparison of the photophysical properties of azobenzene, parent diazocine **1,** and heteroatom-bridged diazocines **18–22**.

| | **Parent azobenzene** | **Parent diazocine 1** | **O-diazocine 18** | **S-diazocine 19** | **NH-diazocine 20** | **NMe-diazocine 21** | **NAc-diazocine 22** |
|---|---|---|---|---|---|---|---|
| Stable isomer | *E* | *Z* | *Z* | *Z* | *Z* | *Z* | *Z* |
| $\Delta E_{rel}$ [a)] | −12.4 | 7.9 | 12.5 | 6.2 | 11.0 | 9.0 | 9.2 |
| $\lambda_{max(Z)}$ [b)] | 435 nm (nπ*) | 404 nm (nπ*) | 385 nm (nπ*) | 405 nm (nπ*) | 409 nm (nπ*) | 401 nm (nπ*) | 398 nm (nπ*) |
| $\lambda_{max(E)}$ [b)] | 314 nm (ππ*) | 490 nm (nπ*) | 525 nm (nπ*) | 525 nm (nπ*) | 559 nm (nπ*) | 554 nm (nπ*) | 516 nm (nπ*) |
| $t_{1/2}$ | 4 h (60 °C) | 4.5 h (28.5 °C) | 89 s (20 °C) | 3.5 d (27 °C) | 131 s (25 °C) | 40 s (25 °C) | 27 min (25 °C) |
| $\Gamma_{Z\to E}$ [c)] | > 400 nm: 79% | 385 nm: 92% | 385 nm: 80% | 405 nm: 70% | 405 nm: 65% | 405 nm: 50% | 400 nm: 88% |
| $\Phi_{Z\to E}$ [d)] | 0.47 (436 nm) | 0.72 (385 nm) | N/A | 0.43 (405 nm) | 0.57 (400 nm) | N/A | 0.48 (400 nm) |
| $\Gamma_{E\to Z}$ [a)] | 317 nm: 90% | 520 nm: > 99% | 520 nm: > 99% | 520 nm: > 99% | 520–690 nm: > 99% | 520–740 nm: > 99% | 520–590 nm: > 99% |
| $\Phi_{E\to Z}$ [d)] | 0.16 (280 nm) | 0.9 (520 nm) | N/A | N/A | 0.8 (520 nm) | N/A | 0.85 (520 nm) |

a) $\Gamma_{Z\to E}$, $\Gamma_{E\to Z}$: conversion yields $Z \to E$ and $E \to Z$ at the photostationary states upon irradiation at the given wavelengths;
b) $\Delta E_{rel} = E_E - E_Z$ in kcal mol$^{-1}$, M06-2X(D3)/def2-TZVP;
c) $\lambda_{max(Z)}$, $\lambda_{max(E)}$: maximum absorption wavelengths of the excitations used for switching (nπ* or ππ*);
d) $\Phi_{Z\to E}$, $\Phi_{E\to Z}$: quantum yields determined at the given wavelengths.

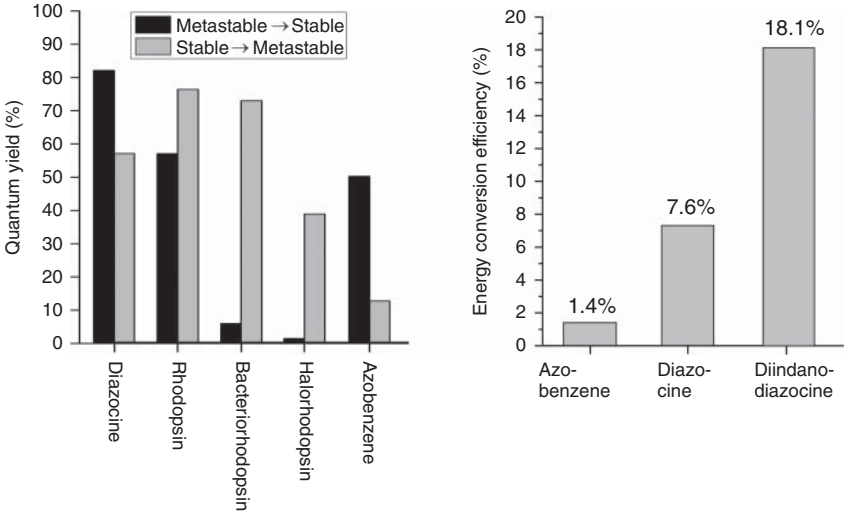


**Figure 4.2** Left: Switching quantum yields of diazocine, azobenzene, and selected natural systems. Right: Energy conversion efficiencies of light to chemical (strain) energy of azobenzene, diazocine, and a diazocine derivative [8].

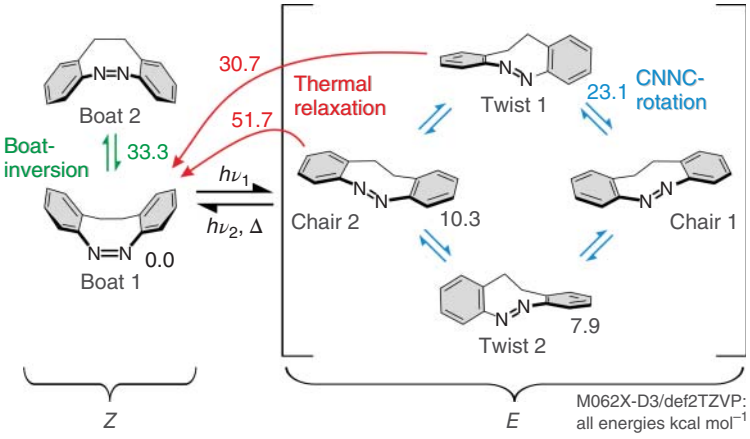


**Figure 4.3** Configurational and conformational space of the parent diazocine **1** [12]. Relative energies (relative to the most stable structure: *Z*-boat **1**) calculated at the M062X-D3/def2TZVP level of density functional theory are given. Numbers in black are minima, and numbers in green and blue color are transition-state energies.

the nπ*-transitions are not much affected by substitution, particularly if the substituents are in *meta* position with respect to the azo group (2,8-positions). The nπ*-transitions seem to be largely independent of the electronic nature of the diazocine. However, in contrast to the nπ*-transitions, the ππ*-transitions are shifting bathochromically if the π-system is enlarged, if it carries amino substituents or a push–pull substitution pattern. Large bathochromic shifts cause an overlap of the

$E$ ππ*-transition with the $Z$ nπ*-transition, and consequently the $Z \rightarrow E$ photostationary state decreases significantly (down to 18%: dithiophene diazocine) [13]. The ππ*-transitions are significantly affected by strong electron-donating substituents (e.g. $NH_2 > OMe$). A decoupling of these substituents from the electronic core (e.g. by inserting $CH_2$ groups) is the best strategy to retain the excellent photophysical properties of diazocines [18].

The photoconversion with visible light in both directions, the well-separated nπ*-transitions, the efficient photoconversion, the high quantum yields, and the ultrafast isomerization are outstanding properties of diazocines. Moreover, no fatigue over thousands of switching cycles was observed in the parent system. The substituted systems investigated so far are obviously long-term stable as well.

## 4.2 Synthesis of Diazocines

A key step of the synthesis of diazocines is the formation of the 8-membered ring. Cyclization can be accomplished by reduction [16, 19–21] of the nitro precursor **2** or oxidation [17] of the amino precursor **4** (Figure 4.4). Direct reduction to the diazocine with zinc or lead under milling was found to give low yields, which are hard to reproduce. Variable product distributions of azoxy, azo, and hydrazo derivatives are observed under reductive conditions, since the reduction is very sensitive to pH, the reducing reagent, or temperature. It is most convenient to reduce the nitro precursor **2** with zinc in basic solution to the hydrazine derivative **3** (58% yield) that can selectively be reoxidized with air in a copper-catalyzed reaction to the diazocine in quantitative yields. Oxidation of a dianiline precursor **4** to the diazocine **1** can be accomplished with yields up to 86% with peroxy reagents such as *m*CPBA [17]

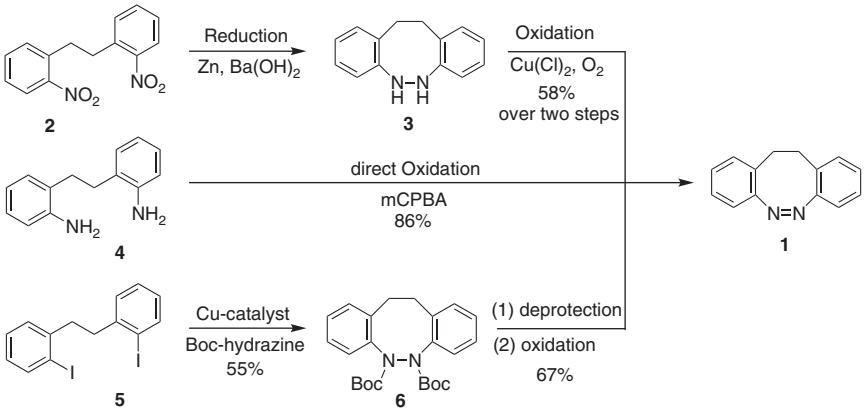


**Figure 4.4** Three strategies to close the 8-membered diazocine ring (azo-cyclization). Reductive approach (top): reduction of nitro precursor **2** via hydrazine **3** and reoxidation to diazocine **1**. Oxidative approach (middle): oxidation of amino precursor **4** with *m*CPBA or oxone. Cross-coupling approach (bottom): Ullmann–Goldberg reaction with Boc-hydrazine, followed by deprotection and oxidation of the free hydrazine.

or Oxone [22]. Another method is the C—N copper-catalyzed Ullmann–Goldberg coupling of 1,2-bis(*t*-butyloxycarbonyl)hydrazine with *o*-iodobibenzyl **5** (55% yield), followed by deprotection of the hydrazo compound **6** with TMSI and oxidation of the hydrazine with NBS in pyridine (67% yield). However, the yields of the cyclization vary strongly, dependent on the substrates (16–70%) [13]. All attempts to form the N=N bond first and to close the 8-membered ring by C—C bond formation in the last step, failed so far.

There is no electrophilic aromatic substitution with diazocines published; however, the aromatic bromination of the parent azoxy derivative was reported [20]. Substitution takes place at the phenyl ring distant from the $N^+$–$O^-$ group. Oxidation of unsymmetrically substituted diazocines and incomplete reduction of unsymmetrical bis-nitro precursors provide two isomeric azoxy compounds. Therefore, only symmetrically substituted diazocines are directly accessible via the "azoxy approach." There is a lack of general methods for the selective reduction of azoxy to azo groups. Each azoxy system requires tedious optimization of reducing agents and conditions. Frequently only moderate yields are obtained [23]. Therefore, substitution prior to cyclization, e.g. substitution of the anilines, or substitution of the nitro compounds and subsequent reduction to the anilines should be considered. Obviously, the reductive approach gives higher yields but is not always favorable.

The first step in diazocine synthesis is the formation of the ethylene bridge. Three general approaches were reported for C—C coupling – (a) Oxidative dimerization of *o*-nitrotoluenes [21], (b) Sonogashira cross-coupling [17], (c) Wittig reaction [15] (Figure 4.5).

The oxidative C—C bond formation (a) requires strongly basic conditions, since the methyl groups of the nitrotoluenes **7**, **8** have to be deprotonated. Substituents that are labile to strong bases or functional groups with more acidic protons than the methyl group in 2-position (e.g. $CH_2$-COR or amines/amides) are not compatible with this method. Moreover, the bridge formation leads to a statistical product distribution (**9**, **10**, **11**) if two different *o*-nitrotoluene molecules are connected. Monosubstituted bis(nitrophenyl)ethanes **9** are accessible by using a large excess of nitrotoluene **8**, which suppresses the self-coupling of the two substituted nitrotoluenes (**7** → **11**); however, self-addition of nitrotoluene might lead to problems to isolate the wanted unsymmetrical product **9** in the presence of large amounts of **10**. Symmetrically substituted bis(nitrophenyl)ethanes **11** are easily accessible in high yields. Moreover, a number of substituted *o*-nitrotoluenes are commercially available [8, 16, 21]. For the synthesis of unsymmetrically substituted dinitro diazocine precursors, the statistical approach **A** is often acceptable, but a C—C bond formation via cross-coupling (b) or Wittig reaction (c) might be favorable if the nitrotoluenes are less accessible or if they include functional groups that are base sensitive. Cross-coupling reactions under Sonogashira conditions (b) often lead to dehalogenation if the phenyl precursors (**12** and **13**) include further halogens (R = Br, I). Steric hindrance also impedes cross-coupling reactions. As an alternative, Wittig reaction is possible under metal-free conditions with a higher tolerance to bulky substituents [24]. Pathways (b) and (c) are resulting in an unsaturated

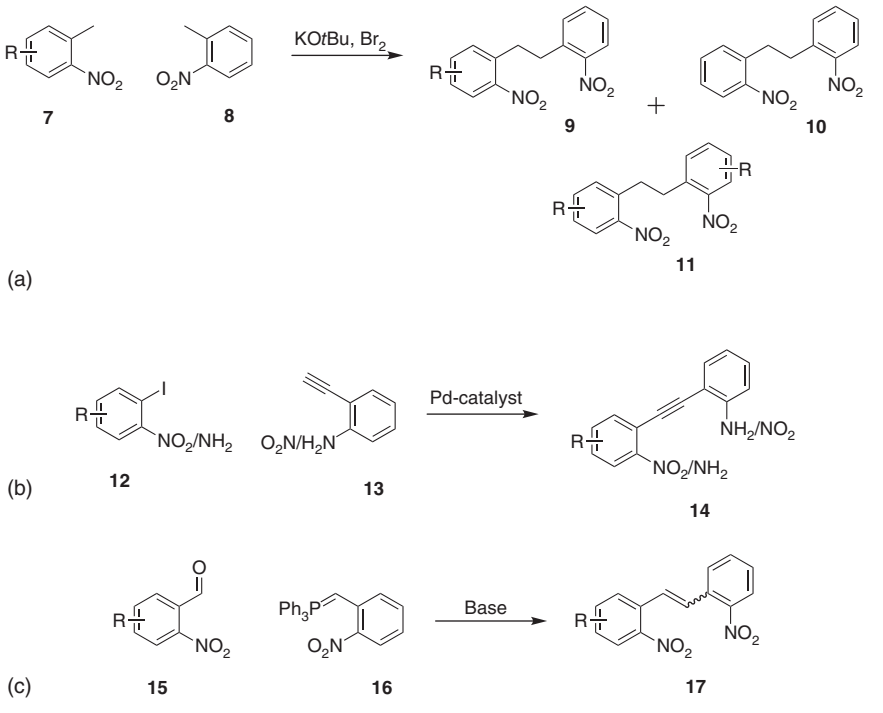


**Figure 4.5** Three C—C bond formation approaches to establish the ethylene bridging unit. (a) Oxidative C—C-coupling under basic conditions and addition of bromine, (b) Sonogashira cross-coupling reaction, (c) Wittig reaction.

bridge (**14**, **17**) that has to be reduced before the azo cyclization. For the complete reduction of stilbenes or tolanes to alkanes, catalytic hydrogenation (Pd/C) is the method of choice. However, aryl halides (R = Cl, Br, I) are partially reduced under these conditions, and therefore ways (b) and (c) are less suitable for the synthesis of halogenated diazocines (except R = F) [17]. The synthetic approach (a) starting from halogenated *o*-nitrotoluenes is most convenient for the preparation of symmetrically halogen-substituted diazocines [22]. Halogenated diazocines are an important starting point for further functionalization via crosscoupling reactions [25].

The synthetic strategies listed above allow the synthesis of a wide range of substituted diazocines [16, 17, 19, 22]. There are practically no functional group limitations. It is justified to state that the synthetic access to functionalized diazocines does not fall behind the well-elaborated preparation methods of azobenzenes. Diazocines for different applications are available or can be rationally designed.

## 4.3 Heteroatom-Bridged Diazocines

Substitution of one $CH_2$ group of the ethylene bridge by heteroatoms such as oxygen **18**, sulfur **19**, or nitrogen **20**–**22** (Figure 4.6) changes the flexibility of the bridge, and the electron-donating effects alter the photophysical properties of the

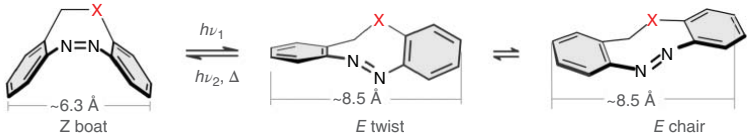


| | X | $E_{strain}$ Z | $E_{rel}$ Twist | $E_{rel}$ Chair |
|---|---|---|---|---|
| **1** | $CH_2$ | 16.3 | 7.6 | 10.5 |
| **2** | O | 19.5 | 12.5 | 15.4 |
| **3** | S | 16.5 | 5.1 | 5.1 |

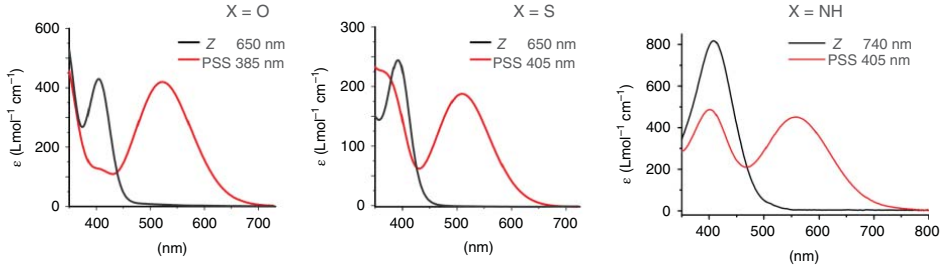


**Figure 4.6** Structures of heteroatom-bridged diazocines with their isodesmic strain energy ($E_{strain}$) and the relative energy differences ($E_{rel}$) of the different *E* conformations (M06-2X(D3)/def2-TZVP) [3, 4]. UV–vis spectra of the photostationary states of **18**, **19,** and **20** are given below. Source: Adapted with permission of the *American Chemical Society* from Hammerich et al. [3] (© 2016) and Lentes et al. [4] (© 2019).

diazocines (Table 4.1). The energy levels of the $Z \rightarrow E$ $n\pi^*$-transitions are slightly bathochromically shifted compared to parent diazocine **1**, which allows a $Z \rightarrow E$ isomerization with 400–405 nm (except O-diazocine **18**). The $E \rightarrow Z$ n$\pi^*$-transitions are strongly bathochromically shifted and a quantitative $E \rightarrow Z$ isomerization is still effective with wavelengths of >600 nm or even near-infrared (NIR) light [3, 4].

$Z \rightarrow E$ Photoconversion yields of S-diazocine **19** (70%) [3, 18], NH-diazocine **20** (60%), and NMe-diazocine **21** (50%) [4] were found to be limited by the presence of a significant amount of the *E*-chair conformation in the *E*-chair $\rightleftharpoons$ *E*-twist equilibrium, due to the overlap of the *Z*-boat and *E*-chair n$\pi^*$-transitions. In contrast to **19**, **20,** and **21**, parent diazocine **1**, O-diazocine **18,** or NAc-diazocine **22** does not suffer from this disadvantage. No significant amount of *E*-chair was observed by NMR or UV–vis spectroscopy.

A systematic investigation of the solvent dependence of the photophysical properties of $CH_2$–$CH_2$-bridged diazocines revealed that the separations of the *Z* and *E* n$\pi^*$-transitions are decreasing with increasing polarity of the solvent. In addition, there is a general trend that the quantum yields of $CH_2$–$CH_2$-bridged diazocines are favoring the $E \rightarrow Z$ and disfavor $Z \rightarrow E$ conversion with increasing solvent polarity. The two effects are systematically decreasing the photoconversion yields of the $CH_2$–$CH_2$-bridged diazocines from 92% in *n*-hexane to ~50% in water. In case of S-diazocine **19**, there is a third effect that decreases $Z \rightarrow E$ conversion yields. The concentration of the *E* chair conformation is increasing with increasing solvent polarity causing a complete overlap with the *Z* boat n$\pi^*$-transition. Therefore, the photoconversion yield of S-diazocine **19** is decreasing from 70% in acetone to <42% in water. The lower $Z \rightarrow E$ conversion yields of $CH_2$–$CH_2$-bridged diazocines and of S-diazocine **19** reduce the efficiency of applications in aqueous media. However, NAc-diazocine **22** is an exception. There is also a decrease of the n$\pi^*$-band separation (*Z*-boat and *E*-twist), but the quantum yields are favoring the $Z \rightarrow E$ conversion with higher solvent polarity. The $Z \rightarrow E$ photoconversion yields of NAc-diazocine **22** are mostly retained in water (72%) compared to organic solvents (82%). Another advantage of NAc-diazocine **22** for applications in biological environments is the fact that it is inherently water-soluble without solubilizing substituents [18].

## 4.4 Applications of Diazocines

Diazocines exhibit inverted stabilities compared to azobenzenes. The bent and sterically more demanding *Z* configuration is thermodynamically more stable than the slender, stretched *E* isomer. This property makes them particularly suitable for applications in photopharmacology and as mechanophores (Figure 4.7).

In photopharmacology, a photoswitchable drug is administered in its biologically inactive state (off state). Upon irradiation at the site of illness (inflammation, tumor, etc.), the drug switches into the active (on) state. Spatiotemporal control of biological activity with light avoids side effects in neighboring healthy tissue, and the thermal backisomerization prevents contamination of the environment after excretion [26, 27]. There are a number of azobenzene-derivativatized, photoswitchable inhibitors published. The majority of these drugs is biologically

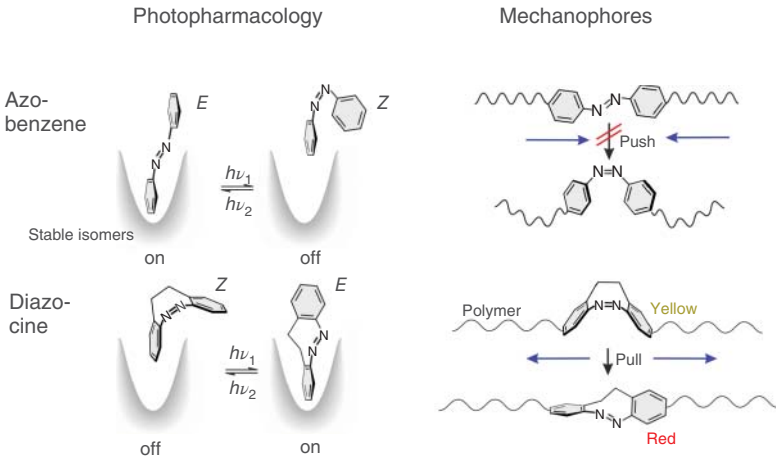


**Figure 4.7** Application of azobenzenes and diazocines in photopharmacology and as mechanophores. Diazocines are more suitable as azobenzenes in these fields because they have a bent *cis* resting state, which is converted to a stretched *trans* geometry upon irradiation (inverted stability). This allows light-induced on-switching of biological activities in photopharmacology as well as mechanically induced $Z \rightarrow E$ switching by applying a stretching force in polymers.

active in the stretched $E$ configuration and inactive in the bent $Z$ form (Figure 4.7). This is probably due to the fact that the slender $E$ configuration fits into the spatially confined active center of the target protein and the sterically more demanding $Z$ isomer does not. Since azobenzenes are stable in their active $E$ configuration, irradiation would rather switch the activity of the drug off than on, which is unfavorable. Diazocines, however, can be administered in their inactive $Z$ state (off) and activated with light (on) at the site of interest. Generally, it is more important to switch a drug effectively to the inactive than to the active state because incomplete conversion to the active state can be accounted for by increasing the concentration, whereas remaining activity of drug due to incomplete deactivation is hard to counterbalance. Off switching ($E \rightarrow Z$) of diazocines, indeed, is quantitative in all cases that were investigated so far. Another obvious advantage of diazocines are the switching wavelengths, which are in the visible region extending to the red and even near infrared (N-diazocines). UV light, needed for $E \rightarrow Z$ isomerization in azobenzenes, is tissue damaging, whereas the $E \rightarrow Z$ switching wavelengths in diazocines (>500 nm) are rather safe. Moreover, at wavelengths >650 nm, light has a larger penetration depth in blood-supported tissue (bio-optical window). Diazocines with their tricyclic structure are conformationally less flexible than azobenzenes and most other photoswitches. Therefore, the force transmission from the photoswitch to the environment should be more efficient and an induced fit of the inhibitor to the binding site of the receptor should be less likely. Diazocines are structurally similar to the family of tricyclic drugs. One can assume that if the photoswitching unit is part of such a binding motif, the change in binding affinity upon isomerization is stronger than in drugs that carry a photoswitch as a substituent.

The first applications of diazocines in photopharmacology were photoswitchable neurotransmitters. Substituted diazocines that are binding as ligands to the tetraethylammonium-binding site or glutamate receptors of potassium channels (external and internal) were used as extracellular ion channel agonists and intracellular ion channel blocker in living neurons [22, 28, 29]. The thermodynamically stable $Z$ isomers of the photoswitches did not influence the postsynaptic currents, while the metastable $E$ isomers exhibit a high affinity to ion channels. In the extracellular media, the ion flow was switched on, while the ion flow was switched off in intracellular experiments. Even though the conversion yield ($Z \rightarrow E$) was comparatively low (~50–60%) and does not limit this application, the dark-adapted $Z$ isomer is physiologically inactive and addressable with a quantitative photoconversion yield. It was possible to trigger neuronal firing selectively and spatiotemporally resolved without any background activity in the dark. This is a big advantage compared to azobenzene-based systems, where only an increase or decrease in current flow through irradiation was achieved in similar studies due to its incomplete photostationary states or thermal relaxation to the active $E$ isomers [30, 31]. Moreover, visible light (~400 nm) for the $Z \rightarrow E$ isomerization of diazocines has a higher tissue penetration depth than UV light that is required for the $E \rightarrow Z$ isomerization of azobenzene (Figure 4.8).

Substituted diazocines were also used as peptide cross-linking, amino-acid analogs in protein backbones [15, 32, 33], or for the modulation of DNA duplexes [34]. The photoinduced isomerization of diazocines allowed a selective manipulation of the three-dimensional structures of the biological macromolecules (protein folding and unfolding or interconversion of DNA duplexes with double-stranded DNA) with a high spatiotemporal resolution and non-toxic and traceless light energy. The ability to control the biological activity of macromolecules with light provides the basis to investigate mechanisms, kinetics, or biochemical pathways on a more sophisticated level as compared to classical methods.

S-diazocine derivates were used as photoswitchable VEGFR-2 Axitinib inhibitors. The sterical clash of the protein-binding site with the $Z$-configurations gave rise to a 40–50 fold difference in bioactivity upon $Z \rightarrow E$ conversion, which is a major improvement compared to previous photoswitchable kinase inhibitors. However, a derivative of parent diazocine **1** did not yield a significant decrease of the inhibitorial

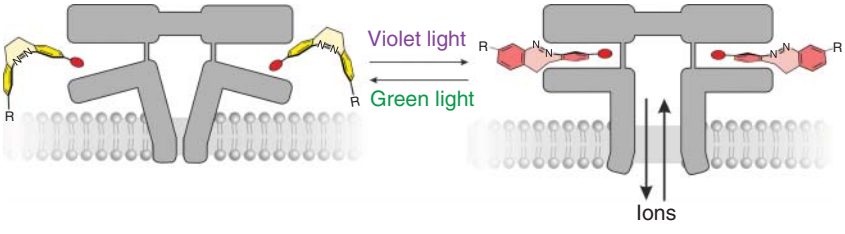


**Figure 4.8** Photoinduced firing of neuronal cells. Irradiation with deep blue light induces a $Z \rightarrow E$ photoisomerization of a diazocine ligand. The $E$ isomer opens the ion channels while the $Z$ isomer is completely inactive.

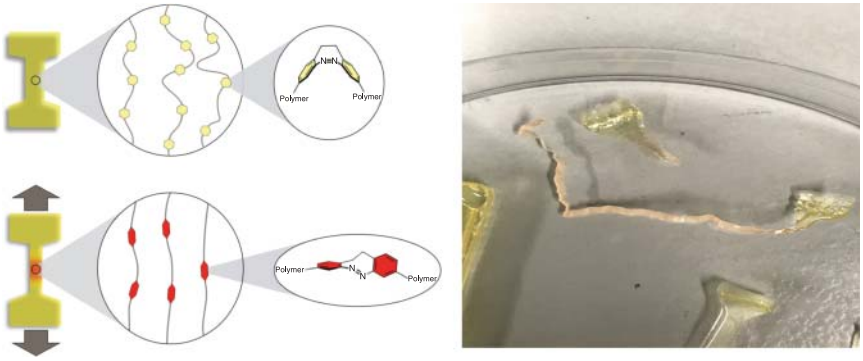


**Figure 4.9** Diazocines in a polymer backbone. The thermodynamically stable *Z* configuration isomerizes to the metastable *E* twist isomer if the material is stretched. The mechanical stress is indicated by a color change from yellow to intense red. Source: van der Schaft and Luijk [38].

strength after irradiation, because of a larger angle between the phenyl rings in its *Z* configuration and a less pronounced sterical clash compared to the S-diazocine [35].

Diazocines in their *Z* resting state are pale yellow, while the metastable *E* twist configurations are intensely red-colored. The color difference is observable with the bare eye even at very small concentrations. Tensile forces lead to the conversion of the shorter bend *Z* conformer to the stretched *E* isomer and, therefore, diazocines are suitable as mechanochromes that are indicating mechanical stress of functional materials by a color change from yellow to red. Linear urea polymers that contain amino-substituted diazocines in their backbone or siloxane copolymers, including vinylated diazocines, were reported. Irradiation caused reversible color changes and bending of the thin polymer films. These functional polymers are promising candidates for applications as smart materials such as photoresponsive mechanophores, visible-light-driven actuators, or rewriteable materials [36, 37] (Figure 4.9).

## 4.5 Conclusion

Diazocines are structurally related to azobenzenes; however, they are superior in most photophysical properties. The bridge between the two phenyl rings forming an 8-membered ring inverts the relative stability of the *E* and *Z* isomers in favor of the *Z* form. Unlike azobenzene, where ππ* ($E \rightarrow Z$) and nπ* ($Z \rightarrow E$) excitations are used for switching, both isomerizations in diazocines are induced by nπ* excitations with light in the visible range or even near infrared. The more rigid structure of diazocines improves quantum yields, light to chemical energy conversion efficiencies, and force transmission to the environment. Long-term stability studies of the parent system did not reveal any fatigue over more than 100 000 switching cycles. Recent strategies for the synthesis of diazocine derivatives improved the accessibility for a number of applications in biochemistry and materials science. Further applications in other areas are to be expected.

## Acknowledgments

The authors are grateful to the Deutsche Forschungsgemeinschaft for support via the SFB 677 Function by Switching.

## References


1 Duval, H. (1910). Recherches sur la benzidination. *Bull. Soc. Chim. Fr.* 7: 727–732.

2 Siewertsen, R., Neumann, H., Buchheim-Stehn, B. et al. (2009). Highly efficient reversible Z-E photoisomerization of a bridged azobenzene with visible light'through resolved S1(nπ*) absorption bands. *J. Am. Chem. Soc.* 131: 15594–15595.

3 Hammerich, M., Schütt, C., Stähler, C. et al. (2016). Heterodiazocines: synthesis and photochromic properties, trans to cis switching within the bio-optical window. *J. Am. Chem. Soc.* 138: 13111–13114.

4 Lentes, P., Stadler, E., Röhricht, F. et al. (2019). Nitrogen Bridged Diazocines: Photochromes Switching within the Near-Infrared Region with High Quantum Yields in Organic Solvents and in Water. *J. Am. Chem. Soc.* 141: 13592–13600.

5 Siewertsen, R., Schönborn, J.B., Hartke, B. et al. (2001). Superior Z → E and E → Z photoswitching dynamics of dihydrodibenzodiazocine, a bridged azobenzene, by S1(nπ*) excitation at λ = 387 and 490 nm. *Phys. Chem. Chem. Phys.* 13: 1054–1063.

6 Bortolus, P. and Monti, S. (1979). *Cis-trans* photoisomerization of azobenzene. Solvent and triplet donors effects. *J. Phys. Chem.* 83: 648–652.

7 Ito, Y., Ito, H., and Matsuura, T. (1988). *Trans-cis* photoisomerization of *meta*-(phenylazo) azobenzenes. *Tetrahedron Lett.* 29: 563–566.

8 Moormann, W., Tellkamp, T., Stadler, E. et al. (2020). Efficient conversion of light to chemical energy: directional, chiral photoswitches with very high quantum yields. *Angew. Chem. Int. Ed.* 132: 15081–15089.

9 Ladányi, V., Dvořák, P., Al Anshori, J. et al. (2017). Azobenzene photoisomerization quantum yields in methanol redetermined. *Photochem. Photobiol. Sci.* 16: 1757–1761.

10 Böckmann, M., Doltsinis, N.L., and Marx, D. (2010). Unraveling a chemically enhanced photoswitch: bridged azobenzene. *Angew. Chem. Int. Ed.* 49: 3382–3384.

11 Jiang, C.-W., Xie, R.-H., Li, F.-L., and Allen, R.E. (2011). Comparative studies of the trans−cis photoisomerizations of azobenzene and a bridged azobenzene. *J. Phys. Chem. A* 115: 244–249.

12 Röhricht, F. (2021). In silico design funktionaler Moleküle: Vorhersage und Erklärung molekularen Verhaltens durch Dichtefunktionaltheorie. Dissertation. Kiel University.

13 Li, S., Eleya, N., and Staubitz, A. (2020). Cross-coupling strategy for the synthesis of diazocines. *Org. Lett.* 22: 1624–1627.

**14** Sell, H., Näther, C., and Herges, R. (2013). Amino-substituted diazocines as pincer-type photochromic switches. *Beilstein J. Org. Chem.* 9: 1–7.

**15** Samanta, S., Quin, C., Lough, A.J., and Woolley, G.A. (2012). Bidirectional photocontrol of peptide conformation with a bridged azobenzene derivative. *Angew. Chem. Int. Ed.* 124: 6558–6561.

**16** Moormann, W., Langbehn, D., and Herges, R. (2019). Synthesis of functionalized diazocines for application as building blocks in photo- and mechanoresponsive materials. *Beilstein J. Org. Chem.* 15: 727–732.

**17** Maier, M.S., Hüll, K., Reynders, M. et al. (2019). Oxidative approach enables efficient access to cyclic azobenzenes. *J. Am. Chem. Soc.* 141: 17295–17304.

**18** Lentes, P., Frühwirt, P., Freißmuth, H. et al. (2021). Photoswitching of diazocines in aqueous media. *J. Org. Chem.* in press. DOI: https://doi.org/10.1021/acs.joc.1c00065.

**19** Paudler, W.W. and Zeiler, A.G. (1969). Diazocine chemistry. VI. An inquiry into the aromaticity of 5,6-dihydrodibenzo[b,f][l,Z]diazocine. *J. Org. Chem* 34: 3237–3239.

**20** Joshi, D.K., Mitchell, M.J., Bruce, D. et al. (2012). Synthesis of cyclic azobenzene analogues. *Tetrahedron* 68: 8670–8676.

**21** Moormann, W., Langbehn, D., and Herges, R. (2017). Solvent-free synthesis of diazocine. *Synthesis* 49: 3471–3475.

**22** Cabré, G., Garrido-Charles, A., González-Lafont, À. et al. (2019). Synthetic photoswitchable neurotransmitters based on bridged azobenzenes. *J. Org. Lett.* 21: 3780–3784.

**23** Merino, E. (2011). Synthesis of azobenzenes: the coloured pieces of molecular materials. *Chem. Soc. Rev.* 40: 3835–3853.

**24** Kiselyov, A.S. (1994). Reaction of *N*-fluoropyridinium salts with wittig reagents: a novel and convenient approach to symmetric trans-olefins. *Tetrahedron Lett.* 35: 8951–8954.

**25** Zhu, Q., Wang, S., and Chen, P. (2019). Diazocine derivatives: a family of azobenzenes for photochromism with highly enhanced turn-on fluorescence. *Org. Lett.* 21: 4025–4029.

**26** Hüll, K., Morstein, J., and Trauner, D. (2018). In vivo photopharmacology. *Chem. Rev.* 118: 10710–10747.

**27** Szymanski, W., Beierle, J.M., Kistemaker, H.A. et al. (2013). Reversible photocontrol of biological systems by the incorporation of molecular photoswitches. *Chem. Rev.* 113: 6114–6178.

**28** Thapaliya, E.K., Zhao, J., and Ellis-Davies, G.C.R. (2019). Locked-azobenzene: testing the scope of a unique photoswitchable scaffold for cell physiology. *ACS Chem. Neurosci.* 10: 2481–2488.

**29** Trads, J.B., Hüll, K., Matsuura, B.S. et al. (2019). Sign inversion in photopharmacology:incorporation of cyclic azobenzenes in photoswitchable potassium channel blockers and openers. *Angew. Chem. Int. Ed.* 58: 15421–15428.

**30** Mourot, A., Herold, C., Kienzler, A.M., and Lramer, R.H. (2018). Understanding and improving photo-control of ion channels in nociceptors with azobenzene photo-switches. *Br. J. Pharmacol.* 175: 2296–2311.